

Like sisters but not twins – vasopressin and oxytocin excite BNST neurons via cell type-specific expression of oxytocin receptor to reduce anxious arousal

Walter Francesconi*¹, Valentina Olivera-Pasilio*^{1,2,3}, Fulvia Berton¹, Susan L. Olson¹, Rachel Chudoba^{1,2}, Lorena M. Monroy^{1,4}, Quirin Krabichler⁵, Valery Grinevich⁵, and Joanna Dabrowska^{1,2#}

* contributed equally

corresponding author

¹ Center for Neurobiology of Stress Resilience and Psychiatric Disorders, Discipline of Cellular and Molecular Pharmacology, The Chicago Medical School, Rosalind Franklin University of Medicine and Science, 3333 Green Bay Road, North Chicago, IL, 60064, USA

² School of Graduate and Postdoctoral Studies, Rosalind Franklin University of Medicine and Science, 3333 Green Bay Road, North Chicago, IL, 60064, USA

³ Center for Psychiatric Neuroscience, Department of Psychiatry and Behavioral Sciences, Northwestern University, Chicago, IL, 60611, USA

⁴ Neuroscience Program, Lake Forest College, Lake Forest, IL, 60045, USA

⁵ Department of Neuropeptide Research in Psychiatry, German Center for Mental Health (DZPG), Medical Faculty Mannheim, Heidelberg University, 68159 Mannheim, Germany

corresponding author

Joanna Dabrowska, PhD, PharmD

Center for the Neurobiology of Stress Resilience and Psychiatric Disorders

Discipline of Cellular and Molecular Pharmacology

The Chicago Medical School

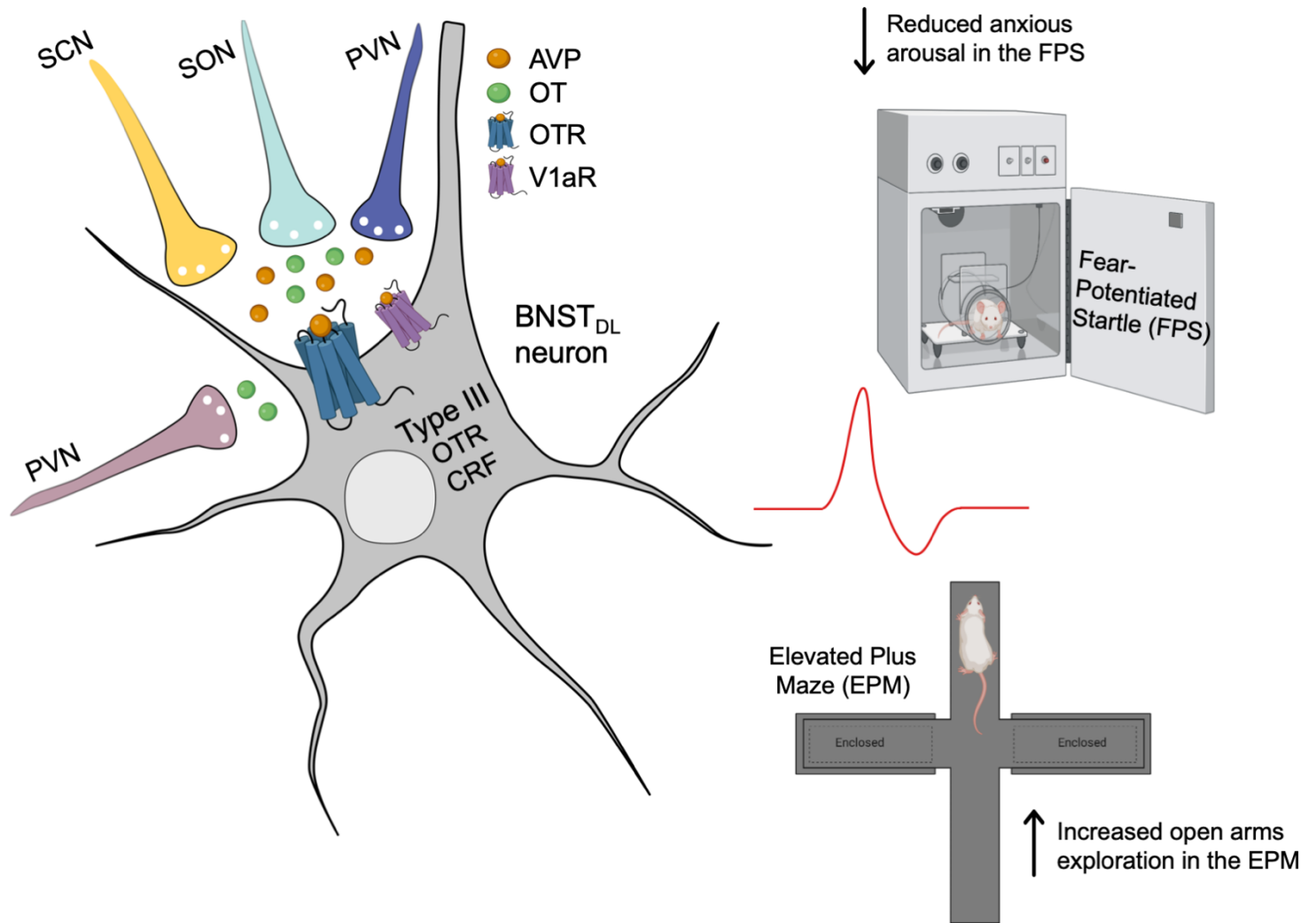
Rosalind Franklin University of Medicine and Science

3333 Green Bay Road, North Chicago, IL, 60064

Tel: 847-578-8664

joanna.dabrowska@rosalindfranklin.edu

Graphical abstract



Highlights

- Exogenous and light-evoked vasopressin peptide excites neurons of the bed nucleus of the stria terminalis (BNST) via oxytocin receptor (OTR) in male rats
- The dorsolateral BNST receives vasopressinergic inputs from suprachiasmatic, supraoptic, and paraventricular nuclei of the hypothalamus
- The majority of OTR- and Corticotropin-releasing factor (CRF) neurons of the BNST are classified as Type III neurons of the BNST_{DL} and are excited by AVP
- OTR-expressing BNST neurons increase exploration of open spaces and reduce anxious arousal in fear-potentiated startle in male rats
- Internal signal-sensitive hypothalamic inputs directly impact BNST excitability via OTR to balance interoceptive signals and defensive behaviors

Abstract

Interoceptive signals dynamically interact with the environment to shape appropriate defensive behaviors. Hypothalamic hormones arginine-vasopressin (AVP) and oxytocin (OT) regulate physiological states, including water and electrolyte balance, circadian rhythmicity, and defensive behaviors. Both AVP and OT neurons project to dorsolateral bed nucleus of stria terminalis (BNST_{DL}), which expresses oxytocin receptors (OTRs) and vasopressin receptors and mediates fear responses. However, understanding the integrated role of neurohypophysial hormones is complicated by the cross-reactivity of AVP and OT and their mutual receptor promiscuity. Here, we provide evidence that the effects of neurohypophysial hormones on BNST_{DL} excitability are driven by input specificity and cell type-specific receptor selectivity. We show that OTR-expressing BNST_{DL} neurons, excited by hypothalamic OT and AVP inputs, play a major role in regulating BNST_{DL} excitability, overcoming threat avoidance, and reducing threat-elicited anxious arousal. Therefore, OTR-BNST_{DL} neurons are perfectly suited to drive the dynamic interactions balancing external threat risk and physiological needs.

1. Introduction

Interoceptive signals dynamically interact with the environment to shape appropriate defensive behaviors. For example, rodents avoid open spaces to escape from predators but must overcome this defensive behavior to locate water when driven by thirst. Further, circadian rhythm-associated interoceptive signals drive animals to follow wake-sleep cycles despite predator threats. Numerous physiological functions, including water and electrolyte balance and circadian rhythmicity, are supported by the hormone and neuromodulator arginine-vasopressin (AVP) ^{1,2}, making AVP a prime candidate for modulating the interaction balancing external risks and internal needs. However, it is not clear how AVP acts in the extended amygdala, which directly influences defensive responses, to shape appropriate, physiologically relevant levels of exploratory and defensive behaviors.

AVP signals via three centrally located receptors: vasopressin receptors (V1aR, V1bR) and the oxytocin receptor (OTR), all of which are implicated in defensive behaviors, including fear, avoidance- and anxiety-like behaviors, for review see ³⁻⁸ (of note V2R is located in the kidneys ⁹). The receptors are differentially expressed in the brain, with V1bR highly expressed in the pituitary and other discrete locations ^{10,11}, whereas V1aR and OTR more highly expressed throughout the central nervous system ¹²⁻¹⁴. Notably, OTR and V1aR seemingly have opposite effects on exploration and fear-related behaviors in rodents ^{15,16}, suggesting that receptor selectivity is one mechanism by which AVP modulates defensive behaviors. The extended amygdala, including the central (CeA) and medial amygdala (MeA), as well as bed nucleus of the stria terminalis (BNST), has a high density of both oxytocin (OT)- and AVP-binding sites ¹⁷. However, specific receptor contributions to behavioral and physiological responses remain unclear and likely underlie the diverse behavioral effects of AVP. For example, there is a mismatch between AVP peptide density and vasopressin receptor expression in some regions of the extended amygdala, such as sparse V1aR but high AVP fiber density and OTR binding sites in posterior BNST, for review see ¹⁸. In addition, OTR contribution to AVP signaling may be obscured in behavioral studies using prominent V1R antagonists that also bind OTRs ^{19,20}. Given the abundance of OTRs and V1Rs in hypothalamic and the extended amygdala, AVP's effects via OTR are likely to be vastly underestimated.

Besides receptor selectivity, the diverse effects of AVP on behavior may also be modulated by input specificity. AVP is produced in neurons of the hypothalamus—including the paraventricular (PVN), supraoptic (SON), and suprachiasmatic nucleus (SCN) ^{21,22}—and the extended amygdala—including the MeA and posterior BNST ²³. As AVP and OT predominantly exist in separate neuronal groups within the hypothalamus ²⁴, AVP and/or OT inputs, prompted by specific physiological cues, might orchestrate the balance between physiological states and defensive behaviors through downstream brain structures. Given the hypothalamus' role in assessing internal physiological states

and the extended amygdala's role in gauging external threats, AVP and OT likely flexibly regulate defensive behaviors based on the interplay between physiological needs and external threats.

The dorsolateral portion of the BNST (BNST_{DL}) is critical for fear processing and vigilant threat monitoring^{25–28} and is one of the few brain regions with high expression of OT and AVP binding sites and fibers^{17,29}, as well as OTR and V1aR^{30–32}. It receives inputs from hypothalamic OT (primarily PVN) and AVP neurons^{23,33,34}, but the origins of the AVP projections to the BNST_{DL} are unknown. Primarily a GABA-ergic and peptidergic structure^{35,36}, the BNST_{DL} contains three major neuron types (Type I-III) defined by their intrinsic electrophysiological membrane properties and firing patterns^{37,38}. Previously, we demonstrated that OT is released in the BNST_{DL} in response to fear stimuli³⁹ where it has distinct cell type-specific effects on neuronal excitability and synaptic transmission⁴⁰. However, the integrative mechanisms by which AVP and OT act via V1R and/or OTR to regulate neuronal excitability and fear processing in the BNST_{DL} are unknown.

In this study, we used slice electrophysiology, neuronal tract tracing, and peptide optogenetics in naïve and AVP-Cre transgenic male rats to show that AVP neurons from the SCN, SON, and PVN project to the BNST_{DL}. Both exogenous AVP application and blue light-evoked AVP release excited Type I and Type III BNST_{DL} neurons, which required OTR transmission. Using OTR-Cre transgenic rats^{41,42}, we confirmed that fluorescent OTR-BNST_{DL} neurons, which match the properties of Type I and Type III cells, were excited by AVP. Single-cell PCR previously showed that Type III BNST_{DL} neurons express both OTR and CRF mRNA³³. Using CRF-Cre transgenic rats⁴³, we demonstrated that AVP and an OTR agonist (TGOT) directly excited these CRF-BNST_{DL} neurons. Finally, using chemogenetics we show that OTR-BNST_{DL} neurons' activity increased exploration in the elevated-plus maze and reduced anxious arousal in the fear-potentiated startle. Our findings show that AVP and OT effects on BNST_{DL} excitability depend on cell-type specific receptor expression and input specificity. Therefore, changes in the activity of internal signal-sensitive hypothalamic nuclei will directly impact BNST_{DL} excitability via specific hypothalamic inputs to balance exploratory and defensive behaviors.

2. Star Methods

Experimental models and subjects

Male wild-type Sprague-Dawley rats (SD, Envigo, Chicago, IL; 240-300 g), male transgenic OTR-Cre (Cre-recombinase (Cre) under OTR promoter), CRF-Cre (Cre under CRF promoter), and AVP-Cre (Cre under AVP promoter) rats (220-400 g) were housed in groups of three on a 12-h light/dark cycle (light 7 a.m. to 7 p.m.) with free access to water and food. Upon arrival from Envigo, wild-type SD rats were habituated to the environment for one week before the experiments began. OTR-Cre (Althamer et al., 2022; Iwasaki et al., 2023) and AVP-Cre transgenic (knock-in) rats were originally generated

and kindly provided by Dr. Valery Grinevich (Heidelberg University, Germany)⁴⁴, and CRF-Cre rats (Pomrenze et al., 2019) were created and kindly provided by Dr. Robert Messing (University of Texas, Austin) and bred at the biological resources facility (BRF) at Rosalind Franklin University of Medicine and Science (RFUMS). Experiments were performed in accordance with the guidelines of the NIH and approved by the Animal Care and Use Committee at RFUMS.

Drug preparation and pharmacological manipulations

The following compounds were used for electrophysiology: arginine (Arg⁸)-vasopressin (AVP; H-Cys-Tyr-Phe-Gln-Asn-Cys-Pro-Arg-Gly-NH₂ (disulfide bond); 0.2 μM, Bachem Americas, Torrance, CA; catalog #4012215); oxytocin (OT; H-Cys-Tyr-Ile-Gln-Asn-Cys-Pro-Leu-Gly-NH₂ (disulfide bond, acetate salt), 0.2 μM, Bachem Americas, Torrance, CA, #4016373); a selective rat V1aR agonist FE201874 (0.2-0.4 μM, generously provided by Ferring Pharmaceuticals, San Diego, CA)⁴⁷, a selective and potent OTR agonist TGOT ([Thr⁴,Gly⁷]-oxytocin (0.4 μM, Bachem Americas, Torrance, #4013837), and V1bR agonist d[Cha⁴]-AVP (1 μM, GlpBio Technology Inc, Montclair, CA, #GC1659)^{3,48}. The following antagonists were used: a V1aR/OTR antagonist (d(CH₂)₅¹,Tyr(Me)²,Arg⁸)-vasopressin, Manning compound⁴⁹; 1 μM, Tocris, Bio-Techne Corporation; MN, #3377); selective OTR antagonist (OTA; d(CH₂)₅(1), D-Tyr(2), Thr(4), Orn(8), des-Gly-NH₂(9))-Vasotocin trifluoroacetate salt⁴⁹; 0.4 μM, Chemical Repository, #V-905 NIMH); selective V1aR antagonist SR49059 (2S)-1-[[[(2R,3S)-5-Chloro-3-(2-chlorophenyl)-1-[(3,4-dimethoxyphenyl)sulfonyl]-2,3-dihydro-3-hydroxy-1H-indol-2-yl]carbonyl]-2-yrrolidinecarboxamide; 5 μM, Tocris, Bio-Techne Corporation, #2310); and a V1bR antagonist Nelivaptan ((2S,4R)-1-[(3R)-5-Chloro-1-[(2,4-dimethoxyphenyl)sulfonyl]-2,3-dihydro-3-(2-methoxyphenyl)-2-oxo-1H-indol-3-yl]-4-hydroxy-N,N-dimethyl-2-pyrrolidinecarboxamide; 1 μM, Tocris, Bio-Techne Corporation, #6195). To block glutamatergic transmission, we used AMPA and kainate receptor antagonist 6-Cyano-7-nitroquinoxaline-2,3-dione disodium salt (CNQX, 10 μM, Tocris, Bio-Techne Corporation, #1045). To block NMDA receptors, we used D-2-Amino-5-phosphopentanoic acid (D-AP5, 50 μM, Tocris, Bio-Techne Corporation, #0106). To block GABA-A receptors we used picrotoxin (PTX, 25 μM, Tocris, Bio-Techne Corporation, #1128). The designer receptor exclusively activated by designer drugs (DREADD) ligand clozapine-N-oxide (CNO), 8-Chloro-11-(4-methyl-4-oxido-1-piperazinyl)-5H-dibenzo[b,e][1,4]diazepine (CNO, Tocris, Bio-Techne Corporation, #4936) was used at 20 μM for chemogenetics manipulations during electrophysiological recordings and at 2 mg/kg for behavioral experiments. All drug stock solutions were dissolved in sterile deionized water, unless stated otherwise, and stored at -20°C until use. The day of the experiment, drugs for electrophysiology were diluted into artificial cerebrospinal fluid (aCSF) and applied to bath solution. CNO was diluted into sterile saline and injected intraperitoneally (i.p.) at 2 mg/kg.

Methods Details

In vitro whole-cell patch-clamp electrophysiology

Slice preparation and electrophysiological recordings were performed as before⁴⁰. Rats were deeply anesthetized by inhalation of isoflurane USP (Patterson Veterinary, Greeley, CO, USA). After decapitation, the brain was rapidly removed from the cranial cavity, and 300- μ m-thick coronal slices containing the BNST were prepared in ice-cold cutting solution (saturated with 95% O₂/ 5% CO₂) containing in mM: 122.5 NaCl, 3.5 KCl, 25 NaHCO₃, 1 NaH₂PO₄, 0.5 CaCl₂·2H₂O, 20 D-glucose, 3 MgCl₂·6H₂O, and 1 ascorbic acid (pH 7.4, 290–300 mOsm). The slices were prepared using a Leica vibratome (VT1200; Leica, Wetzlar, Germany), incubated for 30 min at 34°C, and subsequently transferred to room temperature for 1 hour before the recordings began. Next, the slices were transferred to a recording chamber perfused with oxygenated aCSF at a rate of 2-4 ml/min containing in mM: 122.5 NaCl, 3.5 KCl, 25 NaHCO₃, 1 NaH₂PO₄, 2.5 CaCl₂·2H₂O, 20 D-glucose, and 1 MgCl₂·6H₂O (pH 7.4, 290-300 mOsm), saturated with 95% O₂ and 5% CO₂. The aCSF was warmed to 30–34°C by passing it through a feedback-controlled in-line heater (TC-324C; Warner Instruments, Hamden, CT). The cell bodies of BNST_{DL} neurons were visualized using infrared differential interference contrast (IR-DIC) optics with an upright microscope (Scientifica Slice Scope Pro 1000, Clarksburg, NJ). Neurobiotin (0.1%, Vector Laboratories, Burlingame, CA) was added to the internal solution of the recording pipette to confirm cell location. After recording, slices were immersed in 10% formalin (Fisher Scientific, SF98-4), washed three times (10 min each) in phosphate-buffered saline (PBS 0.05 M), and incubated with streptavidin-Alexa Fluor 594 or Alexa Fluor 488 conjugate (dilution 1:2000, Invitrogen ThermoFisher Scientific, S32356 and S11223, respectively) at room temperature for 2 hours, followed by three washes in PBS and one wash in phosphate buffer (PB 0.05 M) (10 min each). All slices were mounted using Mowiol with antifade reagent (Sigma-Aldrich, 81381), and coverslips were applied before visualization with fluorescent microscopy (Nikon eclipse Ni, Nikon Instruments Inc.)

Electrophysiology recordings were made using Multiclamp 700B amplifiers (Axon Instruments, Union City, CA); current-clamp signals were acquired at 10 kHz with a 16-bit input-output board NI USB-6251 (National Instruments, Austin, TX) using custom MatLab scripts (Math-Work, Natick, MA) written by Dr. Niraj Desai⁵⁰. The access resistance (Ra) was monitored, and recordings were terminated if Ra changed > 15%. Electrophysiological measurements were carried out 10-15 min after reaching the whole-cell configuration. The input resistance was calculated from steady-state voltage responses upon negative current injections (pulses of 450-1000 ms). Whole-cell patch-clamp recordings were made from BNST_{DL} neurons using glass pipettes (4–8 M Ω) pulled from thick-walled borosilicate glass capillaries with a micropipette puller (Model P-97; Sutter Instrument, Novato, CA) filled with a solution

containing the following in mM: 135 potassium gluconate, 2 KCl, 3 MgCl₂·6H₂O, 10 HEPES, 5 Na-phosphocreatine, 2 ATP-K, and 0.2 GTP-Na (pH 7.3 adjusted with KOH, osmolarity 300-305 mOsm; potentials were not corrected for a liquid junction potential), as before⁴⁰.

To study the effects of AVP on intrinsic membrane properties and intrinsic excitability, the recordings were performed in the presence of synaptic transmission blockers: the AMPA receptor antagonist CNQX, the NMDA receptor antagonist D-AP5, and GABA-A receptor antagonist, PTX. To verify the receptor involved in the effects of AVP, in separate experiments, AVP was perfused in the presence of the V1aR/OTR antagonist, selective OTR antagonist OTA, selective V1aR antagonist SR49059, or selective V1bR antagonist Nelivaptan. Each antagonist was first applied alone for 10 min and then maintained during AVP application for another 12-15 min, followed by a 12-15-min drug-free washout in all whole-cell patch-clamp experiments.

Electrophysiological characterization of BNST_{DL} neurons

At the beginning of the recording sessions in current clamp mode, neurons were characterized using current pulses (450 ms in duration) from -250pA to 180pA in 10-pA increments. Based on their characteristic voltage responses³⁷, three major types of neurons were identified in the BNST_{DL}. Type I neurons fire regularly and display moderate spike frequency adaptation. These neurons also display a voltage sag that indicates the presence of the hyperpolarization-activated cation current (I_h). As a distinguishing feature of Type II neurons, post-inhibitory spikes are produced in response to preceding negative current steps that are related to the action of the low-threshold Ca^{2+} current. Additionally, Type II neurons display strong voltage sags under hyperpolarizing current pulses that indicate a high level of I_h current. Type III neurons differ from the previous two types in several aspects: they exhibit high rheobase and no voltage sag under negative current steps; they display prominent inward rectification that is caused by the activation of the inward rectifying K^+ current (I_{KIR}) at membrane potentials more negative than approximately -50 mV; and start firing after a characteristic slow voltage ramp mediated by the K^+ delayed current (I_D).

The effect of AVP on membrane properties and intrinsic excitability of Type I, II, and III BNST_{DL} neurons

We investigated the effects of AVP and other pharmacological manipulations in Type I-III BNST_{DL} neurons on the following membrane properties: resting membrane potential (RMP), input resistance (R_{in}), rheobase (R_h), threshold of the first action potential (first-spike T_h) (calculated as the voltage at which the depolarization rate exceeded 5 mV/ms), and latency of the first spike (first-spike Lat) evoked at the R_h current. We also investigated the intrinsic excitability by measuring the input-output (I/O) relationship before (pre), during, and after AVP application (post). We measured the steady-state frequency (SSF) by applying depolarizing pulses (1 sec in duration) of different

amplitudes (0-180 pA in 10 pA increments) and determining the average of the inverse of the inter-spike intervals (ISI) from all action potentials starting from the second action potential. We used SSF as a function of current to assess the effect of AVP on intrinsic excitability of Type I-III BNST_{DL} neurons from wild-type rats, as well as fluorescent BNST_{DL}-OTR neurons and BNST_{DL}-CRF neurons, from OTR-Cre and CRF-Cre transgenic rats, respectively.

Electrophysiological recordings from fluorescent neurons

To visualize OTR- and CRF-mCherry fluorescent neurons in brain slices from OTR-Cre and CRF-Cre rats or AVP-eYFP neurons in the hypothalamus (SON, SCN, and the PVN), we used an upright microscope (Scientifica Slice Scope Pro 1000 fitted with fluorescent filters (49008_Olympus BX2_Mounted, ET mCherry, Texas Red, ET560/40x ET630/75m T585lpxr for the visualization of mCherry and 49002 ET- EFP (FITC/Cy2) ET470/40x ET525/50m T495LPXR for the visualization of eYFP) and infrared differential interference contrast [IR-DIC] optics), with a CoolLED pE-300^{ultra}, broad-spectrum LED illumination system as the light source. We identified fluorescent neurons using the 40x objective, mCherry or eYFP filter, and a live-image video camera (IR-2000, Dage-MTI). Once these neurons were targeted and considered healthy using an IR-DIC filter, we performed the whole-cell patch-clamp recordings.

Stereotaxic surgeries and adeno-associated virus (AAV) injections

We deeply anesthetized male OTR-Cre rats (n=92), Wistar CRF-Cre rats (n=26), both at approximately 250g of body weight, +/-10 g), and AVP-Cre rats (n=83, at 220g (+/-10 g) body weight) with a mix of isoflurane (2%) and oxygen, placed them in a stereotaxic frame (Model 955, Kopf, CA) as before^{27,51}, and subcutaneously injected ketoprofen (5 mg/kg; Zoetis) for analgesia. After cleaning the rat's head with iodine solution and applying one or two drops of lidocaine (2%, Wockhardt USA, LLC, NDC60432-464-00) to anesthetize the skin, we made a small incision to gently lift the skin and expose the skull. After making two small bilateral holes into the skulls of OTR-Cre and CRF-Cre rats, we bilaterally injected a Cre-dependent adeno-associated viral vector pAAV-hSyn-DIO-hM4D(Gi)-mCherry, which was a gift from Bryan Roth (Addgene plasmid #44362; <http://n2t.net/addgene:44362>; RRID:Addgene_44362)⁵² into the BNST_{DL} (at the following coordinates from Bregma: 15° coronal angle, AP: 0.0 mm, ML: ± 3.4 mm, DV: -7.1 mm, 100 nl) using a 5-µl Hamilton syringe (Hamilton Co., Reno, Nevada) at a rate of 25 nL/min. In a separate group of male AVP-Cre rats, we injected pAAV-hSyn FLEEx-mGFP-2A-synaptophysin-mRuby (gifted by Liqun Luo (Addgene plasmid #71760; <http://n2t.net/addgene:71760>; RRID:Addgene_71760) bilaterally into the SON (n=4, from Bregma: AP -1.44, ML +/-2.07, DV -9.047, angle 0°) or SCN (n=4, AP -0.58, ML +2.015, DV -9.1, angle 12.3°). For optogenetic experiments, we injected the SON (n=28), SCN (n=30), or PVN (n=10, coordinates from Bregma: AP -1.4, ML +/-0.6 DV -7.8 angle 0°) of another cohort of male AVP-Cre rats with a Cre-

dependent AAV driving channelrhodopsin (ChR2) expression pAAV-EF1a-double floxed-hChR2(H134R)-EYFP-WPRE-HGHpA (gifted by Karl Deisseroth; Addgene plasmid #20298; <http://n2t.net/addgene:20298>; RRID:Addgene_20298; 100 nl, diluted 1:4 with sterile saline). A separate cohort of SD rats was injected bilaterally in the PVN (n=10) with the AAV driving ChR2-mCherry expression under the OT promoter (AAV-OTp-ChR2-mCherry, developed by Valery Grinevich⁵³). Coordinates were based on the rat brain atlas⁵⁴ and our prior work^{27,33,53} and adjusted based on body weight, when needed, according to the published formula⁵⁵. Syringes were left in place for 8 min after viral infusion before syringe retraction. Upon completion of surgery, we sutured the skin and applied antibiotic ointment to the incision site. Rats received another injection of ketoprofen 24-hours post-surgery and were housed for another three weeks before experiments began. Fluorescence expression in brain sections from all injected transgenic rats was analyzed prior to inclusion of the animal in the analysis for electrophysiology, neuronal tract tracing, or behavioral experiments.

Neuronal tract tracing, dual-immunofluorescence, and microscopy

Three weeks after surgeries, rats were either used for electrophysiology as above or were perfused for neuronal tract tracing. Following the electrophysiological recordings, all slices were collected, processed, and analyzed for fluorescence in the injection sites and fibers in the BNST_{DL}. In the latter case, rats received an i.p. injection of euthanasia III (Covetrus, Columbus, OH) before transcardial perfusion with cold PBS (0.05 M, pH=7.4), followed by stabilized 10% formalin solution (200-250 ml, Fisher Scientific, SF98-4). Brains were dissected, stored in 10% formalin for an hour at room temperature, and then incubated in 30% sucrose-PBS for 48 h at 4°C. Frontal 50- μ m-thick serial brain sections containing the BNST and the hypothalamus were sliced using a freezing-stage Microtome (model SM2000R, Leica Biosystems, Nussloch, Germany) and processed for immunofluorescence. Brain sections from AVP-Cre rats injected with a Cre-dependent-synaptophysin-mRuby into the SON or SCN for neuronal tract tracing and from AVP-Cre rats injected with a Cre-dependent-ChR2-eYFP (post-electrophysiology) were processed with AVP antibody (dilution 1:7500, rabbit, Millipore Sigma AB-1565) as before³³ or AVP antibody generated and kindly provided by Dr. Harold Gainer (NIH; Bethesda; USA)⁵⁶, and then visualized with goat anti-rabbit IgG Alexa 647 secondary antibody (dilution 1:500, Invitrogen A21245) or Alexa 594 secondary antibody (dilution 1:500, Invitrogen A11037), respectively. These sections were then mounted with Mowiol antifade reagent on gelatin-subbed slides (Fischer Scientific, 12-544-7). We first imaged mRuby or EYFP in AVP cell bodies in the SON or SCN and fibers in the BNST with a Nikon Eclipse fluorescent microscope and then used an Olympus FV10i confocal microscope (Fluoview FV10i confocal laser-scanning microscope, Olympus, Waltham, MA) to take high-magnification images and Z-stacks to visualize hypothalamic cell bodies and fibers in the BNST co-expressing mRuby or EYFP and AVP peptide.

The expression and distribution of OTR neurons in the BNST were determined on the brain sections from OTR-Cre rats (n=9) injected with a Cre-dependent AAV driving Gi-DREADD-mCherry into the BNST_{DL}. To determine the phenotype of OTR neurons, we used BNST sections from these rats combined with antibodies against two enzymes involved in cellular signaling in the BNST^{35,57}, which mark mutually exclusive neuronal populations in the BNST⁵⁸: striatal-enriched protein tyrosine phosphatase (STEP), using anti-STEP primary antibody (mouse, dilution 1:500, Santa Cruz sc-23892)³⁵ and protein kinase C delta (PKC δ), with anti-PKC δ primary antibody (mouse, dilution 1:1000, BD Biosciences 610398)⁵⁷. Both proteins were then visualized with goat anti-mouse IgG Alexa 488 secondary antibody (dilution 1:500, Invitrogen A11029). Confocal microscopy was used for high-resolution images and to acquire multi-Z-stack images at 60x for cell quantification.

To count OTR-, STEP-, and PKC δ -expressing neurons and neurons co-expressing OTR and STEP or OTR and PKC δ , we took z-stacks from the entire dorsal BNST (above the anterior commissure) from 3 rats, selecting the Multi Area Z-stacks Time Lapse function in the confocal Fluoview Fv10i software. Each z-stack contained 25-35 confocal planes with 1- μ m intervals with 60x magnification. Z-stacks were taken at anterior (Bregma -0.12 mm), middle (Bregma -0.24 mm), and posterior (Bregma -0.48 mm) regions of the antero-posterior axis of the BNST_{DL}. OTR-, STEP-, and PKC δ -expressing neurons were counted on the left and right hemispheres from 3 sections per rat and averaged per BNST. After image acquisition, all individual z-stacks were used to create a montage of the entire dorsal BNST using the function Multi Stack Montage, which is part of the BIOP plugin package on the ImageJ 1.53t software (Image processing and analysis in Java,⁵⁹). The final montage was used to manually count each cell type using ImageJ's cell counter, which allows to assign a number to each cell type and label them to prevent counting the same cell twice. OTR-mCherry and STEP or PKC δ co-expressing neurons were assigned three numbers, one for OTR-mCherry, one for STEP or PKC δ , and another to indicate double labeling. Every third consecutive BNST section (150 μ m intervals) from the entire brain was used for quantification.

Diagrams and graphical abstract were created using SciDraw (images/icons created by Dr. Zhe Chen, Dr. Christophe Leterrrie), Biorender (Biorender.com), Adobe Illustrator 2024, Adobe Photoshop 2024, and Microsoft PowerPoint software.

Optogenetic stimulation protocol in AVP-Cre transgenic rats

As we previously reported detailed cellular effects of exogenous OT application in the BNST_{DL}⁴⁰, we first validated the optogenetic approach in the rats injected with the AAV-OTp-ChR2-mCherry virus, generated by the Grinevich Lab³⁴ in the PVN and recorded from brain slices containing the BNST. Tetanic blue light stimulation (TLS, 10-ms single pulse at 30 Hz for 20 s, which previously successfully triggered axonal OT release in the central amygdala⁵³) evoked OT release in the BNST_{DL}

(Supplementary Fig. 1). Three weeks after Cre-dependent AAV-ChR2-eYFP was injected in the SON, PVN, or SCN, we decapitated AVP-Cre rats as above and used brain slices containing the BNST or hypothalamus for electrophysiological recordings combined with optogenetic stimulation. The slices were kept in aCSF in the dark to avoid photobleaching of the fluorescent signal and ChR2 activation. Because high frequencies of action potentials are thought to be necessary to trigger neuropeptide release, we first performed current-clamp recordings from fluorescent AVP neurons in the SON and demonstrated that 10-ms blue light pulses (BL, 470 nm) evoked action potentials in AVP SON neurons that followed frequencies up to 30 Hz applied for 20 s (**Fig. 6e**). Then, to study the effects of AVP released from terminals containing ChR2 in the BNST on the intrinsic excitability of Type I and Type III BNST_{DL} neurons, we determined the input/output (I/O) relationship in response to 80, 100, and 120pA current injections, before and after TLS. Here, we modified the optogenetic stimulation protocol to more closely mimic the physiological firing of AVP neurons in the SCN and SON^{60,61} with 10-ms single pulses at 10 Hz for 20 s. This TLS protocol was used in BNST slices from AVP-Cre rats injected with Cre-dependent AAV-ChR2 in the hypothalamus and was delivered at the recording site using whole-field illumination through a 40x water-immersion objective (Olympus, Tokyo, Japan) with a pE-300^{ultra} CoolLED illumination system (CoolLED Ltd., Andover, UK). In a subset of neurons in each experiment, to confirm peptide receptor-mediated cellular effects, we applied the OTR antagonist, OTA (as above), before TLS.

Acoustic startle response (ASR) and FPS in OTR-Cre rats

OTR-Cre rats (n=45) injected with a Cre-dependent AAV-Gi-DREADD-mCherry were used for chemogenetic inhibition of OTR neurons in the BNST_{DL} before fear conditioning (followed by FPS) and before EPM experiments (body weight 388.7±48.7 g, n=22 saline, n=21 CNO). Only rats that showed moderate to high Gi-DREADD-mCherry expression in the BNST in one or both hemispheres were considered for data analysis (n=43).

Rats were tested in Plexiglas enclosures inside sound-attenuating chambers (San Diego Instruments, Inc., CA), as described before^{27,39}. The Plexiglas enclosures were installed on top of a platform that detected movement (jump amplitude measured within a 200-ms window following the onset of the startle-eliciting noise) and transformed the velocity of the movement into a voltage output⁶² detected by SR-Lab software (Part No: 6300-0000-Q, San Diego Instruments, Inc., CA). ASR was measured during 30 trials of startle-eliciting 95-dB white noise burst (WNB) on day 1 (chamber and startle habituation) and day 2 (baseline pre-shock test). On day 3 (fear conditioning), rats received an i.p. injection of CNO (2 mg/kg) 45 min before exposure to 10 presentations of 3.7-s cue light (conditioned stimulus, CS), each co-terminating with a 0.5-s foot shock (unconditioned stimulus, US; 0.5 mA) in context A. On day 4, rats were tested for recall of cued and non-cued fear in context B, where ASR

was first measured alone (10 trials, post-shock), followed by an additional 20 trials in which ASR was measured in the presence of the cue (light+noise trials) or in the absence of the cue (noise-only trials), presented in a pseudorandom order (**Fig. 4A**). Selected environmental cues were altered in context B to distinguish it from context A: context B lacked the steel grid bars used for conditioning in context A, was cleaned with a different disinfectant (ethanol 70% instead of peroxide), and had a different experimenter performing the testing. On day 5, rats were tested for contextual fear recall, where ASR was measured with no cue presentation in the original context A. To determine the rate of fear extinction, we tested rats for cued/non-cued fear three times and contextual fear two times on alternate days, see **Supplementary Fig. 2** for FPS components.

Elevated plus maze (EPM) in OTR-Cre rats

The behavioral experiments took place in a room under a dim lighting condition. The experimental OTR-Cre rats used for the FPS test were tested on the EPM 3 days after the last FPS test. The EPM apparatus was elevated 32 inches (in) from the ground and consisted of two closed arms (width, length, height: 5 in x 20 in x 18 in), two open arms (width and length: 5 in x 20 in), and a squared center (width and length: 5 in x 5 in). Forty-five min after saline or CNO i.p. injections, we placed rats at the center of the EPM and allowed them to explore for 5 min. We measured total entries and time spent in the open arms, closed arms, and at the center using ANY-Maze 6.34 software (Stoelting, Wood Dale, IL) and quantified time spent freezing in each of these compartments.

Functional verification of Gi-DREADD with *in vitro* whole-cell patch-clamp electrophysiology

The whole-cell patch recordings were performed as above⁴⁰ on 300- μ m-thick brain slices containing the BNST from 5 AAV-injected OTR-Cre male rats. To confirm that OTR-BNST_{DL} neurons expressing Gi-DREADD-mCherry were functionally inhibited by CNO, we depolarized neurons to action potential threshold and recorded spontaneous activity for 5 min before bath application of CNO (20 μ M), for 7 min during CNO application, and for 12 min during washout (**Fig. 4B**).

Breeding protocols and genotyping

Rats were bred at 11-15 weeks of age by pairing Cre^{+/-} male or female rats with wild-type SD (for OTR-Cre and AVP-Cre) or Wistar (for CRF-Cre) rats, such that all offspring were heterozygous for Cre. Wild-type breeders were purchased from Envigo, as above, from diverse litters to keep the Cre lines outbred. Pairs were together for approximately 10-14 days or until females showed signs of pregnancy and then individually housed. Rats were genotyped at weaning (postnatal day 21) for the presence of Cre. During weaning, males and females were separated and ear tagged (Braintree Scientific, Inc. 1005-1LZ). For tagging, we lightly exposed rats to the inhalant isoflurane and used an

ear punch (Braintree Scientific, Inc. EP-S-902) to create a 2-mm hole for tag insertion. Ear tissue was stored in 0.2-ml 8-strip PCR tubes (GeneMate, VWR, 490003-710) labeled with the animals corresponding ID number at -20°C.

For genotyping, we added 50 µl of a lysis buffer (2.5 ml 1M Tris, pH 8.8, 100 µl 0.5M EDTApH8.0, 250ul Tween 20, 1.0 ml) with proteinase K (20 mg added to 1.0 ml 50 nM Tris-HCLpH8.0, 10mM CaCl₂ 15 µl) to each tube of tissue and placed tubes in a Thermo Cycler at 95°C overnight. The next day, we vortexed the tubes slightly and returned them to the Thermo Cycler for another 10 min at 100°C to denature the proteinase K. We then centrifuged the samples for 10 min at 6000 rpm and collected the supernatant for use with the PCR mix. The primers used were specific for the Cre-sequence within the DNA, amplifying only the DNA of Cre⁺ animals with the following sequence (5' → 3') for OTR-Cre and AVP-Cre: Cre 3 (forward) TCGCTGCATTACCGGTCGATGC (22 bp), and Cre 4 (reverse) CCATGAGTGAACGAACCTGGTCG (23 bp), and for CRF-Cre: SG13 (forward) GCATTACCGGTCGATGCAACGAGTGATGAG, and SG14 (reverse) GAGTGAACGAACCTGGTCGAAATCAGTGCG (all from ThermoFisher Scientific), as before ⁴¹. The PCR-mix was composed of the extracted DNA, primers, KAPA2G Fast HS Master Mix (Kapa Biosystems, Inc, KK5621), Ultrapure BSA (Invitrogen, AM2616) and nuclease free H₂O. The PCR-Mix and protocol used for the thermal cycler is below. The PCR samples were loaded on a 2.0% agarose gel (VWR, 0710) made in 1X TAE buffer (VWR, 82021-492) with 50 µl ethidium bromide (0.625 mg/ml, VWR, E406,) in an electrophoresis chamber containing 1X TAE buffer at 80 V for 90 min. A 10-Kb DNA ladder (BioLabs, Inc., N3270S) was run in parallel to verify the size of the amplified DNA fragment.

Statistical analysis

Electrophysiological data are presented as mean ± standard error of mean (SEM). The distribution of data sets was first evaluated with Kolmogorov-Smirnov test. When normal distribution was observed, the effects of AVP and other drugs on membrane properties were analyzed by a repeated measures (RM) one-way analysis of variance (ANOVA) or mixed-effects model, when applicable. The effects of AVP (and other pharmacological manipulations) on intrinsic excitability and firing frequency were analyzed with RM two-way ANOVA with treatment and current as factors. Where the F-ratio was significant, all-pairwise post hoc comparisons were made using Tukey's or Sidak's tests.

Behavioral data are presented as violin plots depicting the median and the 25th and 75th quartiles. FPS data were analyzed by a two-way RM ANOVA with the factors trial type (pre-shock, post-shock, noise-only, light+noise) and treatment (saline vs. CNO). When F-ratio was significant, all *post hoc* analyses were compared using Sidak's multiple comparison test. For analyses of the effect of treatment on cued, non-cued, and contextual fear, data are presented as percentage change scores

of ASR and were analyzed with un-paired *t*-tests. The percentage change of ASR was analyzed according to the following formulas:

Cued fear = (Light Noise – Noise alone) / Noise alone) x 100% in context B

Non-cued fear = (Noise alone – Post shock) / Post shock) x 100% in context B

Contextual fear = (Post shock – Pre shock) / Pre shock) x 100% in context A

Shock reactivity for each individual rat was calculated as the average startle amplitude during each of the 10 foot-shock presentations during fear conditioning (no WNB present) and was analyzed with un-paired *t*-tests, See **Supplementary Fig. 2** for the FPS components.

EPM data are presented as the total number of entries and percentage of time spent in each compartment. Total time freezing in each compartment is expressed in seconds. Comparisons between saline and CNO groups were analyzed for each parameter with an un-paired *t*-test.

All statistical analyses were completed using GraphPad Prism version 10.2.1 (339) (GraphPad Software, Inc., San Diego, CA). *P* < 0.05 was considered significant.

3. Results

3.1. AVP excites Type I BNST_{DL} neurons via OTR and not V1R transmission

3.1.1. The effects of AVP, OT, OTR and V1R antagonists and agonists on intrinsic membrane properties of Type I-III BNST_{DL} neurons are shown in **Table 1** and described in detail in the *Supplementary Results*.

3.1.2. The effect of AVP on intrinsic excitability of Type I BNST_{DL} neurons

To assess the effect of AVP on the intrinsic excitability of Type I BNST_{DL} neurons, we measured steady state firing frequency (SSF) as a function of current (input/output, I/O, relationship) before (pre), during, and after AVP application (washout, post). There was a significant incremental current effect on the action potential frequency (*P*=0.0002, *F*(1.267,10.14)=29.52) and a significant treatment effect, with AVP inducing a leftward shift of the I/O relationship, without affecting its slope (*P*=0.0137, *F*(1.201, 9.611)=8.415). There was no interaction between current and treatment (*P*=0.9013, *F*(1.862,11.55)=0.09175, *n*=9, mixed-effect analysis). *Post hoc* test showed a significant AVP effect on SSF at (in pA) 50 (*P*=0.0298), 60 (*P*=0.0274), 70 (*P*=0.0255), and 80 (*P*=0.0181, vs. pre). The change

in SSF induced by AVP completely recovered during washout for all currents injected (in pA): 50 ($P=0.1187$), 60 ($P=0.2704$), 70 ($P=0.2469$), and 80 ($P=0.2121$, pre vs. post), **Fig. 1A-A'**

When the OTR antagonist, OTA, was applied before AVP, there was a significant current effect on action potential frequency ($P<0.0001$, $F(1.341, 10.73)=59.21$, $n=9$, mixed-effects model) but no treatment effect ($P=0.0574$, $F(1.466, 11.73)=3.999$) and no interaction between current and treatment ($P=0.1642$, $F(1.688, 8.440)=2.281$), **Fig. 1B-B'**

In the presence of the V1aR antagonist, SR49059, there was a significant current effect on action potential frequency ($P<0.0001$, $F(1.312, 10.49)=52.74$, $n=9$, mixed-effect analysis), and AVP in a presence of SR49059 significantly changed the I/O relationship ($P=0.0002$, $F(1.886, 15.09)=16.29$), with no interaction between current and treatment ($P=0.1137$, $F(1.708, 7.075)=3.065$). Multiple comparisons showed an excitatory effect of AVP vs. pre at (pA) 40 ($P=0.0355$), 50 ($P=0.0180$), 60 ($P=0.0189$), 70 ($P=0.0009$), 80 ($P=0.0014$), 90 ($P=0.0092$), 100 ($P=0.0035$), 110 ($P=0.0032$), 120 ($P=0.0070$), 130 ($P=0.0111$), 140 ($P=0.0069$), 150 ($P=0.0052$), 160 ($P=0.0060$), 170 ($P=0.0067$), and 180 ($P=0.0021$). Notably, although SR49059 did not block the AVP effect, it showed an excitatory effect on its own vs. pre at (pA) 70 ($P=0.0323$), 80 ($P=0.0221$), 90 ($P=0.0370$), 100 ($P=0.0328$), 110 ($P=0.0328$), 120 ($P=0.0376$), 150 ($P=0.0397$), 160 ($P=0.0432$), 170 ($P=0.0493$), and 180 ($P=0.0374$), **Fig. 1C-C'**

When the V1bR antagonist, Nelivaptan, was applied before AVP, there was a significant current effect on action potential frequency ($P<0.0001$, $F(2.294, 20.65) = 117.9$, $n=10$, mixed-effects analysis). Meanwhile, contrary to OTA, AVP in the presence of Nelivaptan significantly shifted the I/O relationship ($P<0.0001$, $F(1.651, 14.86)=42.15$), but with no interaction with the current ($P=0.4980$, $F(1.027, 5.475)=0.5382$). Multiple comparisons showed a significant excitatory effect of AVP on SSF at (in pA) 30 ($P=0.0175$), 40 ($P=0.0282$), 50 ($P=0.0184$), 60 ($P=0.0042$), 70 ($P=0.0017$), 80 ($P=0.0034$), 90 ($P=0.0050$), 100 ($P=0.0155$), 110 ($P=0.0159$), 120 ($P=0.0048$), 130 ($P=0.0103$), 140 ($P=0.0083$), 150 ($P=0.0268$), and 160 ($P=0.0256$) but not at 170 ($P=0.2845$) or 180 ($P=0.2847$). Nelivaptan alone had no effect on the SSF at any of the currents injected ($P>0.05$) except at 140pA ($P=0.0474$), **Fig. 1D-D'**

3.2. AVP does not affect excitability of Type II BNST_{DL} neurons

3.2.1. The effect of AVP on the intrinsic excitability of Type II BNST_{DL} neurons

Mixed-effect analysis showed a significant incremental effect of currents injected on evoked action potential frequency in Type II BNST_{DL} neurons ($P<0.0001$, $F(1.256, 8.789)=79.04$, $n=8$, mixed-effect analysis). However, AVP did not show a significant effect on SSF ($P=0.1749$, $F(1.173, 8.210)=2.211$),

and there was no interaction between current and treatment ($P=0.3589$, $F(1.414, 8.200)=1.074$, $n=8$, mixed-effect analysis), **not shown**.

3.3. AVP excites Type III BNST_{DL} neurons via OTR

3.3.1. The effect of OTR and V1R activation on intrinsic excitability of Type III BNST_{DL} neurons

3.3.1.1. The effect of AVP on intrinsic excitability of Type III BNST_{DL} neurons

Next, we examined the effect of AVP on the intrinsic excitability of Type III neurons by measuring the SSF. There was a significant incremental current effect on action potential frequency ($P=0.0036$, $F(0.5547, 5.547)=29.81$, $n=11$, mixed-effect analysis), and AVP induced a leftward shift of the I/O relationship, without affecting its slope ($P=0.0007$, $F(0.9966, 9.966)=23.05$). There was no interaction between current and treatment ($P=0.3127$, $F(1.669, 5.463)=1.410$). *Post-hoc* analysis showed a significant AVP effect (in pA) at 70 ($P=0.0209$), 80 ($P=0.0283$), 90 ($P=0.0076$), 100 ($P=0.0116$), 110 ($P=0.0319$), 120 ($P=0.0226$), 130 ($P=0.0453$), 140 ($P=0.0174$), 150 ($P=0.0487$), 160 ($P=0.0099$), and 170 ($P=0.0486$, pre vs. AVP) and trending at 180 ($P=0.0584$). The leftward shift of the I/O relationship in Type III neurons recovered during washout of AVP for all currents injected (in pA): 70 ($P=0.8664$), 80 ($P=0.7177$), 90 ($P=0.2824$), 100 ($P=0.6043$), 110 ($P=0.7137$), 120 ($P=0.8965$), 130 ($P=0.9965$), 140 ($P=0.9635$), 150 ($P=0.1017$), 160 ($P=0.7445$), 170 ($P=0.9206$), and 180 ($P=0.9845$, pre vs. post), **Fig. 1E-E'**

In the presence of the OTR antagonist, OTA, there was a significant incremental current effect ($P<0.0001$, $F(1.877, 15.01)=61.34$, $n=9$, mixed-effect analysis) but no treatment effect of AVP on the I/O relationship ($P=0.3949$, $F(1.419, 11.35)=0.9149$, $n=9$). There was no interaction between current and treatment ($P=0.3986$, $F(0.6373, 1.880)=0.8231$), **Fig. 1F-F'**

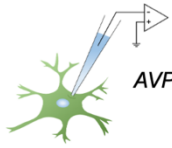
In contrast, in the presence of the V1aR antagonist, SR49059, there was a significant current effect on action potential frequency ($P=0.0003$, $F(0.9437, 5.662)=62.36$, $n=7$, mixed-effect analysis), and AVP application significantly changed the I/O relationship ($P=0.0184$, $F(1.166, 6.997)=8.869$). However, there was no interaction between current and treatment ($P=0.3410$, $F(1.224, 4.841)=1.202$). Multiple comparisons showed an excitatory effect of AVP on SSF at (in pA) 90 ($P=0.0429$), 120 ($P=0.0298$), 130 ($P=0.0311$), 140 ($P=0.0152$), 150 ($P=0.0135$), 160 ($P=0.0236$), 170 ($P=0.0277$), and 180 ($P=0.0270$, pre vs. SR49059+AVP). The effects of AVP were not significant at (in pA) 70 ($P=0.1359$), 80 ($P=0.2954$), 100 ($P=0.1874$), or 110 ($P=0.1720$). Application of SR49059 alone did not have an effect on the SSF at any of the currents injected ($P>0.05$), **Fig. 1G-G'**

When the V1bR antagonist, Nelivaptan, was applied before AVP, there was a significant current effect on action potential frequency ($P < 0.0001$, $F(2.294, 20.65) = 5117.9$, $n = 10$, mixed-effect analysis). Meanwhile, contrary to OTA, AVP in the presence of Nelivaptan significantly shifted the I/O relationship ($P < 0.0001$, $F(1.651, 14.86) = 42.15$, $n = 10$), with no interaction with the current ($P = 0.4980$, $F(1.027, 5.475) = 0.5382$, $n = 10$). Multiple comparisons showed a significant excitatory effect of AVP on SSF at (in pA) 30 ($P = 0.0175$), 40 ($P = 0.0282$), 50 ($P = 0.0184$), 60 ($P = 0.0042$), 70 ($P = 0.0017$), 80 ($P = 0.0034$), 90 ($P = 0.0050$), 100 ($P = 0.0155$), 110 ($P = 0.0159$), 120 ($P = 0.0048$), 130 ($P = 0.0103$), 140 ($P = 0.0083$), 150 ($P = 0.0268$), and 160 ($P = 0.0256$). There was no significant effect at 170 ($P = 0.2845$) or 180 pA ($P = 0.2847$). Nelivaptan alone had a significant effect on SSF at 130 pA ($P = 0.0474$) but not at any of the other currents injected ($P > 0.05$), **Fig. 1H-H'**

Application of AVP in the presence of the V1aR/OTR antagonist showed a significant increase in action potential frequency as the current injected increased ($P < 0.0001$, $F(1.543, 10.80) = 55.46$, $n = 8$, mixed-effect analysis); however, AVP did not change the I/O relationship ($P = 0.2742$, $F(0.6225, 4.358) = 1.293$), suggesting that blocking V1aR and OTR completely abolished the excitatory effects of AVP in Type III neurons, **Fig. 2A**.

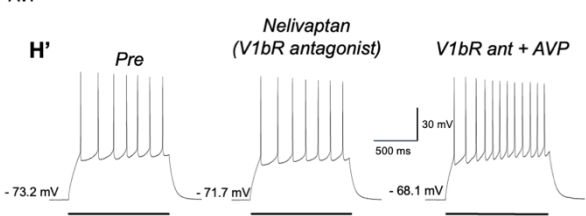
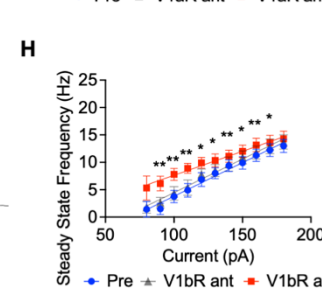
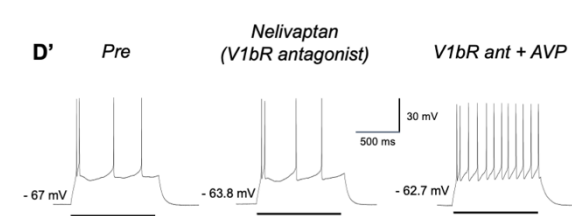
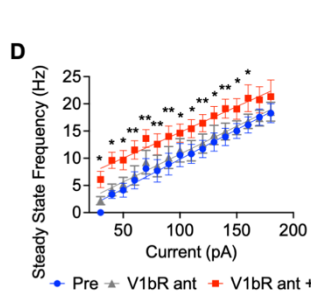
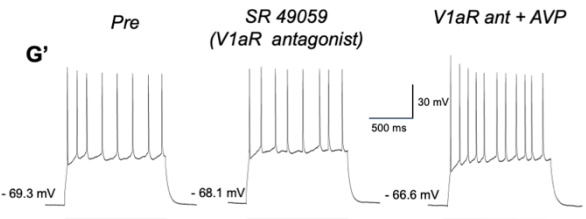
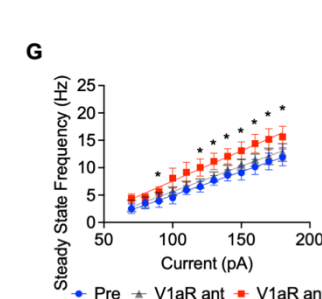
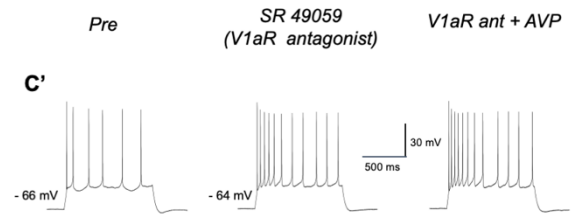
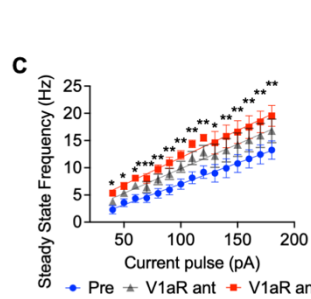
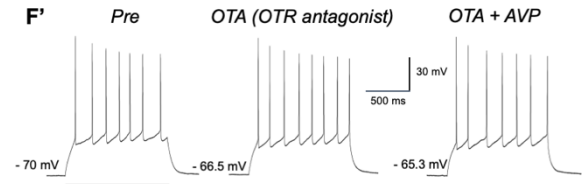
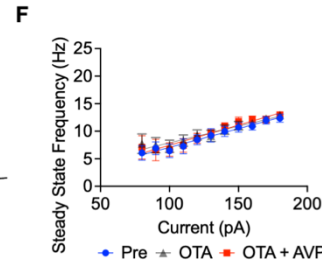
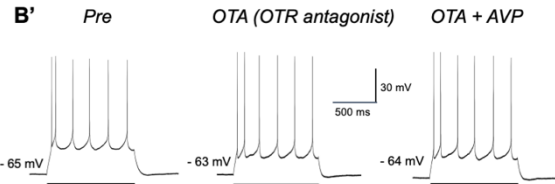
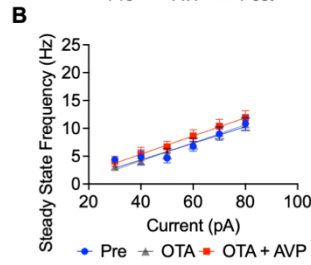
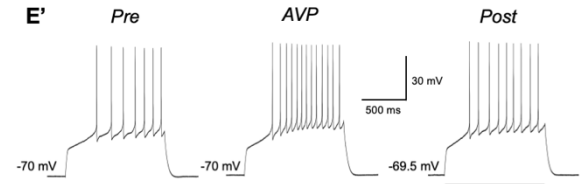
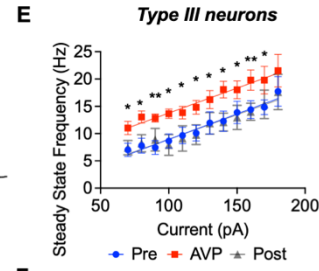
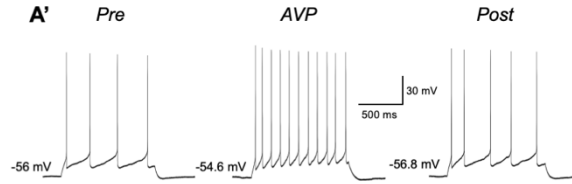
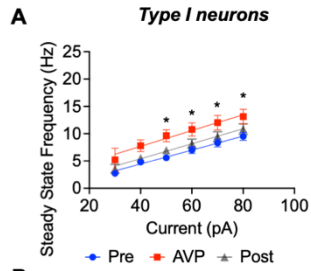
Figure 1. Arginine-vasopressin (AVP) increases intrinsic excitability of Type I and Type III BNST_{DL} neurons, which requires OTR, but not V1aR or V1bR transmission. Steady state firing frequency (SSF) as a function of current (input/output, I/O) is shown before (pre), during, and after AVP application (washout, post). **A)** In Type I neurons, there was a significant treatment effect, with AVP inducing a leftward shift of the I/O relationship, without affecting its slope ($P=0.0137$, $n=11$, mixed-effect analysis). *Post hoc* test showed a significant AVP effect on SSF in most currents injected. **A')** Representative traces of Type I BNST neuron responses to a depolarizing current pulse injection of 40 pA for 1 sec before (Pre), during (AVP) and after AVP (Post). **B)** Application of OTR antagonist, OTA, blocked the excitatory effect of AVP in Type I neurons ($P=0.0574$, $F(1.466, 11.73)=3.999$, $n=9$, mixed-effects model). **B')** Representative traces of Type I neuron responses to a depolarizing current pulse injection of 60 pA for 1 sec before, during OTA alone, and during OTA+AVP. **C)** In the presence of the V1aR antagonist, SR49059, AVP application significantly changed the I/O relationship ($P=0.0009$, $n=7$, mixed-effect analysis). Multiple comparisons showed an excitatory effect of AVP at all currents injected except 40 pA ($P=0.0792$). The SR49059 showed an excitatory effect on its own at (pA) 80 ($P=0.0432$) and 100 ($P=0.0496$). **C')** Representative traces of Type I neuron responses to a depolarizing current pulse injection of 100 pA for 1 sec, before, during SR49059 alone, and during SR49059+AVP. **D)** In a presence of V1bR antagonist, Nelivaptan, AVP significantly shifted the I/O relationship ($P<0.0001$, $n=10$, mixed-effect analysis). Multiple comparisons showed an excitatory effect of AVP on SSF at all current injected except 170 ($P=0.2845$) or 180 pA ($P=0.2847$). Nelivaptan alone had no effect on the SSF at any of the currents injected except at 140 pA ($P=0.0474$). **D')** Representative traces of Type I neuron responses to a depolarizing current pulse injection of 80 pA for 1 sec before, during Nelivaptan alone and Nelivaptan+AVP. **E)** In Type III neurons, AVP induced a leftward shift of the I/O relationship, without affecting its slope ($P=0.0007$, $n=11$, mixed-effect analysis), with a significant AVP effect in all currents injected except 180 ($P=0.0584$). The leftward shift of the I/O relationship in Type III neurons recovered during washout of AVP for all currents injected. **E')** Representative traces of Type III neuron responses to a depolarizing current pulse injection of 140 pA before, during (AVP) and after AVP (Post). **F)** In the presence of OTR antagonist, OTA, there was no treatment effect of AVP on the I/O relationship ($P=0.3949$, $n=9$, mixed-effect analysis). **F')** Representative traces of Type III neuron response to a depolarizing current pulse injection of 100 pA for 1 sec, before, during OTA alone, and during OTA+AVP. **G)** In the presence of the V1aR antagonist, SR49059, AVP application significantly changed the I/O relationship ($P=0.0068$, $n=7$, mixed-effect analysis). Multiple comparisons showed an excitatory effect of AVP on SSF at most current injected except (in pA) at 70 ($P=0.1359$), 80 ($P=0.2954$), 100 ($P=0.1874$), and 110 ($P=0.1720$). Application of SR49059 alone did not have an effect on the SSF at any of the currents injected. **G')** Representative traces of Type III neuron response to a depolarizing current pulse injection of 140 pA for 1 sec, before, during SR49059, and during SR49059+AVP. **H)** When the V1bR antagonist, Nelivaptan, was applied before AVP, AVP significantly shifted the I/O relationship

($P < 0.0001$, $n = 10$, mixed-effect analysis). Multiple comparisons showed a significant excitatory effect of AVP on SSF at most currents injected except 170 ($P = 0.2845$) and 180 pA ($P = 0.2847$). H') Representative traces of Type III neuron responses to a depolarizing current pulse injection of 110 pA for 1 sec, before, during Nelivaptan alone and during Nelivaptan+AVP. * $P < 0.05$, ** $P < 0.01$, *** $P < 0.001$ vs. pre



AVP excites Type I $BNST_{DL}$ neurons, which requires OTR, but not V1aR or V1bR

AVP excites Type III $BNST_{DL}$ neurons, which requires OTR, but not V1aR or V1bR



3.3.1.2. The effect of OT on intrinsic excitability of Type III BNST_{DL} neurons

In Type III neurons, there was a significant incremental current effect on action potential frequency ($P < 0.0001$, $F(1.323, 9.261) = 86.87$, $n = 8$, mixed-effect analysis), and OT induced a leftward shift of the I/O relationship ($P = 0.0077$, $F(1.826, 12.79) = 7.565$). There was no interaction between current and treatment ($P = 0.1023$, $F(1.004, 4.921) = 4.015$). *Post-hoc* analysis showed a significant OT effect (in pA) at 90 ($P = 0.0436$), 100 ($P = 0.0218$), 110 ($P = 0.0392$), 120 ($P = 0.0026$), 130 ($P = 0.0043$), 140 ($P = 0.0088$), 150 ($P = 0.0284$), 160 ($P = 0.0204$), and 170 ($P = 0.0449$). The effects of OT were not significant at (in pA) 80 ($P = 0.3822$) or 180 ($P = 0.2500$), **Fig. 2B**.

3.3.1.3. The effect of OTR agonist, TGOT, on intrinsic excitability of Type III BNST_{DL} neurons

In the presence of TGOT, there was an incremental current effect on action potential frequency ($P = 0.0003$, $F(1.421, 9.944) = 24.05$, $n = 8$, mixed-effect analysis). TGOT induced a significant effect on I/O relationship ($P = 0.0196$, $F(0.8587, 6.011) = 10.48$) with no significant interaction between current and treatment ($P = 0.1344$, $F(2.149, 4.004) = 3.443$). TGOT had a significant excitatory effect at (in pA) 70 ($P = 0.0022$), 80 ($P = 0.0001$), 90 ($P = 0.0350$), 100 ($P = 0.0272$), and 110 ($P = 0.0394$, pre vs. TGOT) and trending at 120 ($P = 0.0673$). These effects were fully reversed with washout at (in pA) 70 ($P = 0.1571$), 80 ($P = 0.1040$), 90 ($P = 0.1552$), 100 ($P = 0.1417$), and 110 ($P = 0.1115$, pre vs. post). The effect of TGOT was not significant at (in pA) 130 ($P = 0.2214$), 140 ($P = 0.2410$), 150 ($P = 0.2090$), 160 ($P = 0.2856$), 170 ($P = 0.1750$), or 180 ($P = 0.1778$), **Fig. 2C-C'**.

3.3.1.4. The effect of V1aR agonist, FE201874, on intrinsic excitability of Type III BNST_{DL} neurons

When FE201874 was tested as a specific agonist of V1aR, mixed-effect analysis revealed a significant effect of current injected on action potential frequency ($P < 0.0001$, $F(1.809, 16.28) = 60.13$, $n = 10$). In addition, FE201874 induced a significant effect on the I/O relationship ($P = 0.0117$, $F(1.283, 11.54) = 8.023$), with no significant interaction between current and treatment ($P = 0.1567$, $F(1.967, 6.230) = 2.535$). Multiple comparison showed a significant effect of FE201874 on SSF at (in pA) 90 ($P = 0.0451$), 100 ($P = 0.0392$), 110 ($P = 0.0287$), 130 ($P = 0.0455$), 170 ($P = 0.0381$), and 180 ($P = 0.0327$) and trends at 140 ($P = 0.0618$) and 150 ($P = 0.0684$). These effects of FE201874 were reversed at all of these currents injected ($P = 0.8557$, $P = 0.9721$, $P = 0.1264$, $P = 0.2114$, $P = 0.1975$, $P = 0.1807$, respectively, pre vs. post), **Fig. 2D-D'**.

3.3.1.5. The effect of V1bR agonist, d[Cha4]-AVP, on intrinsic excitability of Type III BNST_{DL} neurons

In the presence of V1bR agonist, there was an incremental current effect on action potential frequency ($P < 0.0001$, $F(1.123, 7.859) = 34.12$, $n = 8$, mixed-effect analysis), but V1bR agonist did not induce a

significant effect on I/O relationship ($P=0.5334$, $F(0.2668, 1.867)=0.02568$) with no significant interaction between current and treatment ($P=0.2199$, $F(0.4503, 1.551)=2.697$), **Fig. 2E**.

3.4. AVP excites Type III/CRF and Type III/OTR neurons from transgenic rats

3.4.1. AVP excites Type III/OTR neurons from OTR-Cre rats

Here, we tested the effect of AVP on fluorescent OTR neuron intrinsic excitability (measured as SSF) in slices obtained from male OTR-Cre rats injected with Cre-dependent AAV driving mCherry expression in the BNST_{DL}. First, fluorescent OTR-mCherry neurons were characterized as Type I-III neurons based on their electrophysiological properties. We recorded from a total of 45 OTR-mCherry neurons, from which 7 (15.6%) were characterized as Type I, 3 (6.7%) as Type II, and 35 (77.8%) as Type III neurons (**Fig. 2G-H, 2J**). In Type III/OTR fluorescent neurons, mixed-effect analysis revealed a significant current effect on action potential frequency ($P<0.0001$, $F(0.9525, 8.573)=59.68$). Notably, AVP showed a significant incremental effect on SSF ($P<0.0001$, $F(1.267, 11.40)=31.89$, $n=10$, mixed-effect analysis). There was also a significant interaction between current and treatment ($P=0.0168$, $F(2.795, 9.364)=5.850$). Multiple comparisons showed a significant incremental effect of AVP respective to baseline (pre) at (in pA) 80 ($P=0.0130$) and 90 ($P=0.0251$), trends at 100 ($P=0.0678$) and 110 ($P=0.0763$), and a significant effect at 120 ($P=0.0240$), 130 ($P=0.0140$), 140 ($P=0.0077$), 150 ($P=0.0040$), 160 ($P=0.0032$), 170 ($P=0.0036$), and 180 ($P=0.0044$). The effect of AVP in Type III/OTR neurons was reversed during the washout of AVP at (in pA) 80 ($P=0.2158$, pre vs. post), 90 ($P=0.2818$), 100 ($P=0.1373$), 110 ($P=0.3799$), 120 ($P=0.1994$), and 140 ($P=0.0863$), as multiple comparison showed no significant difference from baseline, but was not reversed at 130 ($P=0.0445$), 150 ($P=0.0500$), 160 ($P=0.0450$), 170 ($P=0.0445$), or 180 ($P=0.0294$), **Fig. 2I-I'**.

3.4.2. AVP excites Type III/CRF neurons from CRF-Cre rats

Previous studies have shown that the majority of electrophysiologically defined Type III neurons of the BNST_{DL} express mRNA for CRF at a single-cell level^{35,36}. Therefore, we tested the effect of AVP on the intrinsic excitability, measured as SSF, of fluorescent CRF neurons recorded in slices obtained from male CRF-Cre rats injected with a Cre-dependent AAV driving mCherry expression in the BNST_{DL}. The great majority of recorded fluorescent CRF-mCherry neurons ($n=26$) were characterized as Type III neurons ($n=21$, 80.8%), whereas $n=2$ were classified as Type II (7.7%), and $n=3$ as Type I (11.5%), **Fig. 2K, 2N**. In Type III/CRF neurons, there was a significant effect of current injected on evoked action potential frequency ($P=0.0475$, $F(1.216, 7.293)=5.387$, $n=7$). AVP showed a significant incremental effect on SSF ($P=0.0057$, $F(1.392, 8.351)=11.82$, $n=7$, mixed-effect analysis), and there was a trend in the interaction between current injected and treatment ($P=0.0573$, $F(1.511, 3.399)=7.655$). Multiple comparisons showed a significant effect of AVP at (in pA) 100 ($P=0.0119$), 110 ($P=0.0384$), 120

($P=0.0189$), 130 ($P=0.0235$), 140 ($P=0.0489$), and 150 ($P=0.0425$, pre vs. AVP). The effect of AVP was not fully reversed during washout at (in pA) 100 ($P=0.0118$, pre vs. post), 110 ($P=0.0100$), 120 ($P=0.0443$), 130 ($P=0.0490$), 140 ($P=0.0007$), or 150 ($P=0.0049$), **Fig. 2L-L'**.

3.4.3. TGOT excites CRF/Type III neurons from CRF-Cre rats

In Type III/CRF neurons, there was a significant effect of current injected on evoked action potential frequency ($P=0.0003$, $F(1.723, 10.34)=21.78$), and TGOT induced a significant incremental effect on SSF ($P=0.0167$, $F(1.647, 9.882)=6.823$, $n=7$, mixed-effect analysis). There was a trend in the interaction between current and treatment ($P=0.0583$, $F(1.669, 6.585)=4.686$). However, multiple comparisons showed that the effect of TGOT was not significant (pre) at (in pA) 90 ($P=0.8131$), 100 ($P=0.4264$), 110 ($P=0.2600$), 120 ($P=0.1737$), 130 ($P=0.1953$), 160 ($P=0.2262$), 170 ($P=0.2477$), or 180 ($P=0.2170$) and was trending at 140 ($P=0.0790$) and 150 ($P=0.0884$). Although six (out of 7) CRF neurons showed a clear increase, one neuron recorded showed reduced excitability after AVP administration. Removing this neuron resulted in a significant current effect on the action potential frequency ($P=0.0016$, $F(1.475, 7.373)=19.85$, $n=6$), a significant treatment effect ($P=0.0227$, $F(1.214, 6.069)=8.661$), and a trend in the interaction ($P=0.0729$, $F(1.232, 3.627)=6.151$). Multiple comparisons showed a significant effect of AVP at (in pA): 140 ($P=0.0463$), 150 ($P=0.0370$), and trends at 130 ($P=0.0807$), 160 ($P=0.0978$), and 170 ($P=0.0867$), **Fig. 2O-O'**.

3.5. The BNST_{DL} contains numerous OTR neurons, which co-express STEP or PKC δ

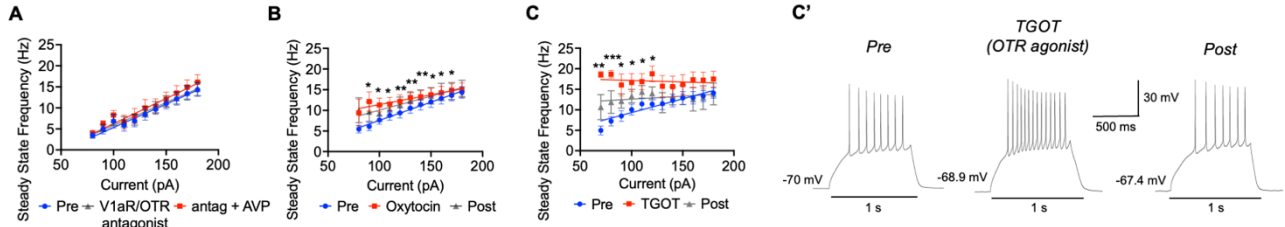
A Numerous OTR-mCherry cell bodies and spiny dendrites were localized in the anterior (bregma 0.20 to -0.00 mm, **Fig. 3b-c**), middle (bregma -0.26 to -0.35 mm, **Fig. 3d-e**), and posterior (bregma -0.60 mm, **Fig. 3f**) subdivisions of the BNST. The majority of the OTR neurons were located in the BNST_{DL}, primarily clustered in the oval nucleus of the BNST_{DL} (BNST_{ov}, Bregma 0.00 mm to -0.35 mm, **Fig. 3c-e**), whereas fewer OTR neurons were found in the anteromedial BNST (BNST_{AM}, **Fig. 3b-e**). In posterior BNST sections, OTR neurons were found in lateral division, posterior BNST (BNST_{LP}), lateral division, intermediate posterior BNST (BNST_{LI}), and to a lesser extent in medial, posterolateral BNST (BNST_{MPL}, **Fig. 3f**). Double-immunofluorescence analysis of confocal images from the BNST_{DL} showed that $16.91\pm 4.41\%$ of OTR-mCherry neurons co-expressed PKC δ (**Fig. 3k**), whereas only $7.87\pm 1.08\%$ of all PKC δ neurons co-expressed OTR-mCherry (**Fig. 3l**). Double-immunofluorescence toward STEP showed that $18.23\pm 2.05\%$ of all OTR-mCherry neurons co-expressed STEP (**Fig. 3p**), whereas $20.22\pm 2.51\%$ of all STEP neurons co-expressed OTR-mCherry (**Fig. 3r**). These results suggest that while OTR neurons constitute a diverse population of BNST_{DL} neurons, STEP is the most reliable marker of OTR-BNST_{DL} neurons identified so far.

Figure 2. *Activation of OTR robustly excites OTR and CRF-expressing Type III BNST_{DL} neurons, whereas activation of V1aR, but not V1bR, has a modest excitatory effect on Type III BNST_{DL} neurons.*

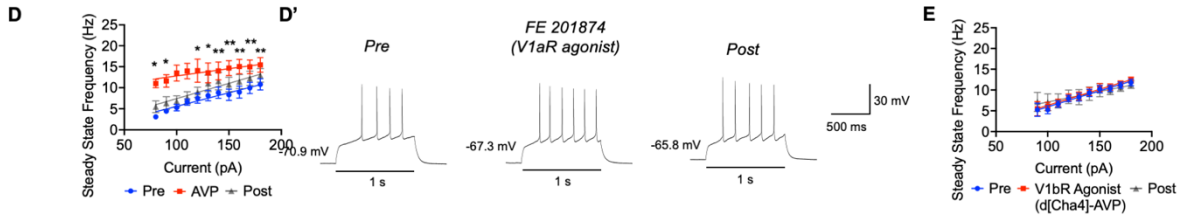
A) In Type III neurons from wild-type Sprague-Dawley rats, application of AVP in the presence of the V1aR/OTR antagonist ((d(CH₂)₅¹, Tyr(Me)², Arg⁸)-vasopressin) did not change the I/O relationship ($P=0.2742$, $n=8$, mixed-effect analysis). **B)** In Type III neurons, application of endogenous OTR agonist oxytocin (OT) induced a leftward shift of the I/O relationship ($P=0.0077$, $n=8$), with significant OT effect on SSF in most currents injected except at 80pA ($P=0.3822$) and 180pA ($P=0.2500$). **C)** Selective and potent OTR agonist ([Thr⁴, Gly⁷]-oxytocin (TGOT) affected the I/O relationship ($P=0.0196$, $n=8$) with significant excitatory effect in the first part of the curve from 70pA to 110pA and trending at 120 ($P=0.0673$). These effects were fully reversed with washout. **C')** Examples of evoked responses of a Type III neuron to a depolarizing pulse of 90 pA for 1 sec before, during, and after TGOT application. **D)** Selective V1aR agonist, FE201874, induced an excitatory effect on the I/O relationship ($P=0.0117$, $n=10$), with significant effects on SSF as shown, which were fully reversed at washout. **D')** Examples of evoked responses of a Type III neuron to a depolarizing pulse of 90pA for 1 sec before, during, and after FE201874 application. **E)** Selective V1bR agonist, d[Cha4]-AVP did not induce a significant effect on I/O relationship ($P=0.5334$, $n=8$), * $P<0.05$, ** $P<0.01$, *** $P<0.001$ vs. pre. **F)** Nissl (left) and anatomical annotations (right) from the Allen Mouse Brain Atlas and Allen Reference Atlas - Mouse Brain ¹¹⁴. High somatodendritic OTR-mCherry expression in the BNST_{DL} after male OTR-Cre transgenic rats were injected with a Cre-dependent AAV-DREADDs-mCherry in the BNST_{DL}. **G)** Example of evoked responses of a Type I/OTR mCherry fluorescent neuron and **H)** Type III/OTR mCherry neuron to a hyperpolarizing and depolarizing current pulses of 1 sec. **I)** In Type III/OTR fluorescent neurons, mixed-effect analysis revealed a significant incremental effect of AVP on SSF ($P<0.0001$, $n=10$), with a significant excitatory effect of AVP on SSF at most current injected except a trend at 100 pA ($P=0.0678$) and 110 pA ($P=0.0763$). **I')** Representative trace of Type III/OTR fluorescent neuron responses to a depolarizing current pulse injection of 130 pA for 1 sec, before, during and after AVP application. **J)** Fluorescent OTR-BNST_{DL}-mCherry neurons were characterized as Type I-III neurons based on their electrophysiological properties, with majority 35/45 (77.8%) characterized as Type III, 7/45 (15.6%) as Type I, and 3/45 (6.7%) as Type II. **K)** The great majority of recorded fluorescent CRF-BNST_{DL}-mCherry neurons (21/26) were characterized as Type III (80.8%), whereas 2/26 as Type II (7.7%), and 3/26 as Type I (11.5%). **L)** In Type III/CRF neurons from CRF-Cre transgenic rats, there was a significant incremental effect of AVP on SSF ($P=0.0057$, $n=7$), with multiple comparisons showed a significant effect of AVP at all current injected except at 90 pA ($P=0.2288$). **L')** Representative traces of Type III/CRF fluorescent neuron responses to a depolarizing current pulse injection of 100 pA for 1 sec before, during, and after AVP application. **M)** Nissl (left) and anatomical annotations (right) from the Allen Mouse Brain Atlas and Allen Reference Atlas - Mouse Brain ¹¹⁴. High somatodendritic CRF-mCherry expression in the BNST_{DL} after male CRF-

Cre transgenic rats were injected with a Cre-dependent AAV-DREADDs-mCherry in the BNST_{DL}. **N**) Example of evoked responses of a Type III/CRF fluorescent neuron to a hyperpolarizing and depolarizing current pulses of 1 sec. **O**) In Type III/CRF neurons, there was a significant TGOT effect on action potential frequency ($P=0.0167$, $n=7$). Multiple comparisons showed a significant effect of TGOT at (in pA): 140 and 150 ($P=0.0370$), and trends at 130 ($P=0.0807$), 160 ($P=0.0978$), and 170 ($P=0.0867$). **O'**) Representative traces of Type III/CRF fluorescent neuron responses to a depolarizing current pulse injection of 150 pA before, during and after TGOT application. * $P<0.05$, ** $P<0.01$, *** $P<0.001$ vs pre.

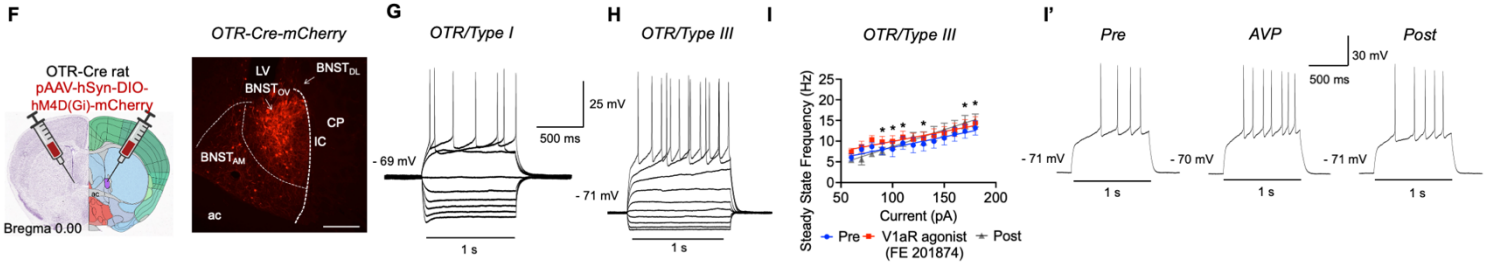
Activation of OTR excites Type III BNST_{DL} neurons



Activation of V1aR, but not V1bR, moderately excites Type III neurons



AVP excites fluorescent OTR-BNST_{DL} neurons (Type I and Type III) from OTR-Cre rat



AVP and TGOT excite fluorescent CRF-BNST_{DL} neurons (Type III) from CRF-Cre rat

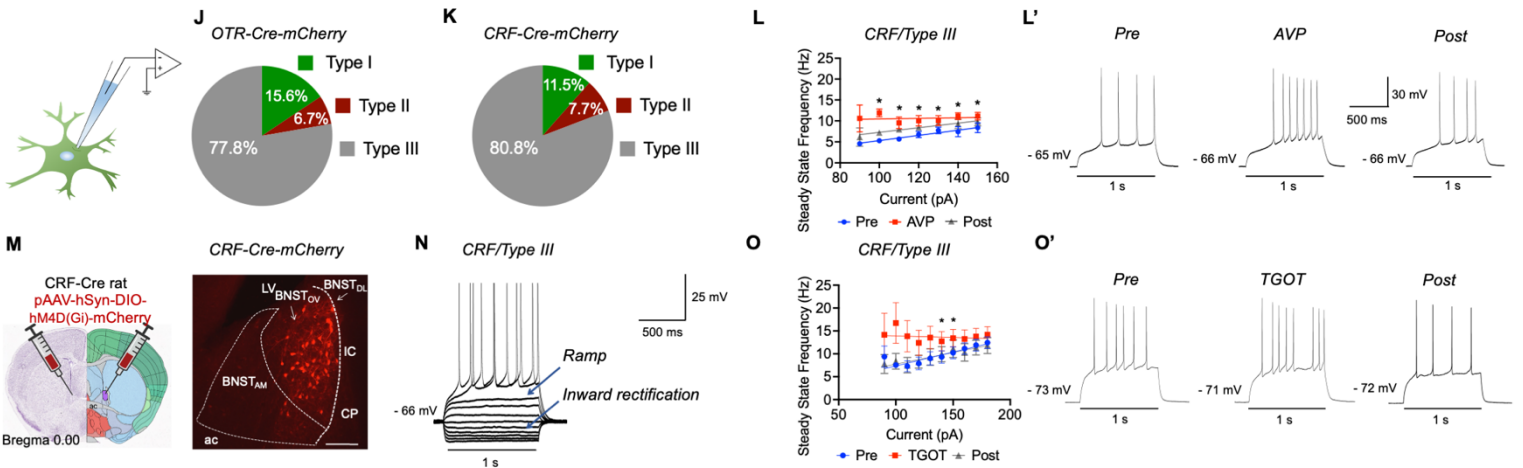
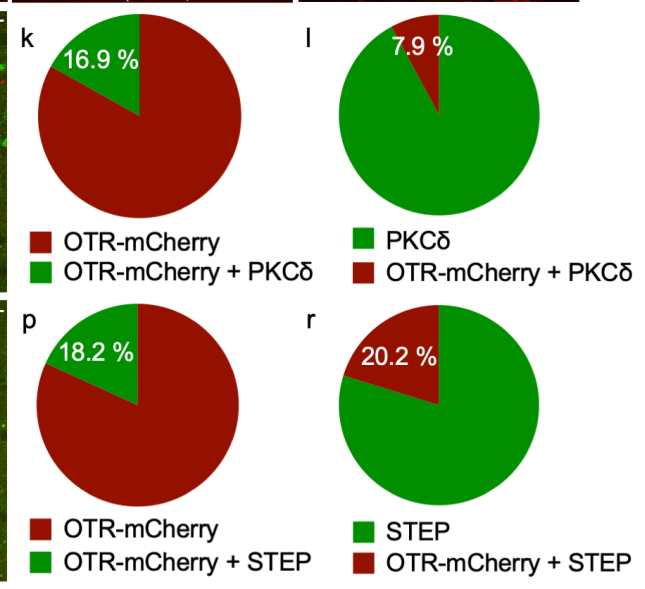
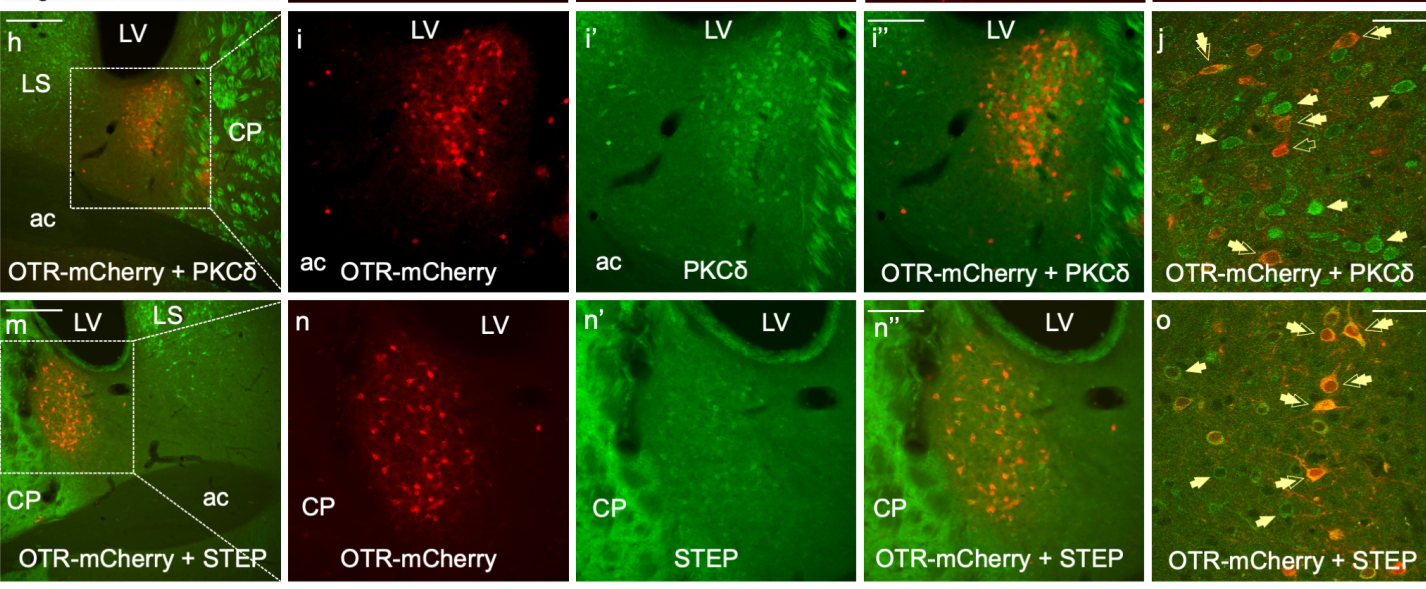
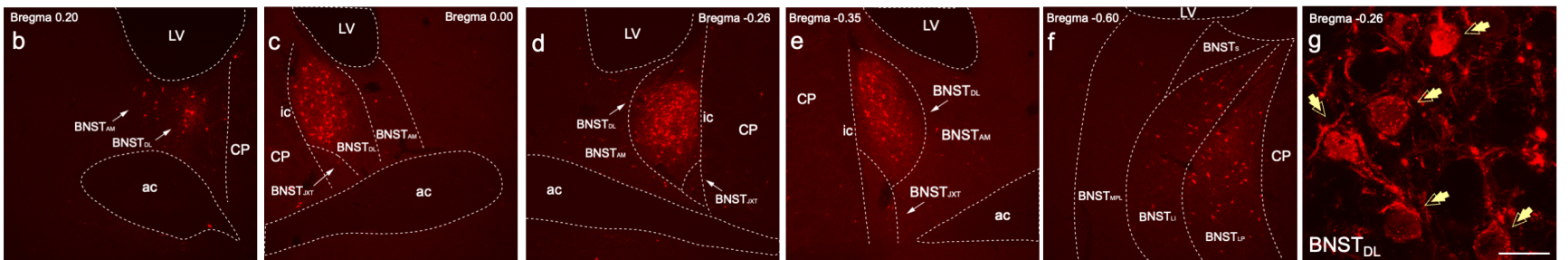
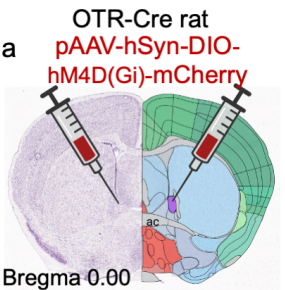


Figure 3. The $BNST_{DL}$ contains numerous OTR-expressing neurons, which co-express *Striatal-enriched Protein Tyrosine Phosphatase (STEP)* or *Protein Kinase C delta (PKC δ)*. Nissl (left) and anatomical annotations (right) from the Allen Mouse Brain Atlas and Allen Reference Atlas – Mouse Brain ¹¹⁴ (a). OTR-mCherry cell bodies and spiny dendrites are localized in the anterior (b-c), middle (d-e), and posterior (f) subdivisions of the BNST. The majority of the OTR neurons were located in the $BNST_{DL}$, primarily in the oval nucleus of the $BNST_{DL}$ ($BNST_{OV}$, c-e), whereas fewer OTR neurons are seen in the anteromedial BNST ($BNST_{AM}$). In posterior BNST sections (f), OTR neurons are found in lateral division, posterior BNST ($BNST_{LP}$), lateral division, intermediate posterior BNST ($BNST_{LI}$), and to a lesser extent in medial, posterolateral BNST ($BNST_{MPL}$). High magnification confocal image shows robust somatodendritic expression of mCherry in $BNST_{DL}$ OTR neurons (scale bar 10 μ m) (g). Double-immunofluorescence microphotographs show high density of OTR and PKC δ neurons in the $BNST_{DL}$ (10x, h) and co-expression between the two populations (20x, i-i’). Double-immunofluorescence confocal images (j, 60x, scale bar 20 μ M) and quantification of neurons from multi-tiles Z-stacks of the entire $BNST_{DL}$ shows that $16.91 \pm 4.41\%$ of OTR-mCherry neurons co-express PKC δ (k), whereas only $7.87 \pm 1.08\%$ of all PKC δ neurons co-express OTR-mCherry (l). High density of OTR and STEP neurons is found in the $BNST_{DL}$ (10x, m) with high co-expression between the two populations (20x, n-n’). Double-immunofluorescence confocal images (o, 60x, scale bar 20 μ M) and quantification of neurons from multi-tiles Z-stacks of the entire $BNST_{DL}$ show that $18.23 \pm 2.05\%$ of all OTR-mCherry neurons co-express STEP (p), whereas $20.22 \pm 2.51\%$ of all STEP neurons co-express OTR-mCherry (r).



3.6. Activity of OTR-BNST_{DL} neurons attenuates threat-elicited vigilant state measured in the FPS

The experimental timeline of behavioral experiments is shown in **Fig. 4A**. First, the inhibitory effect of Gi-DREADD in OTR-BNST_{DL} neurons was confirmed with patch-clamp electrophysiology recordings in brain slices containing the BNST from OTR-Cre rats (n=4) injected with a Cre-dependent Gi-DREADD-mCherry. Here, application of CNO (20 μ M) significantly reduced the spontaneous firing rate recorded near the threshold for action potentials (**Fig. 4B**).

OTR-Cre rats (n=43) injected with a Cre-dependent AAV-Gi-DREADD-mCherry were used to assess the effect of chemogenetic inhibition of OTR neurons in the BNST_{DL} before fear conditioning. All OTR-Cre rats included in the behavioral analysis showed high to moderate expression of OTR-mCherry neurons in the BNST_{DL} in one or both hemispheres. During fear conditioning, there were no significant differences in the reactivity to foot-shocks between saline- and CNO-injected rats ($P=0.1041$, saline n=22, CNO n=21, **not shown**). During the first FPS recall in context B, there was a significant trial effect between the noise-only and light+noise trials ($P=0.0001$, $F(1, 41)=18.25$, two-way RM ANOVA), indicating effective cued fear learning, but no significant effect of treatment (saline vs. CNO) ($P=0.5831$, $F(1, 41)=0.3060$), nor significant interaction between trial and treatment ($P=0.2086$, $F(1, 41)=1.632$, **Fig. 4D**). There was also a significant trial effect between the post-shock and noise-only trials ($P=0.0109$, $F(1, 41)=7.121$), indicating an effective non-cued fear learning, but no significant treatment effect ($P=0.7613$, $F(1, 41)=0.09352$), nor significant interaction between trial and treatment ($P=0.8035$, $F(1, 41)=0.06275$, **Fig. 4D**). During the first contextual fear recall in context A, there was a significant trial effect between the pre-shock and post-shock trials ($P=0.0459$, $F(1, 41)=4.239$) but no significant treatment effect ($P=0.8054$, $F(1, 41)=0.06150$), nor interaction ($P=0.2545$, $F(1, 41)=1.336$, **not shown**). During the first FPS recall test, no significant differences were found in the percentage change of cued fear ($P=0.5698$, **Fig. 4D'**), non-cued fear ($P=0.5069$, **Fig. 4D''**), or contextual fear ($P=0.2541$, not shown).

During the second FPS recall in context B, there was a significant trial effect between the noise-only and light+noise trials ($P<0.0001$, $F(1, 41)=24.68$) and a significant treatment effect (saline vs. CNO) ($P=0.0477$, $F(1, 41)=4.168$) but no significant interaction between trials and treatment ($P=0.5685$, $F(1, 41)=0.3305$, **Fig. 4E**). *Post-hoc* analysis showed that light+noise startle tended to be higher in the CNO group than in the saline group ($P=0.0768$). There was also a significant trial effect between the post-shock and noise-only trials ($P=0.0024$, $F(1, 41)=10.52$), a significant treatment effect ($P=0.0307$, $F(1, 41)=5.009$), and a significant interaction between trials and treatment ($P=0.0430$, $F(1, 41)=4.361$). *Post-hoc* analysis showed that CNO-treated rats ($P=0.0012$) but not saline-treated rats ($P=0.6559$, **Fig. 4E**) exhibited a significantly higher ASR in the noise-only trials than in the post-shock trials. During the second contextual fear recall test in context A, two-way RM ANOVA showed no

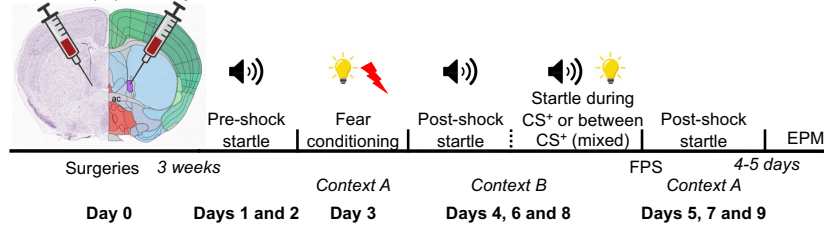
significant trial effect between the pre-shock and post-shock trials ($P=0.9590$, $F(1, 41)=0.002675$), no significant treatment effect ($P=0.7974$, $F(1, 41)=0.06678$), and no significant interaction between trials and treatment ($P=0.5209$, $F(1, 41)=0.4193$, **not shown**). There were no significant differences in the percentage change of cued fear ($P=0.5749$, **Fig. 4E'**) or contextual fear ($p=0.6199$, **not shown**) in the second FPS test. However, there was a significantly higher percentage change of non-cued fear in CNO-treated rats than in saline-treated rats ($P=0.0077$, **Fig. 4E''**). These results show that OTR-BNST_{DL} neuron activity reduces expression of non-cued fear measured during the second FPS test, suggesting that OTR neuron activity in the BNST_{DL} facilitates extinction of non-cued fear (cue-induced vigilant state).

3.7. Activity of OTR-BNST_{DL} neurons increases exploration of open arms in the EPM without affecting locomotor activity

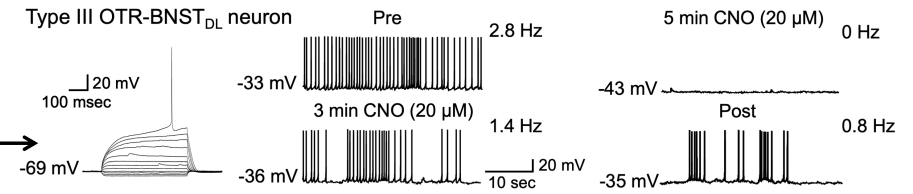
OTR-Cre rats ($n=43$) injected with a Cre-dependent AAV-Gi-DREADD-mCherry into the BNST_{DL} were also used to examine the effect of chemogenetic inhibition of OTR-BNST_{DL} neurons on exploratory behavior in the EPM. Examples of the locomotor activity of saline- vs. CNO-treated rat are shown in **Fig. 4F**. No significant differences between saline and CNO-treated rats were found in the number of entries to the open arms ($P=0.3382$, unpaired t -test, **not shown**), closed arms ($P=0.1835$, **Fig. 4J**), or the center of the EPM ($P=0.8387$, **not shown**), suggesting that silencing OTR-BNST_{DL} neurons does not affect locomotor activity in the EPM. Time spent in each compartment of the EPM was calculated as the percentage of total time in the EPM. CNO-treated OTR-Cre rats spent significantly less time in the open arms ($P=0.0307$, **Fig. 4G**) and significantly more time in the closed arms ($P=0.0168$, **Fig. 4H**) and tended to spend less time at the center ($P=0.0932$, **Fig. 4I**) than saline-treated rats. No significant differences were found in time freezing in open arms ($P=0.3066$, **not shown**), but CNO-treated rats spent significantly more time freezing in closed arms ($P=0.0344$, **Fig. 4K**) than saline-treated rats.

Figure 4. Activity of OTR-neurons in the BNST_{DL} reduces expression of anxious arousal measured in the FPS and increases open arms exploration in the EPM. **A)** Nissl (left) and anatomical annotations (right) from the Allen Mouse Brain Atlas and Allen Reference Atlas – Mouse Brain¹¹⁴. Experimental timeline shows that male OTR-Cre rats were injected with AAV-DREADDs-Gi-mCherry into the BNST_{DL} and were treated with CNO or saline before fear-conditioning in the FPS and once again, before the EPM. **B)** *In vitro* whole-cell patch-clamp electrophysiology in brain slices from the OTR-Cre rats shows that CNO (bath applied continuously for 7 minutes) reduces frequency of spontaneous firing of fluorescent OTR-BNST-mCherry neurons, which recovers during 12 minutes washout (post). **C)** FPS apparatus with Plexiglass animal enclosure and startle detection system underneath the stage. **D-D'')** During the first FPS recall, two-way RM ANOVA showed a significant trial effect of noise only vs. light+noise ($P<0.0001$), and post-shock vs. noise only ($P=0.0109$), but no significant treatment effects (**D**). No significant differences were found in the percentage change of cued fear (**D'**), and non-cued fear (**D''**). **E-E'')** During the second FPS recall, there was a significant trial effect between the noise-only and light+noise trials ($P<0.0001$) and a significant treatment effect ($P=0.0477$) but no significant interaction. There was also a significant trial effect between the post-shock and noise-only trials ($P=0.0024$), a significant treatment effect ($P=0.0307$), and a significant interaction ($P=0.0430$, **E**). *Post-hoc* analysis showed that CNO-treated rats ($P=0.0012$) but not saline-treated rats ($P=0.6559$), exhibited a significantly higher startle in the noise-only trials than in the post-shock trials. There were no significant differences in the percentage change of cued fear (**E'**) but there was a significantly higher percentage change of non-cued fear (cue-induced vigilant state or anxious arousal) in CNO-treated rats than in saline-treated rats ($P=0.0077$, **E''**). **F)** Representative traces of locomotor activity during the EPM exploration by OTR-Cre rats treated with saline or CNO. Rats treated with CNO spent significantly less time in the open arms of the EPM (**G**), spend more time in the closed arms (**H**), and tend to spend less time in the center (**I**) vs. rats treated with saline. No significant differences were found between rats treated with saline vs. CNO in the number of entries to the closed arms (**J**). CNO-treated rats spend significantly more time freezing in the closed arms vs. saline-treated rats ($P=0.0344$). * $P<0.05$, ** $P<0.01$

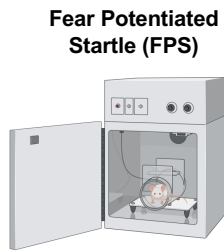
A OTR-Cre rat
pAAV-hSyn-DIO-
hM4D(Gi)-mCherry



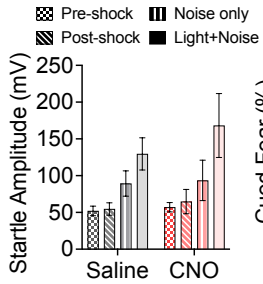
B



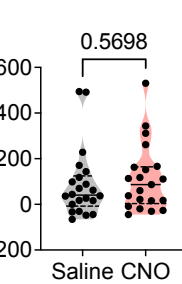
C



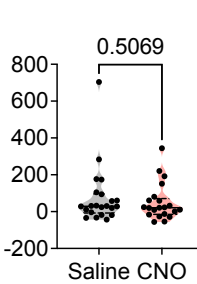
D



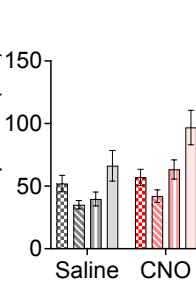
D'



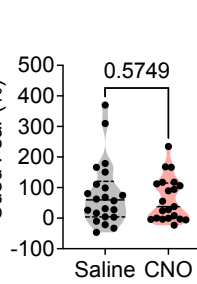
D''



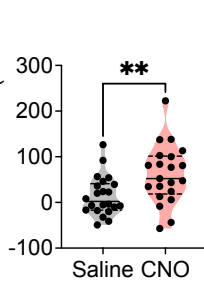
E



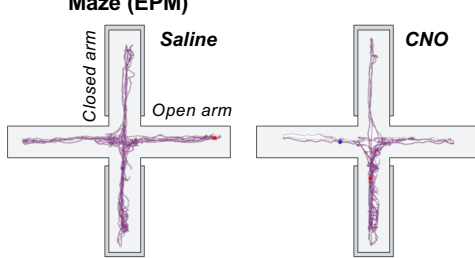
E'



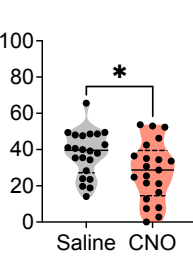
E''



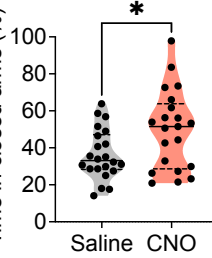
F



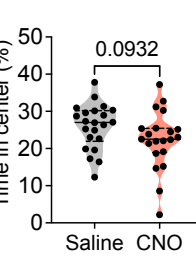
G



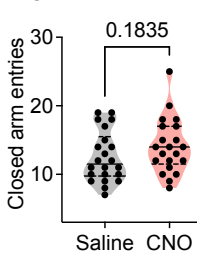
H



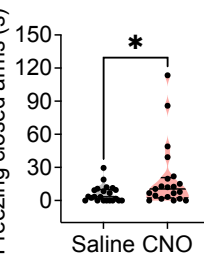
I



J



K



3.8. Hypothalamic AVP neurons from the SON, SCN and the PVN project to the BNST_{DL}

Male AVP-Cre rats injected bilaterally into the SON, SCN, or PVN with a Cre-dependent pAAV hSyn FLEX mGFP-2A-synaptophysin-mRuby were perfused (n=8) or injected with pAAV-EF1a-double floxed-hChR2(H134R)-EYFP-WPRE-HGHpA, used for slice electrophysiology and examined for neuronal projections from the hypothalamic AVP neurons to the BNST_{DL} (SON n=28; SCN n=30; PVN n=10). Fidelity of the Cre expression in the hypothalamic AVP neurons was confirmed in the cell bodies and processes of AVP neurons in the SON, SCN, and PVN, where synaptophysin-mRuby (**Fig. 5a-b''**, **5d-e''**) or EF1a-ChR2-EYFP-expressing neurons and processes co-expressed AVP peptide (**Fig. 6a-d''**, **7a-f''**). Fibers and processes expressing mRuby or EYFP were seen to ascend from the SCN neurons and traversed dorsally along the 3rd ventricle, innervating the anterior hypothalamus and the PVN, and the PVN AVP neurons (**Fig. 7a''''**) and then continued via a right angle toward the posterior BNST and dorsally toward the lateral septum (**Fig. 7b''**). From the SON, mRuby or EYFP-expressing fibers and processes ascended via a lateral-dorsal route toward the hypothalamic accessory nuclei (AN) and the PVN (**Fig. 6a-c''**), and then laterally along the internal capsule (IC) toward the posterior BNST (**Fig. 6g**). From the PVN, eYFP-expressing fibers and processes descended toward SON, and travelled via a lateral route toward the internal capsule (**Fig. 7e**). The eYFP-expressing fibers and processes originating from the SON (**Fig. 6b-c''**), SCN (**Fig. 7b'-b''**), and PVN (**Fig. 7f''**) co-expressed mature AVP peptide. Notably, both synaptophysin-mRuby and EF1a-ChR2-eYFP-expressing fibers originated from the SON (**Fig. 5f-f''**, **6f-f''**), SCN (**Fig. 5c-c''**, **7c-c''**), and PVN (**Fig. 7g-g''**), were found in the BNST_{DL}, and a subset of these fibers co-expressed mature AVP peptide.

3.9. Optogenetically-evoked release of AVP from hypothalamic fibers excites BNST_{DL} neurons

To determine functional peptidergic projections between the hypothalamic nuclei producing AVP and BNST_{DL} neurons, action potentials frequency (Hz) was recorded from Type I and Type III BNST_{DL} neurons, before and after tetanic light stimulation (TLS, 10 Hz) of hypothalamic ChR2-eYFP fibers in BNST slices. These recordings were performed in the presence of synaptic transmission blockers in response to 80, 100, and 120-pA current injections to determine if optogenetically released AVP mimics the excitatory effects of exogenous AVP described above. Here, we stimulated ChR2-eYFP fibers originating from the SON, SCN, and PVN, separately, with and without bath application of the OTR antagonist, OTA. At least 3-4 pre-TLS responses to each current injection were collected for every neuron and averaged as a baseline for repeated measures analyses.

3.9.1 AVP from SON fibers excites Type I and Type III BNST_{DL} neurons via OTR

Only rats with strong bilateral, strong unilateral, or moderate bilateral ChR2-eYFP expression levels in the SON were included in the analysis. First, we demonstrated that TLS (10-ms single pulses at 10 Hz for 20 s) evoked action potentials of fluorescent eYFP-ChR2 expressing AVP neurons in the SON at each light pulse delivered (**Fig. 6d-e**). Following TLS of ChR2-expressing fibers in the BNST, in Type I neurons, there was a significant current effect on spiking frequency ($P=0.0283$, $F(1.234, 7.404)=6.912$, $n=7$) but no TLS effect ($P=0.5131$, $F(1.630, 9.777)=0.6497$) and no interaction between current and TLS ($P=0.3164$, $F(1.918, 11.51)=1.267$). Similarly, there was a significant current effect on Type III neuron firing ($P=0.0123$, $F(0.5618, 2.247)=58.26$, $n=4$, 2-way RM ANOVA) but no TLS effect ($P=0.2023$, $F(1.405, 5.621)=2.137$) nor interaction ($P=0.5631$, $F(1.782, 6.147)=0.5937$).

When the Type I and Type III neurons were pulled together, there was no significant overall TLS effect ($P=0.1212$, $F(2.804, 28.04)=2.138$), $n=11$, 2-way RM ANOVA) despite a significant current effect ($P<0.0004$, $F(1.204, 12.04)=21.51$). However, when the responses to 80 pA were analyzed separately, there was a significant TLS effect ($P=0.0459$, $F(3.166, 31.66)=2.936$, RM ANOVA) and *post-hoc* showed a significant TLS effect at (in min) 4 ($P=0.0199$), 6 ($P=0.0255$), 8 ($P=0.0245$), and 12 ($P=0.0255$) (**Fig. 6h**).

When the OTR antagonist, OTA, was applied before TLS in response to 80 pA current injection, there was no TLS effect on firing frequency ($P=0.2863$, $F(3.286, 23.00)=1.339$, $n=3$ Type I and $n=5$ Type III neurons, RM ANOVA, **Fig. 6h'**). As TLS evoked the most significant increase in firing at 4 min following stimulation, we also compared firing with and without OTA at baseline vs. 4 min in response to 80 pA current for all neurons recorded. There was a significant TLS effect ($P=0.0055$, $F(1, 17)=10.09$, $n=19$, 2-way RM ANOVA), with no treatment effect ($P=0.1705$, $F(1, 17)=2.048$) and no interaction ($P=0.3088$, $F(1, 17)=1.101$). *Post-hoc* showed that TLS increased firing of BNST_{DL} neurons ($P=0.0093$) but had no effect when OTRs were blocked ($P=0.3277$, **Fig. 6h''**).

Figure 5. *Suprachiasmatic nucleus and supraoptic nucleus of the hypothalamus send AVP-containing peptidergic fibers to the BNST_{DL}.* AVP-Cre transgenic rats were bilaterally injected with pAAV-hSyn-FLEX-mGFP-2A-Synaptophysin-mRuby in the SCN or SON and AVP peptide was visualized by Alexa Fluor 647. **a-a''')** Co-expression of GFP (green) and AVP peptide (red) in the SCN, but no SON contamination with GFP, is observed at 4x (**a''**, scale bar 100 μ m) and 20x (**a'''**, bar 25 μ m) magnification. **b-b''')** Confocal images (60x, bar 10 μ m) show the co-expression of hSyn-GFP (green, **b**), 2A-Synaptophysin-mRuby (red, open arrows, **b'**), and AVP peptide (magenta, closed arrows, **b''**) in neurons of the SCN (double arrows, **b'''**). **c-c''')** Confocal images (60x) showing the co-localization of 2A-Synaptophysin-mRuby (red, open arrows, **c'**) and AVP peptide (magenta, closed arrows, **c''**) in fibers of the BNST_{DL} that originated from the SCN (scale bar 10 μ m, double arrows, **c'''**). **d-d''')** Co-expression of GFP (green) and AVP peptide (red) in the SON, but no SCN contamination with GFP, is observed at 4x (**d''**, bar 100 μ m) and 20x (**d'''**, 25 μ m) magnification. **e-e''')** Confocal images (60x, bar 10 μ m) show co-expression of hSyn-GFP (green, **e**), 2A-Synaptophysin-mRuby (red, open arrows, **e'**), and AVP peptide (magenta, closed arrows, **e''**) in neurons of the SON (double arrows, **e'''**). **f-f''')** Confocal images (60x, bar 10 μ m) show co-expression of 2A-Synaptophysin-mRuby (red, open arrows, **f'**) and AVP peptide (magenta, closed arrows, **f''**) in fibers of the BNST_{DL} that originated from the SON (double arrows, **f'''**), opt – optic track, 3rdV – 3rd Ventricle.

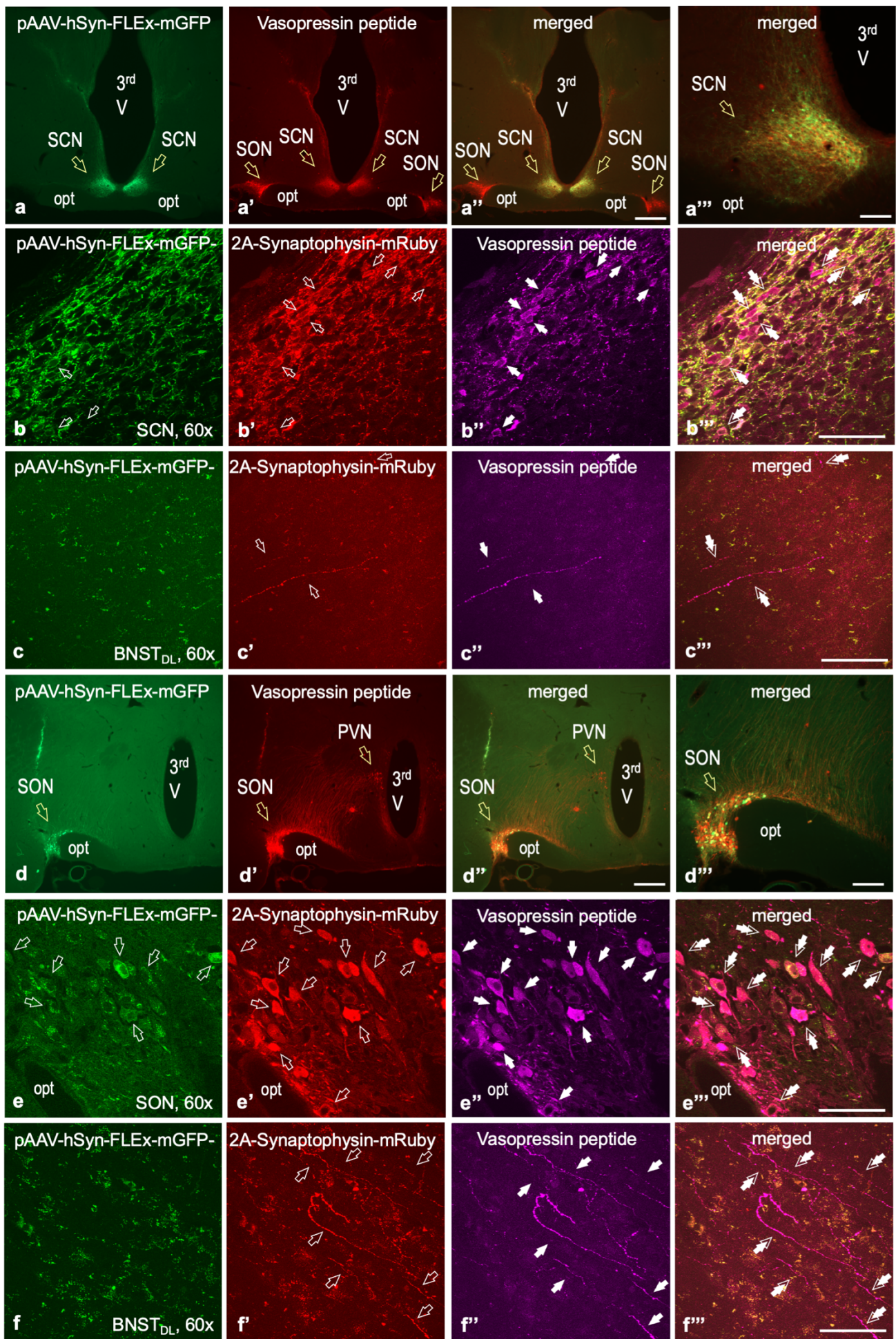
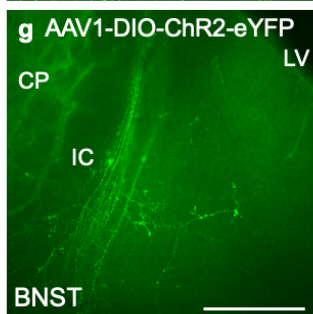
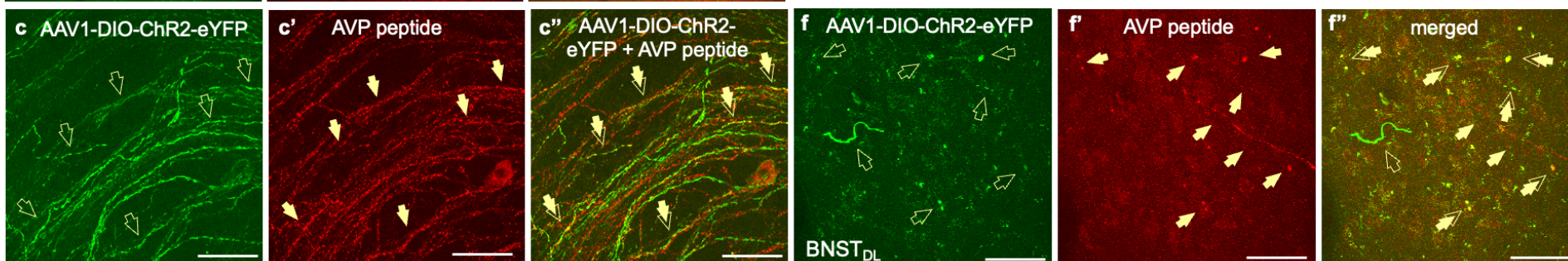
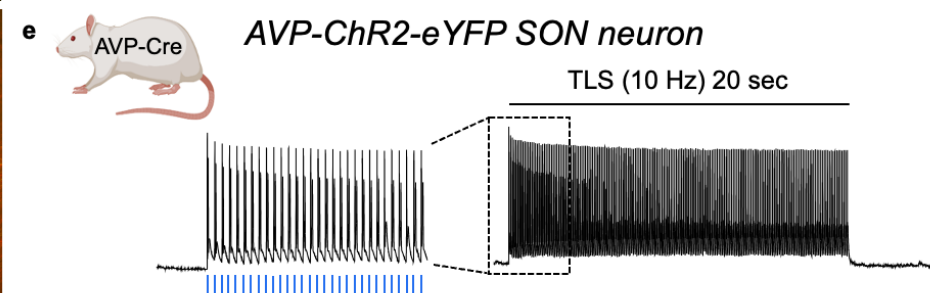
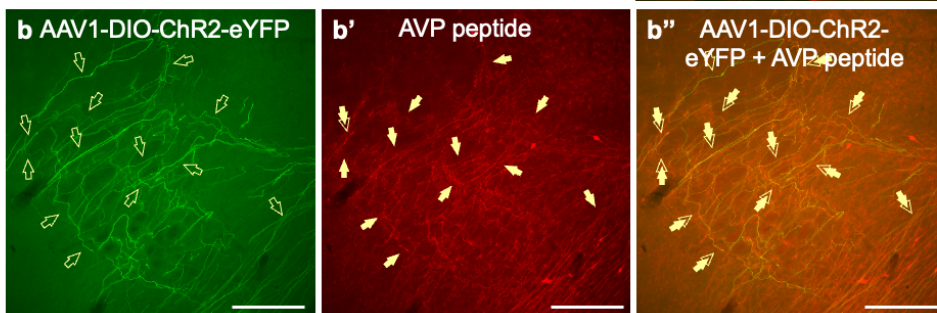
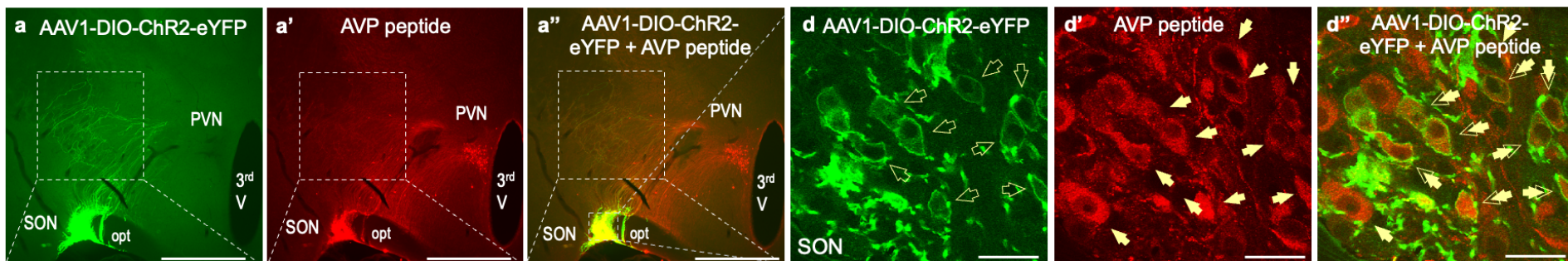
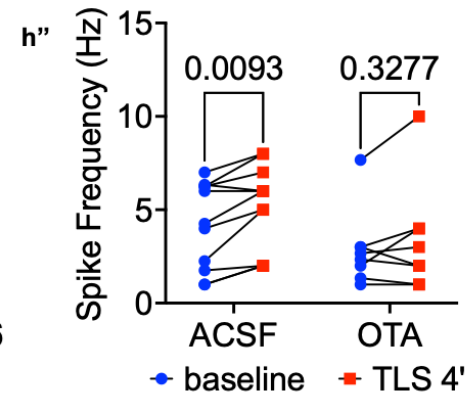
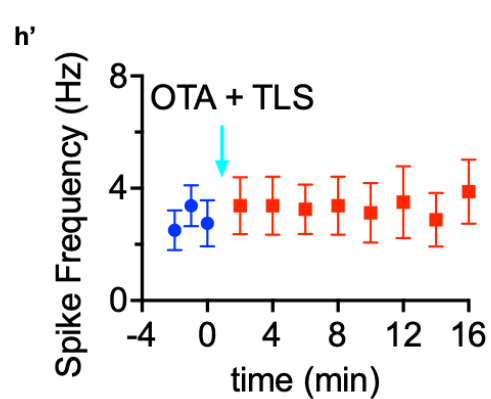
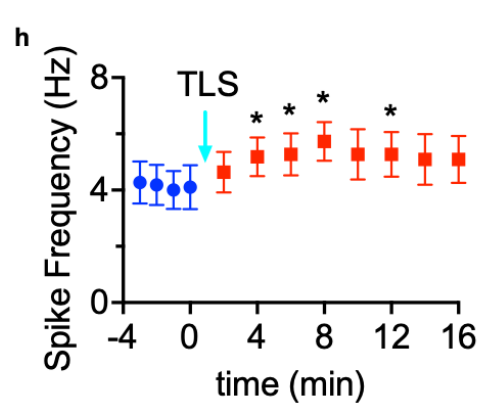


Figure 6. *Tetanic light stimulation of AVP fibers from the SON excite Type I and Type III BNST_{DL} neurons in an OTR-dependent fashion.* AVP-Cre transgenic rats were bilaterally injected with AAV-EF1a-DIO-ChR2-eYFP (green) in the SON and AVP peptide was visualized with Alexa Fluor 594 (red). Co-expression of eYFP-ChR2 and AVP peptide in the SON, but not the PVN, is observed at 4x magnification (**a-a''**, scale bar 100 μ m). High co-expression of ChR2-eYFP (green, open arrows) and AVP peptide (red, closed arrows) is seen in SON-originating fibers, which ascend dorso-laterally from the SON toward internal capsulae (IC), as seen at 20x (**b-b''**, scale bar 50 μ m) and 60x magnification (**c-c''** confocal images, scale bar 10 μ m). Confocal images (60x) show high co-localization of ChR2-eYFP (green, open arrows) and AVP (red, closed arrows) in the soma and dendrites of SON neurons (**d-d''**, scale bar 10 μ m). In the BNST_{DL}, confocal images show ChR2-eYFP-expressing (green, open arrows) and AVP-containing fibers (red, closed arrows) converging on boutons which co-express ChR2-eYFP and AVP peptide (double arrows, scale bar 10 μ m, **f-f''**). Action potentials recorded from fluorescent ChR2-eYFP-expressing SON neurons from brain slices containing hypothalamus shows burst firing following tetanic blue light stimulation (TLS, 10 Hz) for 20 sec, where each pulse of blue light evokes action potential (**e**). High expression of fluorescent ChR2-eYFP-expressing processes and fibers with fluorescent boutons (presumptive peptide release sites), originating from the SON, is seen in the BNST from brain slice processed *post-electrophysiology* (scale bar 100 μ m, **g**). In brain slices containing the BNST, action potentials frequency (Hz) was recorded from identified Type I and Type III BNST_{DL} neurons, before and after TLS (TLS, 10 Hz) of hypothalamic ChR2-eYFP fibers in response to 80pA current injection, with and without bath application of the OTR antagonist, OTA. Only rats with strong bilateral, strong unilateral, or moderate bilateral ChR2-eYFP expression levels in the SON were included in the analysis. In Type I and Type III BNST_{DL} neurons, there was a significant TLS effect ($P=0.0459$, $n=11$, **h**). When the OTR antagonist, OTA, was applied before TLS, there was no TLS effect on firing frequency ($P=0.2863$, $n=8$, **h'**). As TLS evoked the most significant increase in firing at 4 min following stimulation, we also compared firing with and without OTA at baseline vs. 4 min in response to 80pA current for all neurons recorded, which showed a significant TLS effect ($P=0.0055$), with increased firing following TLS, but not when OTR neurons were blocked with OTA. CP – Caudate Putamen, LV – Lateral Ventricle, 3rdV – 3rd Ventricle, * $P<0.05$



Blue-light evoked AVP from SON excites Type I and Type III BNST_{DL} neurons via OTR



3.9.2. AVP from the SCN fibers excites Type III BNST_{DL} neurons via OTR

In Type I BNST_{DL} neurons from rats with strong bilateral, strong unilateral, or moderate bilateral ChR2-eYFP expression in the SCN, there was a current effect on spike frequency ($P=0.0001$, $F(1.338, 10.70) = 28.60$, $n=9$, two-way RM ANOVA), but no TLS effect ($P=0.3718$, $F(1.888, 15.10)=1.045$, nor interaction ($P=0.2841$, $F(3.111, 24.89)=1.340$). Similarly, when firing in response to 80 pA was analyzed separately, there was no TLS effect ($P=0.5633$, $F(2.918, 23.34)=0.6903$, $n=9$).

However, in Type III BNST_{DL} neurons, there was a trend in TLS effect on spike frequency in Type III BNST_{DL} neurons ($P=0.0586$, $F(1.383, 8.297)=4.443$, 2-way RM ANOVA, $n=7$), and a significant current effect ($P=0.0088$, $F(1.051, 6.306)=13.70$), with no interaction ($P=0.1178$, $F(2.840, 17.04)=2.286$). *Post-hoc* analysis showed a significant TLS effect in response to 80-pA injection at (in min) 12 (vs. baseline $P=0.0364$), 14 ($P=0.0154$), 16 ($P=0.0289$), trend at 18 ($P=0.0761$), and an effect at 20 ($P=0.0243$). We then analyzed the response to 80-pA current separately and found a significant TLS effect ($P=0.0251$, $F(1.739, 10.43)=5.611$, $n=7$, RM ANOVA), with multiple comparisons showing significant TLS effects as above (**Fig.7d**).

In the presence of the OTR antagonist, OTA, TLS had no effect on firing of Type III neurons from rats with strong bilateral or strong unilateral ChR2-eYFP expression in the SCN, in response to 80-pA current injection ($P=0.4261$, $F(1.945, 5.836)=0.9831$, RM ANOVA, $n=4$, **Fig.7d'**). When Type III neurons' firing following TLS (at 80 pA) was analyzed with and without OTA, 2-way ANOVA showed a significant interaction between the TLS and OTA treatment ($P=0.0059$, $F(1, 9)=12.84$, $n=11$, 2-way RM ANOVA), with no TLS ($P=0.7535$, $F(1, 9)=0.1048$) or treatment effect ($P=0.4243$, $F(1, 9)=0.7004$). *Post-hoc* analysis showed that TLS increased firing of Type III neurons ($P=0.0202$), but this effect was not observed in neurons in which OTR receptors were blocked ($P=0.1377$, **Fig.7d''**). We chose this time point as TLS evoked the most significant increase in firing at 14 min following stimulation.

3.9.3. AVP from the PVN fibers excites a subset of III BNST_{DL} neurons via OTR

In Type I and III BNST_{DL} neurons from rats with strong bilateral, strong unilateral, or moderate bilateral ChR2-eYFP expression in the PVN, there was a current effect on spike frequency ($P=0.0001$, $F(1.338, 10.70)=28.60$, $n=9$, two-way RM ANOVA), no TLS effect ($P=0.3718$, $F(1.888, 15.10)=1.045$, nor interaction ($P=0.2841$, $F(3.111, 24.89)=1.340$). When spiking in response to 80 pA was analyzed separately, there was no TLS effect ($P=0.3404$, $F(1.375, 12.38)=1.092$, $n=11$, **Fig.7h'**). Similarly, there was no TLS effect in a presence of OTA ($P=0.2920$, $F(1.668, 6.671)=1.457$, $n=5$, **Fig.7h''**). No treatment effect ($P=0.4868$, $F(1, 14)=0.5102$), TLS effect ($F(1, 14)=1.145$, $P=0.3028$), nor interaction ($P=0.5684$, $F(1, 14)=0.3412$, $n=16$) emerged when Type I and III neurons' firing following TLS (at 80 pA) was analyzed with and without OTA (**Fig.7h'''**). However, two out of seven Type I BNST_{DL}

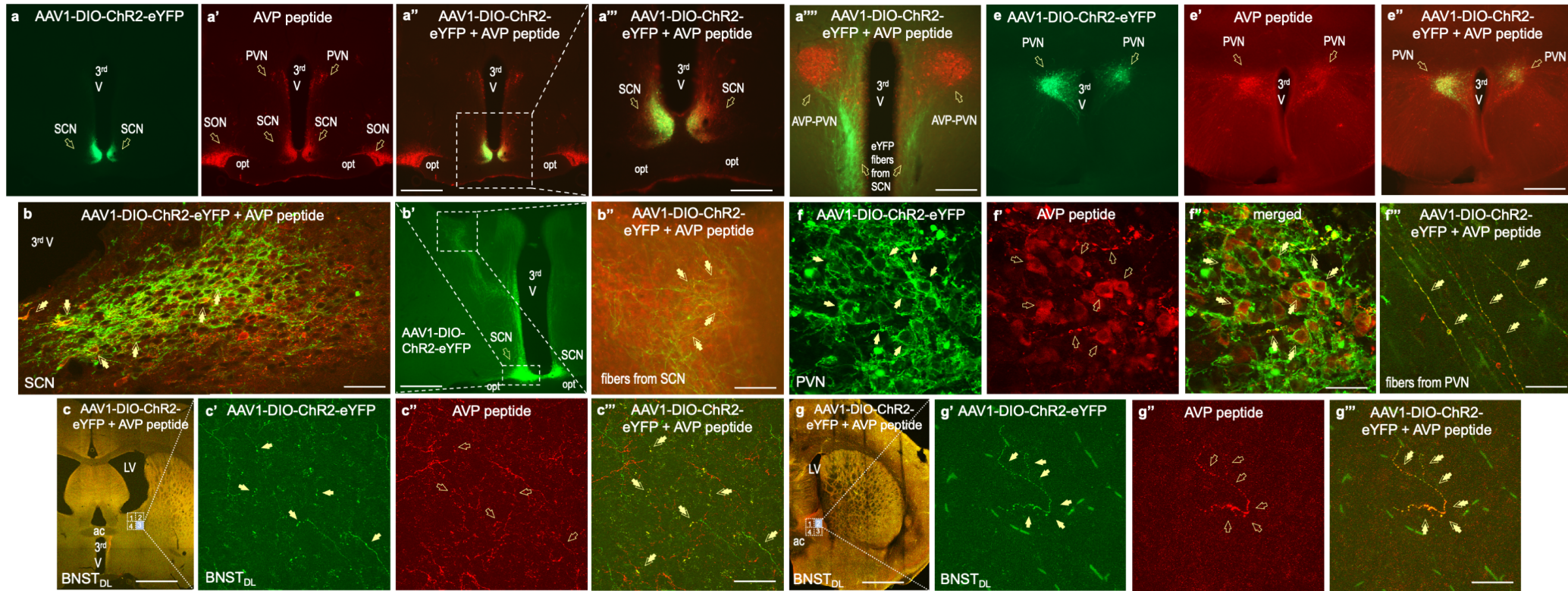
neurons, both from rats with a very high bilateral PVN ChR2-eYFP expression, showed significant spiking increase to 283 and 144% of baseline at 6 min post TLS, whereas no Type I neurons showed increase in firing frequency when OTA was applied before TLS (**Fig.7h**”).

Figure 7. *Tetanic light stimulation of AVP fibers from the SCN or PVN excites BNST_{DL} neurons in an OTR-dependent fashion.* AVP-Cre transgenic rats were bilaterally injected with AAV-EF1a-DIO-ChR2-eYFP (green) in the SCN (**a-b''**) or PVN (**e-g'''**) and AVP peptide was visualized with Alexa Fluor 594 (red). **In rats injected in the SCN**, co-expression of eYFP-ChR2 and AVP peptide in the SCN, but not SON or PVN, is observed at 4x (**a-a''**, scale bar 100 μ m) and 10x magnification (**a'''**, scale bar 50 μ m). High co-expression of ChR2-eYFP (green) and AVP peptide (red) is seen in the SCN neurons (**b**, double arrows, confocal image, 60x, bar 10 μ m) and SCN-originating fibers, which ascend dorsally from the SCN toward the PVN (**a''''**, **b'**, 10x), and travel at a straight angle toward posterior BNST (**b'**, 10x), where they co-express AVP peptide (**b''**, double arrows, 20x, bar 20 μ m). In the BNST_{DL}, confocal images show ChR2-eYFP-expressing (green, open arrows) and AVP-containing fibers and processes (red, closed arrows) which co-express ChR2-eYFP and AVP peptide (double arrows, 60x, scale bar 10 μ m, **c-c'''**). In brain slices containing the BNST, action potentials frequency (Hz) was recorded from identified Type I and Type III BNST_{DL} neurons, before and after TLS (10 Hz) of SCN-originating ChR2-eYFP fibers in response to 80pA current injection, with and without OTR antagonist, OTA. In Type III BNST_{DL} neurons, there was a significant TLS effect ($P=0.0251$, $F(1.739, 10.43)=5.611$, $n=7$, RM ANOVA), with multiple comparisons showing significant increases in firing frequency at 14, 16, and 18 min following TLS (**d**). In the presence of the OTR antagonist, OTA, TLS had no effect on firing of Type III neurons ($P=0.4261$, $F(1.945, 5.836)=0.9831$, $n=4$, **d'**). When firing following TLS was analyzed with and without OTA, 2-way ANOVA showed a significant interaction between the TLS and OTA treatment ($P=0.0059$, $n=11$) with increased firing frequency following TLS but not in the presence of OTA (**d''**). **In rats injected in the PVN**, co-expression of eYFP-ChR2 and AVP peptide is observed in the PVN, but not SON (**e-e''**, 4x, scale bar 100 μ m). High co-expression of ChR2-eYFP (closed arrows, **f**) and AVP peptide (open arrows, **f'**) is seen in the PVN neurons (double arrows, **f''**, confocal image, 60x, bar 10 μ m) and PVN-originating fibers (**f''''**, 60x). In the BNST_{DL}, confocal images show ChR2-eYFP-expressing (**g'**, green, closed arrows) and AVP-containing fibers and processes (**g''**, red, closed arrows) which co-express ChR2-eYFP and AVP peptide (double arrows, 60x, bar 10 μ m, **g'''**). In brain slices containing the BNST, action potentials frequency (Hz) was recorded from identified Type I and Type III BNST_{DL} neurons, before and after TLS (10 Hz) of PVN-originating ChR2-eYFP fibers in response to 80pA current injection, with and without OTR antagonist, OTA. In Type I and III BNST_{DL} neurons, there was no TLS effect ($P=0.3404$, $n=11$, **h**) and no TLS effect in a presence of OTA ($P=0.2920$, $n=5$, **h'**). No treatment or TLS effect ($P=0.3028$, $n=16$) emerged when firing following TLS was analyzed with and without OTA (**h''**). However, individual Type I BNST_{DL} neurons (2/7), from rats with a very high bilateral PVN ChR2-eYFP expression, showed significant spiking increase to 283 and 144% of baseline at 6 min post TLS, whereas no Type I neurons showed increase in firing frequency when OTA was applied

before TLS (**h''**). ac – anterior commissure, CP – Caudate Putamen, LV – Lateral Ventricle, opt – optic track, 3rdV – 3rd Ventricle, * $P < 0.05$

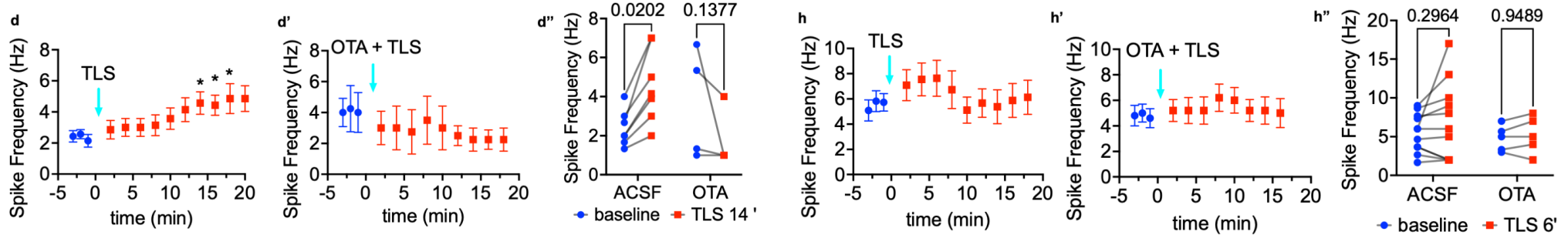
AVP neurons from the SCN project to the BNST_{DL}

AVP neurons from the PVN project to the BNST_{DL}



Blue-light evoked AVP from SCN excites Type III BNST_{DL} neurons via OTR

Blue-light evoked AVP from PVN excites a subset of Type I BNST_{DL} neurons



Discussion

We provide evidence that AVP-OT crosstalk via OTR-expressing BNST_{DL} neurons modulates defensive and exploratory behavior. Exogenous AVP directly and robustly excited Type I and Type III neurons in the BNST_{DL}, a region critical for fear processing and vigilant threat monitoring^{25–28}, and this excitatory effect required OTR transmission. Specifically, OTR, but not V1aR or V1bR antagonists, blocked the excitatory effects of AVP on intrinsic membrane properties and firing frequency of BNST_{DL} neurons. In a subset of Type III BNST_{DL} neurons, V1aR activation by a selective V1aR agonist FE201874, which also blocks OTR⁴⁷, moderately increased firing without affecting intrinsic membrane properties. Excitatory effects of OTR have been documented in the cortex, hippocampus, and BNST^{40,63–65}, and both OTR and V1aR show excitatory effects in the central amygdala (CeA), though on different neuronal populations^{66–68}. AVP and OT differ by only two amino acids, and the cross-talk between these neuropeptides and their respective receptors has been well documented^{69–71}. OTR and V1aR, both centrally located G protein-coupled receptors (GPCRs) for OT and AVP⁷², share 85% structural homology^{73,74}, while V1bR shares 40% identity with V1aR¹⁰. Although OT and AVP have a similar affinity for OTR, OT has a higher affinity for OTR than for V1aR or V1bR^{75,76}.

The greater excitatory response of Type III neurons to AVP, which acts via OTR and V1aR, than to the endogenous OTR agonist, OT, or the highly selective and potent OTR agonist, TGOT, which acts via OTR alone^{77,78}, may be explained by the combined action of these receptors as well as the differences in the affinities of the neurohypophysial hormones toward the receptors. While AVP activates both OTR and V1aR signaling in Type III BNST_{DL} neurons to robustly increase excitability, in Type I neurons, V1aR appears to provide tonic inhibition to a subset of neurons, despite the excitatory effect of OTR. This inhibition was unmasked by the excitatory effect of V1aR antagonist (SR49059), and the inhibitory effects of central V1aR transmission have been reported before⁷⁹. However, OTR remains the key player in regulating BNST_{DL} neuron excitability and BNST_{DL}-dependent behaviors, which are directly influenced by AVP-OT crosstalk.

In many brain regions, the impact of OT and AVP crosstalk on physiology and behavior is less pertinent because OTR and V1R are frequently located in anatomically separate neuronal circuits. In these cases, the effects of OT and AVP depend on the brain site-specific expression of their receptors^{80,81}. However, the BNST_{DL} expresses both OTR^{82,83} and V1aR⁸⁴ and here, we show cell type-specific functional expression of these receptors in Type I and III neurons. This finding aligns with our recent study showing postsynaptic expression of OTR in these neuron types⁴⁰. We further confirmed the excitatory effect of AVP on fluorescent OTR-BNST_{DL} neurons, with the great majority of OTR neurons characterized as Type III. Furthermore, previous single-cell PCR studies have shown that Type III BNST_{DL} neurons express OTR, CRF, and Striatal Enriched Protein Tyrosine Phosphatase (STEP) mRNA³³. Using CRF-Cre transgenic rats, we showed that recorded CRF-mCherry-BNST_{DL} neurons,

which exhibit electrophysiological properties of Type III neurons, are directly excited by both AVP and TGOT. While the co-expression of CRF and OTR in BNST_{DL} neurons was first described in 2011³³, this study provides the first functional evidence of OTR activation directly exciting CRF-BNST_{DL} neurons. Consistent with previous *in situ* hybridization and OTR binding studies^{18,82,85}, identifying the BNST as one of the highest OTR-expressing regions in the rodent brain, we found numerous OTR-expressing neurons throughout the BNST of OTR-Cre rats. Recent single-cell RNAseq analysis in mice revealed that OTRs are expressed in diverse populations of GABA-ergic neurons in the BNST⁸⁶. Here, we found that OTR-BNST_{DL} neurons co-expressed either PKC δ or STEP, two enzymes present on mutually exclusive populations of neurons in the BNST_{DL}⁵⁸. STEP is a unique marker of CRF neurons in the oval nucleus of the BNST_{DL} and is exclusively expressed by Type III BNST_{DL} neurons on a single-cell level³⁵. While our study primarily focused on the BNST_{DL}, different types of OTR neurons might be present in the posterior BNST. Our results contrast with the functional expression and roles of OTR and V1aR in the CeA, where these receptors are located on mutually exclusive neuronal populations in the lateral and medial CeA, respectively, where they play opposite roles in inhibiting and exciting medial CeA output neurons and fear behaviors^{16,53,63}. Thus, Type III BNST_{DL} neurons represent a unique cell population in the extended amygdala in which OTR and V1aR signaling converge to increase excitability in response to AVP.

OTR signaling in the extended amygdala plays an intricate role in fear and vigilance. OTR activation in the CeA reduced contextual fear^{53,87,88}, whereas OTR in the basolateral nucleus of the amygdala (BLA) strengthened fear discrimination toward discrete cues predicting danger⁸⁹. Our previous behavioral studies showed that blocking OTR transmission in the BNST_{DL} reduced the acquisition and recall of learned cued fear measured in the FPS²⁷. Interestingly, blocking OTR in the BNST_{DL} also reduced the ratio between cued and non-cued fear in the same rats, suggesting that BNST_{DL} OTR transmission strengthens fear responses to discrete (cued) threats while reducing threat-induced anxious arousal^{27,39}. Systemic or intracerebroventricular OT similarly reduces non-cued fear in the FPS⁹⁰⁻⁹². In this study, chemogenetic silencing of OTR-BNST_{DL} neurons prolonged the expression of non-cued fear measured in FPS. The non-cued fear reflects potentiation of the startle response that occurs between cue presentations during the cued fear recall, emerging only after the cue is being presented^{27,91}. Hence, this response is thought to reflect a cue-induced vigilant state or anxious arousal, which is independent from contextual fear⁹³. These findings underscore the unique role of OTR and OTR-BNST_{DL} neurons in biasing fear learning toward imminent and signaled threats while dampening threat-induced anxious arousal.

We also found that in the fear-conditioned rats, OTR-BNST_{DL} neuron activity increased open-arm exploration time in the EPM. This aligns with extensive literature showing anxiolytic-like effects of OTR activation in the EPM, especially in stressed animals, for review see^{7,8,94}. BNST_{DL} activity is generally thought to promote anxiety-like behavior by mediating hypervigilance and anticipatory anxiety in response to unpredictable or un-signaled threats^{26,95,96}. Although this appears in contrast

with the role of OTR-BNST_{DL} neurons, our recent study demonstrated that OTR activation excites BNST_{DL} interneurons, thereby increasing inhibitory synaptic transmission that inhibits Type II BNST_{DL} output neurons. This results in a primarily inhibitory effect of OTR activation on BNST_{DL} output to the CeA⁸³, a projection which has been shown before to reduce open arms exploration in the EPM⁹⁷.

AVP and OT influence fear- and anxiety-like behaviors, and are often labeled as ‘anxiogenic’ and ‘anxiolytic’ peptides, respectively. The anxiogenic label for AVP originates from early studies on AVP-deficient Brattleboro rats, which showed reduced vigilance in open spaces and reduced contextual fear memory^{98–100}. Consistent with this, systemic V1aR activation reduces exploration of open arms in the EPM, while V1aR antagonism or knockout increases exploration^{19,101–103}. However, V1aR activation in the lateral septum and posterior BNST can increase EPM exploration and reduce defensive behaviors^{31,104}, suggesting a more complex role of V1aR in modulating fear behavior. Notably, the commonly used V1aR-selective antagonist, d(CH₂)₅[Tyr(Me)²]AVP (Manning compound)^{19,20}, though not binding V1bR or V2R, acts as a potent OTR antagonist⁴⁹. Given the abundant expression of OTR and V1R in the hypothalamus and extended amygdala, the behavioral effects of AVP via OTR may be underestimated. Our finding that AVP increased BNST_{DL} neuronal excitability, requiring OTR signaling (with V1aR showing a moderate excitatory effect), suggests that OTR and V1aR, modulated by specific hypothalamic inputs, work in tandem rather than in opposition to impact BNST neuron activity and behaviors. However, since we used blockers of synaptic transmission in the current study, we cannot exclude the possibility that V1aR, similarly to OTR^{34,40}, has a distinct effect on synaptic activity in the BNST_{DL}.

This study has other limitations. Firstly, female rats were not included. Although we aim to explore potential sex differences (or the lack thereof) in the effects of the AVP and OT systems on BNST excitability and behavior, including both sexes for a detailed analysis was beyond the scope of this study. Combining males and females in the same experimental groups could obscure the significant role the BNST_{DL} OTR and V1aR^{29,105} play in mediating sex differences and similarities in stress-related behaviors, including non-cued fear, which also differs between male and female rats⁹³. Additionally, we cannot rule out the possibility that local AVP neurons from the posterior BNST, which exhibit strong sex-dependent expression and function (with high levels in male rats)¹⁰⁶, may also project to the BNST_{DL}²³.

Previous studies have shown that the rat BNST_{DL} receives OT inputs from the PVN^{33,39,53}, which we confirmed in the current study using optogenetic approach. We also showed that the BNST_{DL} receives AVP inputs from the SON, SCN, and the PVN and that optogenetic high-frequency stimulation of AVP terminals in the BNST_{DL} increased Type I and III BNST_{DL} neurons’ excitability via OTR. Cell-selective genetic manipulations have facilitated our understanding of the contributions of specific populations of hypothalamic and extra-hypothalamic AVP neurons to defensive behaviors.

For example, eliminating AVP neurons in the PVN or SCN using caspase-mediated methods in AVP-Cre mice reduced open-arm exploration in the EPM¹⁰⁷, whereas removing AVP cells in the posterior BNST did not influence open-arm exploration. Overall, these findings suggest that hypothalamic AVP neurons diminish vigilance and promote open-space exploration in the EPM. Although the specific role of AVP SON neurons in defensive behavior is not yet known, it is noteworthy that the activity of AVP neurons in the SCN¹⁰⁷ and the activity of OTR neurons in the BNST_{DL} both increase rodents' open-arm exploration time in the EPM. Thus, in periods when AVP neuron activity in the SCN is high, such as during preparation for the rest phase¹, the system may be primed for AVP release in the BNST_{DL} in response to physiological stimuli, which would activate OTR neurons in the BNST_{DL} and reduce defensive behaviors. Our study reveals cell type and receptor-specific modulation of BNST_{DL} neuron activity via unique hypothalamic projections containing neurohypophysial hormone AVP. We showed that although both OT and AVP have excitatory effects on Type III OTR-expressing neurons of the BNST_{DL}, they differed in the receptors that contributed to the response (OTR alone vs. OTR and V1aR) and hence, the magnitude of the excitatory response. These results suggest that changes in internal states favoring the release of OT vs. AVP (e.g. lactation vs. thirst/salt intake) will have a scaled excitatory impact on Type III OTR-expressing neurons of the BNST_{DL} and will fine tune their input-output responses, thus providing them with greater flexibility in response to specific neurohypophysial inputs.

Acknowledgements

This work was supported by grant MH113007 from National Institute of Mental Health (NIMH) to JD and by the Synergy European Research Council (ERC) grant "OxytocINspace" 101071777, SFB Consortium 1158-3, and German-Israeli Project cooperation (DIP) GR3619-1 to VG.

We thank Dr. Robert Messing, University of Texas Austin for providing us with the CRF-Cre transgenic rats breeders.

We would like to thank Dr. Sarah Daniel of In Scripto, LLC, for edits and comments on this manuscript.

Declaration of interest

The authors declare no competing interest. JD reports US patent 11,559,231 issued on 1.24.2023 entitled: System and method for determining a discrimination index for fear-potentiated startle, which has no competing interest with the current study.

Authors contributions

Conceptualization: JD; Methodology: WF, VOP, FB, SLO, QK, VG, JD; Formal analyses: FB, WF, VOP, RC, JD; Investigation: WF, VOP, FB, SLO, RC, LMM, QR, JD; Resources: QK, VG, JD; Writing - original draft: WF, VOP, JD; Writing – review and editing: WF, VOP, FB, RC, VG, JD; Visualization: JD; Supervision: JD; Project administration: JD; Funding acquisition: VG, JD

References:

1. Kalsbeek, A., Fliers, E., Hofman, M.A., Swaab, D.F., and Buijs, R.M. (2010). Vasopressin and the output of the hypothalamic biological clock. *J Neuroendocrinol* 22, 362–372. <https://doi.org/10.1111/j.1365-2826.2010.01956.x>.
2. Brown, C.H., Ludwig, M., Tasker, J.G., and Stern, J.E. (2020). Somato-dendritic vasopressin and oxytocin secretion in endocrine and autonomic regulation. *J Neuroendocrinol* 32, e12856. <https://doi.org/10.1111/jne.12856>.
3. Serradeil-Le Gal, C., Wagnon, J., Tonnerre, B., Roux, R., Garcia, G., Griebel, G., and Aulombard, A. (2005). An overview of SSR149415, a selective nonpeptide vasopressin V(1b) receptor antagonist for the treatment of stress-related disorders. *CNS Drug Rev* 11, 53–68. <https://doi.org/10.1111/j.1527-3458.2005.tb00035.x>.
4. Caldwell, H.K., Lee, H.-J., Macbeth, A.H., and Young, W.S. (2008). Vasopressin: behavioral roles of an “original” neuropeptide. *Prog Neurobiol* 84, 1–24. <https://doi.org/10.1016/j.pneurobio.2007.10.007>.
5. Veenema, A.H. (2012). Toward understanding how early-life social experiences alter oxytocin- and vasopressin-regulated social behaviors. *Horm Behav* 61, 304–312. <https://doi.org/10.1016/j.yhbeh.2011.12.002>.
6. Jurek, B., and Neumann, I.D. (2018). The Oxytocin Receptor: From Intracellular Signaling to Behavior. *Physiological Reviews* 98, 1805–1908. <https://doi.org/10.1152/physrev.00031.2017>.
7. Janeček, M., and Dabrowska, J. (2019). Oxytocin facilitates adaptive fear and attenuates anxiety responses in animal models and human studies—potential interaction with the corticotropin-releasing factor (CRF) system in the bed nucleus of the stria terminalis (BNST). *Cell Tissue Res* 375, 143–172. <https://doi.org/10.1007/s00441-018-2889-8>.
8. Olivera-Pasilio, V., and Dabrowska, J. (2020). Oxytocin Promotes Accurate Fear Discrimination and Adaptive Defensive Behaviors. *Front. Neurosci.* 14, 583878. <https://doi.org/10.3389/fnins.2020.583878>.
9. Khan, S., Raghuram, V., Chen, L., Chou, C.-L., Yang, C.-R., Khundmiri, S.J., and Knepper, M.A. (2024). Vasopressin V2 receptor, tolvaptan, and ERK1/2 phosphorylation in the renal collecting duct. *Am J Physiol Renal Physiol* 326, F57–F68. <https://doi.org/10.1152/ajprenal.00124.2023>.
10. Lolait, S.J., O’Carroll, A.M., Mahan, L.C., Felder, C.C., Button, D.C., Young, W.S., Mezey, E., and Brownstein, M.J. (1995). Extrahypothalamic expression of the rat V1b vasopressin receptor gene. *Proc Natl Acad Sci U S A* 92, 6783–6787. <https://doi.org/10.1073/pnas.92.15.6783>.
11. Corbani, M., Marir, R., Trueba, M., Chafai, M., Vincent, A., Borie, A.M., Desarménien, M.G., Ueta, Y., Tomboly, C., Olma, A., et al. (2018). Neuroanatomical distribution and function of the vasopressin V1B receptor in the rat brain deciphered using specific fluorescent ligands. *Gen Comp Endocrinol* 258, 15–32. <https://doi.org/10.1016/j.ygcen.2017.10.011>.

12. Tribollet, E., Barberis, C., Jard, S., Dubois-Dauphin, M., and Dreifuss, J.J. (1988). Localization and pharmacological characterization of high affinity binding sites for vasopressin and oxytocin in the rat brain by light microscopic autoradiography. *Brain Research* 442, 105–118. [https://doi.org/10.1016/0006-8993\(88\)91437-0](https://doi.org/10.1016/0006-8993(88)91437-0).
13. Tribollet, E., Dubois-Dauphin, M., Dreifuss, J.J., Barberis, C., and Jard, S. (1992). Oxytocin receptors in the central nervous system. Distribution, development, and species differences. *Ann. N. Y. Acad. Sci.* 652, 29–38.
14. Johnson, A.E., Audigier, S., Rossi, F., Jard, S., Tribollet, E., and Barberis, C. (1993). Localization and characterization of vasopressin binding sites in the rat brain using an iodinated linear AVP antagonist. *Brain Res* 622, 9–16. [https://doi.org/10.1016/0006-8993\(93\)90795-o](https://doi.org/10.1016/0006-8993(93)90795-o).
15. Roozendaal, B., Schoorlemmer, G.H., Wiersma, A., Sluyter, S., Driscoll, P., Koolhaas, J.M., and Bohus, B. (1992). Opposite effects of central amygdaloid vasopressin and oxytocin on the regulation of conditioned stress responses in male rats. *Ann N Y Acad Sci* 652, 460–461. <https://doi.org/10.1111/j.1749-6632.1992.tb34384.x>.
16. Viviani, D., and Stoop, R. (2008). Opposite effects of oxytocin and vasopressin on the emotional expression of the fear response. *Prog Brain Res* 170, 207–218. [https://doi.org/10.1016/S0079-6123\(08\)00418-4](https://doi.org/10.1016/S0079-6123(08)00418-4).
17. Veinante, P., and Freund-Mercier, M.J. (1997). Distribution of oxytocin- and vasopressin-binding sites in the rat extended amygdala: a histoautoradiographic study. *J. Comp. Neurol.* 383, 305–325.
18. Smith, C.J.W., DiBenedictis, B.T., and Veenema, A.H. (2019). Comparing vasopressin and oxytocin fiber and receptor density patterns in the social behavior neural network: Implications for cross-system signaling. *Frontiers in Neuroendocrinology* 53, 100737. <https://doi.org/10.1016/j.yfrne.2019.02.001>.
19. Bayerl, D.S., Hönig, J.N., and Bosch, O.J. (2016). Vasopressin V1a, but not V1b, receptors within the PVN of lactating rats mediate maternal care and anxiety-related behaviour. *Behav. Brain Res.* 305, 18–22. <https://doi.org/10.1016/j.bbr.2016.02.020>.
20. Hernández-Pérez, O.R., Crespo-Ramírez, M., Cuza-Ferrer, Y., Anias-Calderón, J., Zhang, L., Roldan-Roldan, G., Aguilar-Roblero, R., Borroto-Escuela, D.O., Fuxe, K., and Perez de la Mora, M. (2018). Differential activation of arginine-vasopressin receptor subtypes in the amygdaloid modulation of anxiety in the rat by arginine-vasopressin. *Psychopharmacology (Berl.)* 235, 1015–1027. <https://doi.org/10.1007/s00213-017-4817-0>.
21. Rood, B.D., Stott, R.T., You, S., Smith, C.J.W., Woodbury, M.E., and De Vries, G.J. (2013). Site of origin of and sex differences in the vasopressin innervation of the mouse (*Mus musculus*) brain. *J Comp Neurol* 521, 2321–2358. <https://doi.org/10.1002/cne.23288>.
22. Brown, C.H., Ludwig, M., Tasker, J.G., and Stern, J.E. (2020). Somato-dendritic vasopressin and oxytocin secretion in endocrine and autonomic regulation. *J Neuroendocrinol* 32. <https://doi.org/10.1111/jne.12856>.
23. Rigney, N., de Vries, G.J., and Petrulis, A. (2023). Sex differences in afferents and efferents of vasopressin neurons of the bed nucleus of the stria terminalis and medial amygdala in mice. *Horm Behav* 154, 105407. <https://doi.org/10.1016/j.yhbeh.2023.105407>.

24. Mohr, E., Bahnsen, U., Kiessling, C., and Richter, D. (1988). Expression of the vasopressin and oxytocin genes in rats occurs in mutually exclusive sets of hypothalamic neurons. *FEBS Lett* 242, 144–148. [https://doi.org/10.1016/0014-5793\(88\)81003-2](https://doi.org/10.1016/0014-5793(88)81003-2).
25. Sullivan, G.M., Apergis, J., Bush, D.E.A., Johnson, L.R., Hou, M., and Ledoux, J.E. (2004). Lesions in the bed nucleus of the stria terminalis disrupt corticosterone and freezing responses elicited by a contextual but not by a specific cue-conditioned fear stimulus. *Neuroscience* 128, 7–14. <https://doi.org/10.1016/j.neuroscience.2004.06.015>.
26. Duvarci, S., Bauer, E.P., and Pare, D. (2009). The Bed Nucleus of the Stria Terminalis Mediates Inter-individual Variations in Anxiety and Fear. *Journal of Neuroscience* 29, 10357–10361. <https://doi.org/10.1523/JNEUROSCI.2119-09.2009>.
27. Moaddab, M., and Dabrowska, J. (2017). Oxytocin receptor neurotransmission in the dorsolateral bed nucleus of the stria terminalis facilitates the acquisition of cued fear in the fear-potentiated startle paradigm in rats. *Neuropharmacology* 121, 130–139. <https://doi.org/10.1016/j.neuropharm.2017.04.039>.
28. Goode, T.D., Ressler, R.L., Acca, G.M., Miles, O.W., and Maren, S. (2019). Bed nucleus of the stria terminalis regulates fear to unpredictable threat signals. *Elife* 8. <https://doi.org/10.7554/eLife.46525>.
29. DiBenedictis, B.T., Nussbaum, E.R., Cheung, H.K., and Veenema, A.H. (2017). Quantitative mapping reveals age and sex differences in vasopressin, but not oxytocin, immunoreactivity in the rat social behavior neural network. *J Comp Neurol* 525, 2549–2570. <https://doi.org/10.1002/cne.24216>.
30. Dabrowska, J., Hazra, R., Ahern, T.H., Guo, J.-D., McDonald, A.J., Mascagni, F., Muller, J.F., Young, L.J., and Rainnie, D.G. (2011). Neuroanatomical evidence for reciprocal regulation of the corticotrophin-releasing factor and oxytocin systems in the hypothalamus and the bed nucleus of the stria terminalis of the rat: Implications for balancing stress and affect. *Psychoneuroendocrinology* 36, 1312–1326. <https://doi.org/10.1016/j.psyneuen.2011.03.003>.
31. Duque-Wilckens, N., Steinman, M.Q., Laredo, S.A., Hao, R., Perkeybile, A.M., Bales, K.L., and Trainor, B.C. (2016). Inhibition of vasopressin V1a receptors in the medioventral bed nucleus of the stria terminalis has sex- and context-specific anxiogenic effects. *Neuropharmacology* 110, 59–68. <https://doi.org/10.1016/j.neuropharm.2016.07.018>.
32. Luo, P.X., Zakharenkov, H.C., Torres, L.Y., Rios, R.A., Gegenhuber, B., Black, A.M., Xu, C.K., Minie, V.A., Tran, A.M., Tollkuhn, J., et al. (2022). Oxytocin receptor behavioral effects and cell types in the bed nucleus of the stria terminalis. *Horm Behav* 143, 105203. <https://doi.org/10.1016/j.yhbeh.2022.105203>.
33. Dabrowska, J., Hazra, R., Ahern, T.H., Guo, J.-D., McDonald, A.J., Mascagni, F., Muller, J.F., Young, L.J., and Rainnie, D.G. (2011). Neuroanatomical evidence for reciprocal regulation of the corticotrophin-releasing factor and oxytocin systems in the hypothalamus and the bed nucleus of the stria terminalis of the rat: Implications for balancing stress and affect. *Psychoneuroendocrinology* 36, 1312–1326. <https://doi.org/10.1016/j.psyneuen.2011.03.003>.
34. Knobloch, H.S., Charlet, A., Hoffmann, L.C., Eliava, M., Khrulev, S., Cetin, A.H., Osten, P., Schwarz, M.K., Seeburg, P.H., Stoop, R., et al. (2012). Evoked axonal oxytocin release in the central amygdala attenuates fear response. *Neuron* 73, 553–566. <https://doi.org/10.1016/j.neuron.2011.11.030>.

35. Dabrowska, J., Hazra, R., Guo, J.-D., Li, C., DeWitt, S., Xu, J., Lombroso, P.J., and Rainnie, D.G. (2013). Striatal-Enriched Protein Tyrosine Phosphatase—STEPS Toward Understanding Chronic Stress-Induced Activation of Corticotrophin Releasing Factor Neurons in the Rat Bed Nucleus of the Stria Terminalis. *Biological Psychiatry* 74, 817–826. <https://doi.org/10.1016/j.biopsych.2013.07.032>.
36. Dabrowska, J., Hazra, R., Guo, J.-D., DeWitt, S., and Rainnie, D.G. (2013). Central CRF neurons are not created equal: phenotypic differences in CRF-containing neurons of the rat paraventricular hypothalamus and the bed nucleus of the stria terminalis. *Front. Neurosci.* 7. <https://doi.org/10.3389/fnins.2013.00156>.
37. Hammack, S.E., Mania, I., and Rainnie, D.G. (2007). Differential Expression of Intrinsic Membrane Currents in Defined Cell Types of the Anterolateral Bed Nucleus of the Stria Terminalis. *Journal of Neurophysiology* 98, 638–656. <https://doi.org/10.1152/jn.00382.2007>.
38. Rodríguez-Sierra, O.E., Turesson, H.K., and Pare, D. (2013). Contrasting distribution of physiological cell types in different regions of the bed nucleus of the stria terminalis. *J. Neurophysiol.* 110, 2037–2049. <https://doi.org/10.1152/jn.00408.2013>.
39. Martinon, D., Lis, P., Roman, A.N., Tornesi, P., Applebey, S.V., Buechner, G., Olivera, V., and Dabrowska, J. (2019). Oxytocin receptors in the dorsolateral bed nucleus of the stria terminalis (BNST) bias fear learning toward temporally predictable cued fear. *Transl Psychiatry* 9, 140. <https://doi.org/10.1038/s41398-019-0474-x>.
40. Francesconi, W., Berton, F., Olivera-Pasilio, V., and Dabrowska, J. (2021). Oxytocin excites BNST interneurons and inhibits BNST output neurons to the central amygdala. *Neuropharmacology* 192, 108601. <https://doi.org/10.1016/j.neuropharm.2021.108601>.
41. Althammer, F., Roy, R.K., Lefevre, A., Najjar, R.S., Schoenig, K., Bartsch, D., Eliava, M., Feresin, R.G., Hammock, E.A.D., Murphy, A.Z., et al. (2022). Altered PVN-to-CA2 hippocampal oxytocin pathway and reduced number of oxytocin-receptor expressing astrocytes in heart failure rats. *J Neuroendocrinol* 34, e13166. <https://doi.org/10.1111/jne.13166>.
42. Iwasaki, M., Lefevre, A., Althammer, F., Clauss Creusot, E., Łapieś, O., Petitjean, H., Hilfiger, L., Kerspern, D., Melchior, M., Küppers, S., et al. (2023). An analgesic pathway from parvocellular oxytocin neurons to the periaqueductal gray in rats. *Nat Commun* 14, 1066. <https://doi.org/10.1038/s41467-023-36641-7>.
43. Pomrenze, M.B., Millan, E.Z., Hopf, F.W., Keiflin, R., Maiya, R., Blasio, A., Dadgar, J., Kharazia, V., De Guglielmo, G., Crawford, E., et al. (2015). A Transgenic Rat for Investigating the Anatomy and Function of Corticotrophin Releasing Factor Circuits. *Front Neurosci* 9, 487. <https://doi.org/10.3389/fnins.2015.00487>.
44. Zhang, L., Zetter, M.A., Hernández, V.S., Hernández-Pérez, O.R., Jáuregui-Huerta, F., Krabichler, Q., and Grinevich, V. (2024). Morphological Signatures of Neurogenesis and Neuronal Migration in Hypothalamic Vasopressinergic Magnocellular Nuclei of the Adult Rat. *Int J Mol Sci* 25, 6988. <https://doi.org/10.3390/ijms25136988>.
45. Millan, E.Z., Hopf, F.W., Keiflin, R., Maiya, R., Blasio, A., Dadgar, J., Kharazia, V., De Guglielmo, G., Crawford, E., Janak, P.H., et al. (2015). A Transgenic Rat for Investigating the Anatomy and Function of Corticotrophin Releasing Factor Circuits. *Front. Neurosci.* 9. <https://doi.org/10.3389/fnins.2015.00487>.
46. Pomrenze, M.B., Tovar-Diaz, J., Blasio, A., Maiya, R., Giovanetti, S.M., Lei, K., Morikawa, H., Hopf, F.W., and Messing, R.O. (2019). A Corticotropin Releasing Factor Network in the Extended

Amygdala for Anxiety. *J. Neurosci.* 39, 1030–1043. <https://doi.org/10.1523/JNEUROSCI.2143-18.2018>.

47. Marir, R., Virsolvy, A., Wisniewski, K., Mion, J., Haddou, D., Galibert, E., Meraihi, Z., Desarménien, M.G., and Guillon, G. (2013). Pharmacological characterization of FE 201874, the first selective high affinity rat V_{1A} vasopressin receptor agonist: FE 201874, a selective rat V_{1A} agonist. *Br J Pharmacol* 170, 278–292. <https://doi.org/10.1111/bph.12249>.
48. Griffante, C., Green, A., Curcuruto, O., Haslam, C.P., Dickinson, B.A., and Arban, R. (2005). Selectivity of d[Cha4]AVP and SSR149415 at human vasopressin and oxytocin receptors: evidence that SSR149415 is a mixed vasopressin V1b/oxytocin receptor antagonist. *Br J Pharmacol* 146, 744–751. <https://doi.org/10.1038/sj.bjp.0706383>.
49. Manning, M., Misicka, A., Olma, A., Bankowski, K., Stoev, S., Chini, B., Durroux, T., Mouillac, B., Corbani, M., and Guillon, G. (2012). Oxytocin and Vasopressin Agonists and Antagonists as Research Tools and Potential Therapeutics: Oxytocin and vasopressin agonists and antagonists. *Journal of Neuroendocrinology* 24, 609–628. <https://doi.org/10.1111/j.1365-2826.2012.02303.x>.
50. Desai, N.S., Siegel, J.J., Taylor, W., Chitwood, R.A., and Johnston, D. (2015). MATLAB-based automated patch-clamp system for awake behaving mice. *Journal of Neurophysiology* 114, 1331–1345. <https://doi.org/10.1152/jn.00025.2015>.
51. Dabrowska, J., Martinon, D., Moaddab, M., and Rainnie, D.G. (2016). Targeting Corticotropin-Releasing Factor Projections from the Oval Nucleus of the Bed Nucleus of the Stria Terminalis Using Cell-Type Specific Neuronal Tracing Studies in Mouse and Rat Brain. *J Neuroendocrinol* 28. <https://doi.org/10.1111/jne.12442>.
52. Krashes, M.J., Koda, S., Ye, C., Rogan, S.C., Adams, A.C., Cusher, D.S., Maratos-Flier, E., Roth, B.L., and Lowell, B.B. (2011). Rapid, reversible activation of AgRP neurons drives feeding behavior in mice. *J. Clin. Invest.* 121, 1424–1428. <https://doi.org/10.1172/JCI46229>.
53. Knobloch, H.S., Charlet, A., Hoffmann, L.C., Eliava, M., Khrulev, S., Cetin, A.H., Osten, P., Schwarz, M.K., Seeburg, P.H., Stoop, R., et al. (2012). Evoked Axonal Oxytocin Release in the Central Amygdala Attenuates Fear Response. *Neuron* 73, 553–566. <https://doi.org/10.1016/j.neuron.2011.11.030>.
54. Paxinos, G., and Watson, C. (2009). *The rat brain in stereotaxic coordinates Compact 6. ed.* (Elsevier, Academic Press).
55. Yang, P., Wang, Z., Zhang, Z., Liu, D., Manolios, E.N., Chen, C., Yan, X., Zuo, W., and Chen, N. (2018). The extended application of *The Rat Brain in Stereotaxic Coordinates* in rats of various body weight. *J Neurosci Methods* 307, 60–69. <https://doi.org/10.1016/j.jneumeth.2018.06.026>.
56. Ben-Barak, Y., Russell, J.T., Whitnall, M.H., Ozato, K., and Gainer, H. (1985). Neurophysin in the hypothalamo-neurohypophysial system. I. Production and characterization of monoclonal antibodies. *J Neurosci* 5, 81–97. <https://doi.org/10.1523/JNEUROSCI.05-01-00081.1985>.
57. Williford, K.M., Taylor, A., Melchior, J.R., Yoon, H.J., Sale, E., Negasi, M.D., Adank, D.N., Brown, J.A., Bedenbaugh, M.N., Luchsinger, J.R., et al. (2023). BNST PKC δ neurons are activated by specific aversive conditions to promote anxiety-like behavior. *Neuropsychopharmacol.* <https://doi.org/10.1038/s41386-023-01569-5>.
58. Daniel, S.E., and Rainnie, D.G. (2016). Stress Modulation of Opposing Circuits in the Bed Nucleus of the Stria Terminalis. *Neuropsychopharmacol* 41, 103–125. <https://doi.org/10.1038/npp.2015.178>.

59. Schneider, C.A., Rasband, W.S., and Eliceiri, K.W. (2012). NIH Image to ImageJ: 25 years of image analysis. *Nat Methods* 9, 671–675. <https://doi.org/10.1038/nmeth.2089>.
60. Zaelzer, C., Gizowski, C., Salmon, C.K., Murai, K.K., and Bourque, C.W. (2018). Detection of activity-dependent vasopressin release from neuronal dendrites and axon terminals using sniffer cells. *Journal of Neurophysiology* 120, 1386–1396. <https://doi.org/10.1152/jn.00467.2017>.
61. Thirouin, Z.S., and Bourque, C.W. (2021). Mechanism and function of phasic firing in vasopressin-releasing magnocellular neurosecretory cells. *J Neuroendocrinol* 33. <https://doi.org/10.1111/jne.13048>.
62. Walker, D., and Davis, M. (2002). Quantifying fear potentiated startle using absolute versus proportional increase scoring methods: implications for the neurocircuitry of fear and anxiety. *Psychopharmacology* 164, 318–328. <https://doi.org/10.1007/s00213-002-1213-0>.
63. Viviani, D., Charlet, A., van den Burg, E., Robinet, C., Hurni, N., Abatis, M., Magara, F., and Stoop, R. (2011). Oxytocin selectively gates fear responses through distinct outputs from the central amygdala. *Science* 333, 104–107. <https://doi.org/10.1126/science.1201043>.
64. Owen, S.F., Tuncdemir, S.N., Bader, P.L., Tirko, N.N., Fishell, G., and Tsien, R.W. (2013). Oxytocin enhances hippocampal spike transmission by modulating fast-spiking interneurons. *Nature* 500, 458–462. <https://doi.org/10.1038/nature12330>.
65. Hu, B., Boyle, C.A., and Lei, S. (2021). Activation of Oxytocin Receptors Excites Subicular Neurons by Multiple Signaling and Ionic Mechanisms. *Cereb Cortex* 31, 2402–2415. <https://doi.org/10.1093/cercor/bhaa363>.
66. Migita, K., Hori, N., Manako, J., Saito, R., Takano, Y., and Kamiya, H. (1998). Effects of arginine-vasopressin on neuronal interaction from the area postrema to the nucleus tractus solitarius in rat brain slices. *Neurosci Lett* 256, 45–48. [https://doi.org/10.1016/s0304-3940\(98\)00753-8](https://doi.org/10.1016/s0304-3940(98)00753-8).
67. Boyle, C.A., Hu, B., Quaintance, K.L., and Lei, S. (2021). Involvement of TRPC5 channels, inwardly rectifying K⁺ channels, PLC β and PIP2 in vasopressin-mediated excitation of medial central amygdala neurons. *J Physiol* 599, 3101–3119. <https://doi.org/10.1113/JP281260>.
68. Viviani, D., Charlet, A., van den Burg, E., Robinet, C., Hurni, N., Abatis, M., Magara, F., and Stoop, R. (2011). Oxytocin Selectively Gates Fear Responses Through Distinct Outputs from the Central Amygdala. *Science* 333, 104–107. <https://doi.org/10.1126/science.1201043>.
69. Manning, M., Misicka, A., Olma, A., Bankowski, K., Stoev, S., Chini, B., Durroux, T., Mouillac, B., Corbani, M., and Guillon, G. (2012). Oxytocin and vasopressin agonists and antagonists as research tools and potential therapeutics. *J. Neuroendocrinol.* 24, 609–628. <https://doi.org/10.1111/j.1365-2826.2012.02303.x>.
70. Song, Z., Borland, J.M., Larkin, T.E., O'Malley, M., and Albers, H.E. (2016). Activation of oxytocin receptors, but not arginine-vasopressin V1a receptors, in the ventral tegmental area of male Syrian hamsters is essential for the reward-like properties of social interactions. *Psychoneuroendocrinology* 74, 164–172. <https://doi.org/10.1016/j.psyneuen.2016.09.001>.
71. Waltenspühl, Y., Ehrenmann, J., Vacca, S., Thom, C., Medalia, O., and Plückthun, A. (2022). Structural basis for the activation and ligand recognition of the human oxytocin receptor. *Nat Commun* 13, 4153. <https://doi.org/10.1038/s41467-022-31325-0>.
72. Gimpl, G., and Fahrenholz, F. (2001). The oxytocin receptor system: structure, function, and regulation. *Physiol Rev* 81, 629–683. <https://doi.org/10.1152/physrev.2001.81.2.629>.

73. Sala, M., Braidà, D., Lentini, D., Busnelli, M., Bulgheroni, E., Capurro, V., Finardi, A., Donzelli, A., Pattini, L., Rubino, T., et al. (2011). Pharmacologic rescue of impaired cognitive flexibility, social deficits, increased aggression, and seizure susceptibility in oxytocin receptor null mice: a neurobehavioral model of autism. *Biol Psychiatry* 69, 875–882. <https://doi.org/10.1016/j.biopsych.2010.12.022>.
74. Neumann, I.D., and Landgraf, R. (2012). Balance of brain oxytocin and vasopressin: implications for anxiety, depression, and social behaviors. *Trends Neurosci.* 35, 649–659. <https://doi.org/10.1016/j.tins.2012.08.004>.
75. Chini, B., Mouillac, B., Ala, Y., Balestre, M.N., Trumpp-Kallmeyer, S., Hoflack, J., Elands, J., Hibert, M., Manning, M., and Jard, S. (1995). Tyr115 is the key residue for determining agonist selectivity in the V1a vasopressin receptor. *EMBO J* 14, 2176–2182. <https://doi.org/10.1002/j.1460-2075.1995.tb07211.x>.
76. Song, Z., and Albers, H.E. (2018). Cross-talk among oxytocin and arginine-vasopressin receptors: Relevance for basic and clinical studies of the brain and periphery. *Front Neuroendocrinol* 51, 14–24. <https://doi.org/10.1016/j.yfrne.2017.10.004>.
77. Lowbridge, J., Manning, M., Haldar, J., and Sawyer, W.H. (1977). Synthesis and some pharmacological properties of [4-threonine, 7-glycine]oxytocin, [1-(L-2-hydroxy-3-mercaptopropanoic acid), 4-threonine, 7-glycine]oxytocin (hydroxy[Thr4, Gly7]oxytocin), and [7-Glycine]oxytocin, peptides with high oxytocic-antidiuretic selectivity. *J Med Chem* 20, 120–123. <https://doi.org/10.1021/jm00211a025>.
78. Busnelli, M., Bulgheroni, E., Manning, M., Kleinau, G., and Chini, B. (2013). Selective and potent agonists and antagonists for investigating the role of mouse oxytocin receptors. *J Pharmacol Exp Ther* 346, 318–327. <https://doi.org/10.1124/jpet.113.202994>.
79. Gillard, E.R., Coburn, C.G., de Leon, A., Snissarenko, E.P., Bauce, L.G., Pittman, Q.J., Hou, B., and Currás-Collazo, M.C. (2007). Vasopressin autoreceptors and nitric oxide-dependent glutamate release are required for somatodendritic vasopressin release from rat magnocellular neuroendocrine cells responding to osmotic stimuli. *Endocrinology* 148, 479–489. <https://doi.org/10.1210/en.2006-0995>.
80. Goodson, J.L., and Thompson, R.R. (2010). Nonapeptide mechanisms of social cognition, behavior and species-specific social systems. *Curr Opin Neurobiol* 20, 784–794. <https://doi.org/10.1016/j.conb.2010.08.020>.
81. Lukas, M., and Neumann, I.D. (2013). Oxytocin and vasopressin in rodent behaviors related to social dysfunctions in autism spectrum disorders. *Behav Brain Res* 251, 85–94. <https://doi.org/10.1016/j.bbr.2012.08.011>.
82. Veinante, P., and Freund-Mercier, M.J. (1997). Distribution of oxytocin- and vasopressin-binding sites in the rat extended amygdala: a histoautoradiographic study. *J. Comp. Neurol.* 383, 305–325.
83. Francesconi, W., Berton, F., Olivera-Pasilio, V., and Dabrowska, J. (2021). Oxytocin excites BNST interneurons and inhibits BNST output neurons to the central amygdala. *Neuropharmacology* 192, 108601. <https://doi.org/10.1016/j.neuropharm.2021.108601>.
84. Grundwald, N.J., Benítez, D.P., and Brunton, P.J. (2016). Sex-Dependent Effects of Prenatal Stress on Social Memory in Rats: A Role for Differential Expression of Central Vasopressin-1a Receptors. *J. Neuroendocrinol.* 28. <https://doi.org/10.1111/jne.12343>.

85. Nair, H.P., Gutman, A.R., Davis, M., and Young, L.J. (2005). Central oxytocin, vasopressin, and corticotropin-releasing factor receptor densities in the basal forebrain predict isolation potentiated startle in rats. *J Neurosci* 25, 11479–11488. <https://doi.org/10.1523/JNEUROSCI.2524-05.2005>.
86. Luo, P.X., Zakharenkov, H.C., Torres, L.Y., Rios, R.A., Gegenhuber, B., Black, A.M., Xu, C.K., Minie, V.A., Tran, A.M., Tollkuhn, J., et al. (2022). Oxytocin receptor behavioral effects and cell types in the bed nucleus of the stria terminalis. *Hormones and Behavior* 143, 105203. <https://doi.org/10.1016/j.yhbeh.2022.105203>.
87. Hasan, M.T., Althammer, F., Silva da Gouveia, M., Goyon, S., Eliava, M., Lefevre, A., Kerspern, D., Schimmer, J., Raftogianni, A., Wahis, J., et al. (2019). A Fear Memory Engram and Its Plasticity in the Hypothalamic Oxytocin System. *Neuron* 103, 133-146.e8. <https://doi.org/10.1016/j.neuron.2019.04.029>.
88. Rasie Abdullahi, P., Eskandarian, S., Ghanbari, A., and Rashidy-Pour, A. (2018). Oxytocin receptor antagonist atosiban impairs consolidation, but not reconsolidation of contextual fear memory in rats. *Brain Research* 1695, 31–36. <https://doi.org/10.1016/j.brainres.2018.05.034>.
89. Fam, J., Holmes, N., Delaney, A., Crane, J., and Westbrook, R.F. (2018). Oxytocin receptor activation in the basolateral complex of the amygdala enhances discrimination between discrete cues and promotes configural processing of cues. *Psychoneuroendocrinology* 96, 84–92. <https://doi.org/10.1016/j.psyneuen.2018.06.006>.
90. Missig, G., Ayers, L.W., Schulkin, J., and Rosen, J.B. (2010). Oxytocin Reduces Background Anxiety in a Fear-Potentiated Startle Paradigm. *Neuropsychopharmacol* 35, 2607–2616. <https://doi.org/10.1038/npp.2010.155>.
91. Ayers, L.W., Missig, G., Schulkin, J., and Rosen, J.B. (2011). Oxytocin Reduces Background Anxiety in a Fear-Potentiated Startle Paradigm: Peripheral vs Central Administration. *Neuropsychopharmacol* 36, 2488–2497. <https://doi.org/10.1038/npp.2011.138>.
92. Ayers, L., Agostini, A., Schulkin, J., and Rosen, J.B. (2016). Effects of oxytocin on background anxiety in rats with high or low baseline startle. *Psychopharmacology* 233, 2165–2172. <https://doi.org/10.1007/s00213-016-4267-0>.
93. Olivera-Pasilio, V., and Dabrowska, J. (2023). Fear-Conditioning to Unpredictable Threats Reveals Sex and Strain Differences in Rat Fear-Potentiated Startle (FPS). *Neuroscience* 530, 108–132. <https://doi.org/10.1016/j.neuroscience.2023.08.030>.
94. Neumann, I.D., and Slattery, D.A. (2016). Oxytocin in General Anxiety and Social Fear: A Translational Approach. *Biol. Psychiatry* 79, 213–221. <https://doi.org/10.1016/j.biopsych.2015.06.004>.
95. Walker, D.L., and Davis, M. (2008). Role of the extended amygdala in short-duration versus sustained fear: a tribute to Dr. Lennart Heimer. *Brain Struct Funct* 213, 29–42. <https://doi.org/10.1007/s00429-008-0183-3>.
96. Davis, M., Walker, D.L., Miles, L., and Grillon, C. (2010). Phasic vs Sustained Fear in Rats and Humans: Role of the Extended Amygdala in Fear vs Anxiety. *Neuropsychopharmacol* 35, 105–135. <https://doi.org/10.1038/npp.2009.109>.
97. Yamauchi, N., Takahashi, D., Sugimura, Y.K., Kato, F., Amano, T., and Minami, M. (2018). Activation of the neural pathway from the dorsolateral bed nucleus of the stria terminalis to the central amygdala induces anxiety-like behaviors. *Eur. J. Neurosci.* 48, 3052–3061. <https://doi.org/10.1111/ejn.14165>.

98. Fodor, A., Kovács, K.B., Balázsfi, D., Klausz, B., Pintér, O., Demeter, K., Daviu, N., Rabasa, C., Rotllant, D., Nadal, R., et al. (2016). Depressive- and anxiety-like behaviors and stress-related neuronal activation in vasopressin-deficient female Brattleboro rats. *Physiol Behav* 158, 100–111. <https://doi.org/10.1016/j.physbeh.2016.02.041>.
99. Stoehr, J.D., Cheng, S.W., and North, W.G. (1993). Homozygous Brattleboro rats display attenuated conditioned freezing responses. *Neurosci Lett* 153, 103–106. [https://doi.org/10.1016/0304-3940\(93\)90087-2](https://doi.org/10.1016/0304-3940(93)90087-2).
100. Ambrogi Lorenzini, C., Bucherelli, C., Giachetti, A., and Tassoni, G. (1988). Aversive conditioning of homozygous and heterozygous D.I. Brattleboro rats in the light-dark box. *Physiol Behav* 42, 439–445. [https://doi.org/10.1016/0031-9384\(88\)90173-4](https://doi.org/10.1016/0031-9384(88)90173-4).
101. Pitkow, L.J., Sharer, C.A., Ren, X., Insel, T.R., Terwilliger, E.F., and Young, L.J. (2001). Facilitation of affiliation and pair-bond formation by vasopressin receptor gene transfer into the ventral forebrain of a monogamous vole. *J Neurosci* 21, 7392–7396. <https://doi.org/10.1523/JNEUROSCI.21-18-07392.2001>.
102. Bielsky, I.F., Hu, S.-B., Szegda, K.L., Westphal, H., and Young, L.J. (2004). Profound impairment in social recognition and reduction in anxiety-like behavior in vasopressin V1a receptor knockout mice. *Neuropsychopharmacology* 29, 483–493. <https://doi.org/10.1038/sj.npp.1300360>.
103. Egashira, N., Tanoue, A., Matsuda, T., Koushi, E., Harada, S., Takano, Y., Tsujimoto, G., Mishima, K., Iwasaki, K., and Fujiwara, M. (2007). Impaired social interaction and reduced anxiety-related behavior in vasopressin V1a receptor knockout mice. *Behav Brain Res* 178, 123–127. <https://doi.org/10.1016/j.bbr.2006.12.009>.
104. Appenrodt, E., Schnabel, R., and Schwarzberg, H. (1998). Vasopressin administration modulates anxiety-related behavior in rats. *Physiol Behav* 64, 543–547. [https://doi.org/10.1016/s0031-9384\(98\)00119-x](https://doi.org/10.1016/s0031-9384(98)00119-x).
105. Bredewold, R., and Veenema, A.H. (2018). Sex differences in the regulation of social and anxiety-related behaviors: insights from vasopressin and oxytocin brain systems. *Curr. Opin. Neurobiol.* 49, 132–140. <https://doi.org/10.1016/j.conb.2018.02.011>.
106. Whylings, J., Rigney, N., Peters, N.V., de Vries, G.J., and Petruslis, A. (2020). Sexually dimorphic role of BNST vasopressin cells in sickness and social behavior in male and female mice. *Brain, Behavior, and Immunity* 83, 68–77. <https://doi.org/10.1016/j.bbi.2019.09.015>.
107. Whylings, J., Rigney, N., de Vries, G.J., and Petruslis, A. (2021). Reduction in vasopressin cells in the suprachiasmatic nucleus in mice increases anxiety and alters fluid intake. *Horm Behav* 133, 104997. <https://doi.org/10.1016/j.yhbeh.2021.104997>.
108. Busnelli, M., and Chini, B. (2018). Molecular Basis of Oxytocin Receptor Signalling in the Brain: What We Know and What We Need to Know. *Curr Top Behav Neurosci* 35, 3–29. https://doi.org/10.1007/7854_2017_6.
109. Marir, R., Virsolvy, A., Wisniewski, K., Mion, J., Haddou, D., Galibert, E., Meraihi, Z., Desarménien, M.G., and Guillon, G. (2013). Pharmacological characterization of FE 201874, the first selective high affinity rat V1A vasopressin receptor agonist. *Br J Pharmacol* 170, 278–292. <https://doi.org/10.1111/bph.12249>.
110. Pena, A., Murat, B., Trueba, M., Ventura, M.A., Wo, N.C., Szeto, H.H., Cheng, L.L., Stoev, S., Guillon, G., and Manning, M. (2007). Design and synthesis of the first selective agonists for the

rat vasopressin V(1b) receptor: based on modifications of deamino-[Cys1]arginine vasopressin at positions 4 and 8. *J Med Chem* 50, 835–847. <https://doi.org/10.1021/jm060928n>.

111. Manning, M., Misicka, A., Olma, A., Bankowski, K., Stoev, S., Chini, B., Durroux, T., Mouillac, B., Corbani, M., and Guillon, G. (2012). Oxytocin and vasopressin agonists and antagonists as research tools and potential therapeutics. *J. Neuroendocrinol.* 24, 609–628. <https://doi.org/10.1111/j.1365-2826.2012.02303.x>.
112. Serradeil-Le Gal, C., Wagnon, J., Garcia, C., Lacour, C., Guiraudou, P., Christophe, B., Villanova, G., Nisato, D., Maffrand, J.P., and Le Fur, G. (1993). Biochemical and pharmacological properties of SR 49059, a new, potent, nonpeptide antagonist of rat and human vasopressin V1a receptors. *J Clin Invest* 92, 224–231. <https://doi.org/10.1172/JCI116554>.
113. Griffante, C., Green, A., Curcuruto, O., Haslam, C.P., Dickinson, B.A., and Arban, R. (2005). Selectivity of d[Cha4]AVP and SSR149415 at human vasopressin and oxytocin receptors: evidence that SSR149415 is a mixed vasopressin V1b/oxytocin receptor antagonist. *Br J Pharmacol* 146, 744–751. <https://doi.org/10.1038/sj.bjp.0706383>.
114. Allen Institute for Brain Science. (2024). *Allen Mouse Brain Atlas (2004)*. Retrieved from <https://mouse.brain-map.org> (Accessed March 30, 2024). <http://atlas.brain-map.org/atlas?atlas=1#atlas=1&plate=100960312&structure=554&x=5222.879464285715&y=3571.841212681362&zoom=-3&resolution=11.97&z=6>

Table 1. The effect of OTR and V1R activation on intrinsic membrane properties of Type I-III BNST_{DL} neurons

Type of Neuron	Treatment	Membrane Properties	Pre-Treatment (Mean ± SEM)	Post-Treatment (Mean ± SEM)	Statistical Analysis	p-value	n
Type I	AVP	RMP (mV)	-59.1±1.77	-53.87±1.25	F(2, 15)=6.340	0.0101	9
		Rin (MΩ)	139.54±11.74	165.42±16.62	F(1.774, 13.31)=5.695	0.0187	9
		Rh (pA)	27.08±3.24	15.42±2.01	F(2, 13)=7.374	0.0072	8
		First-spike Th (mV)	-35.83±0.79	-35.80±0.65	F(1.300, 9.750)=0.6786	0.4681	9
		First-spike Lat (ms)	221.50±56.41	137.50±33.78	F(2, 15)=7.393	0.0058	9
<i>OTR antagonist</i>	OTA + AVP	RMP (mV)	-63.17±1.48	-57.04±2.15	F(1.088, 9.788)=6.851	0.0244	10
		Rin (MΩ)	191.60±15.27	202.60±14.01	F(1.719, 15.47)=5.789	0.0162	10
		Rh (pA)	36.58±4.16	30.17±4.73	F(1.584, 14.26)=1.938	0.1840	10
		First-spike Th (mV)	-35.38± 0.71	-35.72±0.88	F(1.720, 15.48)=0.3976	0.6484	10
		First-spike Lat (ms)	188.20±33.61	134.30±32.14	F(1.967, 17.70)=4.366	0.0293	9
<i>V1aR antagonist</i>	SR49059 + AVP	RMP (mV)	-64.22 ± 1.93	-62.47 ± 2.12	F(1.571, 12.57)=5.548	0.0240	9
		Rh (pA)	45.37 ± 7.00	38.61 ± 6.76	F(1.806, 14.45)=6.361	0.0120	9
		Rin (MΩ)	180.1 ± 15.50	202.1 ± 16.27	F(1.216, 9.730)=3.353	0.0930	9
		First-spike Lat (ms)	161.1 ± 18.26	143.4 ± 21.08	F(1.273, 10.19)=0.7476	0.4393	9
		Th (mV)	-36.23 ± 1.51	-34.88 ± 1.72	F(1.260, 10.08)=2.523	0.1401	9
<i>V1bR antagonist</i>	Nelivaptan + AVP	RMP (mV)	-63.13±2.28	-56.76±2.73	F(1.352, 12.17)=15.50	0.0010	10
		Rin (MΩ)	189.5±16.30	214.6±17.92	F(1.421, 12.79)=4.299	0.0480	10
		Rh (pA)	39.50±5.70	31.00±5.36	F(1.387, 12.48)=8.143	0.0093	10
		First-spike Th (mV)	-30.28±1.69	-28.59±2.22	F(1.292, 11.63)=2.541	0.1335	10
		First-spike Lat (ms)	187.2±28.40	113.6±18.15	F(1.707, 15.37)=6.963	0.0090	10
Type II	AVP	RMP (mV)	-53.12±1.46	-51.29±1.69	F(1.155, 6.927)=2.219	0.1815	8
		Rin (MΩ)	135.9±15.83	151.3±21.57	F(2,12)= 3.348	0.0699	8
		Rh (pA)	25.10±5.39	25.62±8.73	F(1.016, 6.095)=0.08300	0.7867	8
		First-spike Th (mV)	-36.82±0.82	-34.65±1.53	F(1.818, 10.91)=1.199	0.3336	8

Type of Neuron	Treatment	Membrane Properties	Pre-Treatment (Mean ± SEM)	Post-Treatment (Mean ± SEM)	Statistical Analysis	p-value	n
		First-spike Lat (ms)	97.3±7.3	75.27±8.7	F(1.403, 8.415)=1.146	0.3397	8
Type III	AVP	RMP (mV)	-68.34±1.36	-65±1.93	F(2, 15)=5.717	0.0143	10
		Rin (MΩ)	108.8±10.29	128.9±13.83	F(1.602, 5.608)=30.90	0.0011	5
		Rh (pA)	75.15±9.45	63.5±9.65	F(1.114, 8.356)=12.18	0.0068	10
		First-spike Th (mV)	-33.12±1.89	-33.46±1.92	F(1.187, 8.902)=0.4559	0.5495	10
		First-spike Lat (ms)	419.08±64.09	257.5±52.13	F(1.869, 13.08)=11.79	0.0014	10
	OTR/V1aR Antagonist + AVP	RMP (mV)	-69.79±1.21	-67.97±1.17	F(1.211, 7.264)=3.616	0.0936	7
		Rin (MΩ)	94.74±16.92	97.37±17.56	F(1.904, 11.42)=2.037	0.1761	7
		Rh (pA)	88.33±8.97	83.33±4.42	F(1.335, 8.007)=0.8376	0.4213	7
		First-spike Th (mV)	-33.41±0.95	-34.69±0.79	F(1.344, 8.063)=2.478	0.1517	7
		First-spike Lat (ms)	203.2±29.08	176.2±32.81	F(1.174, 7.041)=0.3909	0.5843	7
	OTA + AVP	RMP (mV)	-67.37±1.72	-66.59±1.9	F(1.039, 6.235)=0.6159	0.4675	7
		Rin (MΩ)	110.99±8.5	132.79±15.	F(1.042, 4.169)=5.504	0.0758	5
		Rh (pA)	77.02±10.75	75.71±12.74	F(1.197, 7.185)=0.0635	0.8495	7
		First-spike Th (mV)	-38.86±1.96	-37.58±2.46	F(1.926, 11.56)=1.482	0.2667	7
		First-spike Lat (ms)	327.6±60.45	300.3±60.50	F(2, 10)=0.5830	0.5761	6
	SR49059 + AVP	RMP (mV)	-66.95 ± 1.88	-63.94 ± 2.38	F(1.341, 9.386)=11.51	0.0052	8
		Rin (MΩ)	159 ± 13.93	181.5 ± 14.85	F(1.764, 12.35)=5.944	0.0179	8
		Rh (pA)	68.96± 7.48	56.67 ± 7.13	F(1.249, 8.745)=7.536	0.0193	8
		First-spike Th (mV)	-34.09 ± 1.33	-33.25 ± 2.33	F(1.844, 12.91)=1.825	0.2014	8
		First-spike Lat (ms)	404 ± 72.91	261.2 ± 65.96	F(1.546, 10.83)=7.551	0.0121	8
	Nelivaptan + AVP	RMP (mV)	-74.24 ± 1.46	-69.45 ± 1.74	F(1.331 10.65) = 15.67	0.0014	9
		Rin (MΩ)	124.9 ± 9.76	186.6 ± 24.8	F(1.196, 9.565) = 9.060	0.0114	9
		Rh (pA)	94.44 ± 5.86	84.26 ± 6.5	F(1.507, 12.06) = 5.441	0.0272	9

Type of Neuron	Treatment	Membrane Properties	Pre-Treatment (Mean ± SEM)	Post-Treatment (Mean ± SEM)	Statistical Analysis	p-value	n
		First-spike Th (mV)	-29.9 ± 1.76	-24.24 ± 3.12	F(1.077, 8.613) = 4.558	0.0610	9
		First-spike Lat (ms)	377.2 ± 64.25	248.4 ± 37.86	F(1.539, 12.31) = 4.491	0.0402	9
Type III	OT	RMP (mV)	-68.54±1.03	-67.79±0.87	F(2, 13)=1.374	0.2875	8
		Rin (MΩ)	137.15±23.61	142.41±26.16	F(0.8062, 3.628)=14.14	0.0251	6
		Rh (pA)	83.02±4.81	69.33±4.74	F(2, 13)=13.22	0.0007	8
		First-spike Th (mV)	-29.27±1.86	-29.49±1.98	F(0.04181, 0.2717)=2.479	0.1480	8
		First-spike Lat (ms)	497.8±63.95	281.05±43.37	F(1.827, 10.96)=11.13	0.0027	8
<i>OTR agonist</i>	TGOT	RMP (mV)	-71.86±1.00	-70.00±1.22	F(1.168, 8.177)=5.241	0.0469	9
		Rin (MΩ)	85.79±6.63	91.24±7.02	F(1.076, 4.841)=8.456	0.0338	7
		Rh (pA)	93.61±9.88	82.69±10.97	F(1.776, 11.54)=6.129	0.0174	9
		First-spike Th (mV)	-30.84±0.98	-30.79±1.13	F(1.120, 7.838)=0.6998	0.4439	9
		First-spike Lat (ms)	594.03±76.46	355.24±68.69	F(0.9019, 5.412)=7.726	0.0373	9
<i>V1aR agonist</i>	FE 201874	RMP (mV)	-70.72±0.9	-69.44±1.25	F(1.242, 9.312)=3.093	0.1068	10
		Rin (MΩ)	118.21±1.25	117.57±9.69	F(1.219, 6.094)=0.2128	0.70748	7
		Rh (pA)	77.83±9.55	73.66±10.5	F(1.209, 9.066)=1.728	0.2256	10
		First-spike Th (mV)	-30.45±1.22	-31.93±1.1	F(1.550, 11.63)=2.515	0.1312	10
		First-spike Lat (ms)	432.8±65.72	345.3±57.68	F(1.710, 11.12)=3.780	0.0610	9
<i>V1bR agonist</i>	d[Cha4]-AVP	RMP (mV)	-70.42±0.84	-69.81±1.15	F(1.987, 12.91)=1.327	0.2988	8
		Rin (MΩ)	105.18±7.85	110.98±10.05	F(0.9314, 6.054)=2.663	0.1532	8
		Rh (pA)	86.25±5.96	81.46±6.2	F(1.160, 7.540)=1.193	0.3195	8
		First-spike Th (mV)	-33.38±1.67	-34.00±1.79	F(0.9257, 6.017)=2.467	0.1666	8
		First-spike Lat (ms)	475.1±59.48	426.6±60.20	F(1.063, 5.848)=10.24	0.0185	8

Supplementary Materials

Supplementary Table 1. Pharmacological compounds used to manipulate OTR, V1aR, and V1bR

Compound	Alternative name, Abbreviation	Company Catalog #	Concentration	Receptor activity profile
Arginine-vasopressin	AVP, Arg ⁸ -vasopressin	Bachem Americas, #4012215	0.2 μM	V1R, V2, and OTR agonist ⁶⁶
Oxytocin	OT	Bachem Americas, #4016373	0.2 μM	OTR and V1R agonist ¹⁰⁸
(Thr ⁴ , Gly ⁷)-Oxytocin H-Cys-Tyr-Asn-Cys-Gly-Leu-Gly-NH ₂	TGOT	Bachem Americas, 4013837	0.4 μM	Selective OTR agonist ⁶⁵
FE 201874		Ferring Pharmaceuticals	0.2-0.4 μM	Selective V1aR agonist, OTR antagonist ¹⁰⁹
d(Cha4)-AVP		GLP BIO, #GC1659	1 μM	Selective V1bR agonist ¹¹⁰
(d(CH ₂) ₅ ¹ , Tyr(Me) ² , Arg ⁸)-vasopressin	Manning compound	Tocris, Bio-Techne Corporation, #3377	1 μM	V1aR/OTR receptor antagonist ¹¹¹
SR 49059	Relcovaptan	Tocris, Bio-Techne Corporation, #2310	5 μM	Selective V1aR antagonist ¹¹²
d(CH ₂) ₅ (1), D-Tyr(2), Thr(4), Orn(8), des-Gly-NH ₂ (9)]-Vasotocin	OTA	Chemical Repository, #V-905 NIMH	0.4 μM	Selective OTR antagonist ¹¹⁰
SSR 149415	Nelivaptan	Tocris, Bio-Techne Corporation, #6195	1 μM	Selective V1bR antagonist ¹¹³

Supplementary results

1. The effect of AVP on intrinsic membrane properties of Type I BNST_{DL} neurons

We first determined the effect of AVP on membrane properties of Type I-III BNST_{DL} neurons (see **Table 1**). In Type I neurons, AVP induced a significant depolarization of the RMP (mV) from -59.1 ± 1.77 to -53.87 ± 1.25 ($P=0.0101$, $F(2, 15)=6.340$, $n=9$, mixed-effect model). This change was associated with a significant increase in R_{in} ($M\Omega$; at -100 pA) from 139.54 ± 11.74 to 165.42 ± 16.62 ($P=0.0187$, $F(1.774, 13.31)=5.695$, $n=9$). AVP induced a significant reduction in R_h (pA) from 27.08 ± 3.24 to 15.42 ± 2.01 ($P=0.0072$, $F(2, 13)=7.374$, $n=8$). The first-spike Th (mV) was not significantly changed from -35.83 ± 0.79 to -35.80 ± 0.65 after AVP ($P=0.4681$, $F(1.300, 9.750)=0.6786$, $n=9$), but the first-spike Lat (ms) was significantly reduced from 221.50 ± 56.41 to 137.50 ± 33.78 ($P=0.0058$, $F(2, 15)=7.393$, $n=9$, mixed-effect analysis).

In the presence of the OTR antagonist, OTA, AVP did not significantly affect the R_h (pA) at 36.58 ± 4.16 and 30.17 ± 4.73 ($P=0.1840$, $F(1.584, 14.26)=1.938$, $n=10$), or first-spike Th (mV) at -35.38 ± 0.71 and -35.72 ± 0.88 ($P=0.6484$, $F(1.720, 15.48)=0.3976$, $n=10$). The first-spike Lat (ms), however, was significantly reduced from 188.20 ± 33.61 to 134.30 ± 32.14 ($P=0.0293$, $F(1.967, 17.70)=4.366$, $n=9$, RM one-way ANOVA), but multiple comparisons only showed a trend in differences between the groups ($P=0.0599$, pre vs. OTA+AVP). There was also a treatment effect on the RMP (in mV) from -63.17 ± 1.48 to -57.04 ± 2.15 ($P=0.0244$, $F(1.088, 9.788)=6.851$, $n=10$), but multiple comparisons showed that this effect was driven by OTA alone ($P=0.0497$, pre vs. OTA). Lastly, R_{in} ($M\Omega$) (at -100 pA) was increased from 191.60 ± 15.27 to 202.60 ± 14.01 ($P=0.0162$, $F(1.719, 15.47)=5.789$, $n=10$), but multiple comparisons showed only a trend for the AVP effect ($P=0.0575$, pre vs. OTA+AVP).

In contrast, AVP application in a presence of V1aR antagonist, SR49059, induced a significant depolarization of RMP (mV) from -64.22 ± 1.93 to -62.47 ± 2.12 ($P=0.0240$, $F(1.571, 12.57)=5.548$, $n=9$, RM ANOVA), and the R_h (pA) from 45.37 ± 7.00 to 38.61 ± 6.76 ($P=0.0120$, $F(1.806, 14.45)=6.361$). However, it did not affect R_{in} ($M\Omega$) from 180.1 ± 15.50 to 202.1 ± 16.27 (-100 pA, $P=0.0930$, $F(1.216, 9.730)=3.353$), the first-spike Lat (ms) from 161.1 ± 18.26 to 143.4 ± 21.08 ($P=0.4393$, $F(1.273, 10.19)=0.7476$), or Th (mV) from -36.23 ± 1.51 to -34.88 ± 1.72 ($P=0.1401$, $F(1.260, 10.08)=2.523$).

AVP application in the presence of the V1bR antagonist Nelivaptan significantly reduced the RMP (mV) from -63.13 ± 2.28 to -56.76 ± 2.73 ($P=0.0010$, $F(1.352, 12.17)=15.50$, $n=10$, RM one-way ANOVA) and the R_h (pA) from 39.50 ± 5.70 to 31.00 ± 5.36 ($P=0.0093$, $F(1.387, 12.48)=8.143$, $n=10$). It also increased the R_{in} ($M\Omega$) (at -250 pA) from 189.5 ± 16.30 to 214.6 ± 17.92 ($P=0.0480$, $F(1.421, 12.79)=4.299$, $n=10$). While there was no effect on first-spike Th (mV) at -30.28 ± 1.69 and -28.59 ± 2.22

($P=0.1335$, $F(1.292, 11.63)=2.541$, $n=10$), the first-spike Lat (ms) was reduced from 187.2 ± 28.40 to 113.6 ± 18.15 ($P=0.0090$, $F(1.707, 15.37)=6.963$, $n=10$) after Nelivaptan and AVP application.

2. The effect of AVP on membrane properties of Type II BNST_{DL} neurons

AVP did not induce a significant depolarization of the RMP (mV) in Type II BNST_{DL} neurons from -53.12 ± 1.46 to -51.29 ± 1.69 ($P=0.1815$, $F(1.155, 6.927)=2.219$, $n=8$, mixed-effect analysis). Rin (M Ω) (at -100 pA) remained unchanged at 135.9 ± 15.83 and 151.3 ± 21.57 ($P=0.0699$, $F(2, 12)=3.348$, $n=8$), as did Rh (pA) at 25.10 ± 5.39 and 25.62 ± 8.73 ($P=0.7867$, $F(1.016, 6.095)=0.08300$, $n=8$). Similarly, neither the first-spike Th (mV) at -36.82 ± 0.82 and -34.65 ± 1.53 ($P=0.3336$, $F(1.818, 10.91)=1.199$, $n=8$), nor the first-spike Lat (ms) at 97.3 ± 7.3 and 75.27 ± 8.7 ($P=0.3397$, $F(1.403, 8.415)=1.146$, $n=8$) were changed after AVP.

3. The effect of AVP on membrane properties of Type III BNST_{DL} neurons

In Type III neurons, AVP induced a significant depolarization of RMP (mV) from -68.34 ± 1.36 to -65.1 ± 1.93 ($P=0.0143$, $F(2, 15)=5.717$, $n=10$, mixed-effect analysis), associated with a significant increase in Rin (M Ω ; at -100 pA) from 108.8 ± 10.29 to 128.9 ± 13.83 ($P=0.0011$, $F(1.602, 5.608)=30.90$, $n=5$). Consequently, the Rh (pA) was significantly reduced from 75.15 ± 9.45 to 63.5 ± 9.65 ($P=0.0068$, $F(1.114, 8.356)=12.18$, $n=10$). The first-spike Th (mV) was not changed, at -33.12 ± 1.89 and -33.46 ± 1.92 before and after AVP, respectively ($P=0.5495$, $F(1.187, 8.902)=0.4559$, $n=10$), but AVP induced a significant reduction in the first-spike Lat (ms) from 419.08 ± 64.09 to 257.5 ± 52.13 ($P=0.0014$, $F(1.869, 13.08)=11.79$, $n=10$).

Next, we applied a series of OTR/V1R antagonists to determine whether the effects of AVP were mediated via V1aR, V1bR, or OTR. In the presence of the OTR/V1aR antagonist ($(d(CH_2)_5^1, Tyr(Me)^2, Arg^8)$ -Vasopressin), AVP did not affect the RMP (mV) at -69.79 ± 1.21 and -67.97 ± 1.17 ($P=0.0936$, $F(1.211, 7.264)=3.616$, $n=7$, RM one-way ANOVA), Rin (M Ω) (at -100 pA) at 94.74 ± 16.92 and 97.37 ± 17.56 ($P=0.1761$, $F(1.904, 11.42)=2.037$, $n=7$), Rh (pA) at 88.33 ± 8.97 and 83.33 ± 4.42 ($P=0.4213$, $F(1.335, 8.007)=0.8376$, $n=7$), first-spike Th (mV) at -33.41 ± 0.95 and -34.69 ± 0.79 ($P=0.1517$, $F(1.344, 8.063)=2.478$, $n=7$), or first-spike Lat (ms) at 203.2 ± 29.08 and 176.2 ± 32.8 ($P=0.5843$, $F(1.174, 7.041)=0.3909$, $n=7$) before and after AVP application, respectively.

Further, in the presence of OTA, AVP did not significantly affect RMP (mV) at -67.37 ± 1.72 and -66.59 ± 1.9 ($P=0.4675$, $F(1.039, 6.235)=0.6159$, $n=7$, RM one-way ANOVA), Rin (M Ω , at -100 pA) at 110.99 ± 8.5 and 132.79 ± 15 ($P=0.0758$, $F(1.042, 4.169)=5.504$, $n=5$), Rh (pA) at 77.02 ± 10.75 and 75.71 ± 12.74 ($P=0.8495$, $F(1.197, 7.185)=0.06355$, $n=7$), first-spike Th (mV) at -38.86 ± 1.96 and -37.58 ± 2.46 ($P=0.2667$, $F(1.926, 11.56)=1.482$, $n=7$, RM one-way ANOVA), or first-spike Lat (ms) at

327.56±60.45 and 300.3±60.50 ($P=0.5761$, $F(2, 10)=0.5830$, $n=6$) before and after AVP application, respectively.

However, in the presence of the V1aR antagonist, SR49059, AVP induced a significant depolarization of RMP (mV) from -66.95 ± 1.88 to -63.94 ± 2.38 ($P=0.0052$, $F(1.341, 9.386)=11.51$, $n=8$, RM one-way ANOVA) and a significant increase in R_{in} ($M\Omega$) (at -100 pA) from 159 ± 13.93 to 181.5 ± 14.85 ($P=0.0179$, $F(1.764, 12.35)=5.944$, $n=8$), as well as a significant decrease in R_h (pA) from 68.96 ± 7.48 to 56.67 ± 7.13 ($P=0.0193$, $F(1.249, 8.745)=7.536$, $n=8$). The first-spike Lat (ms) was also significantly decreased when AVP was applied in the presence of the V1aR blocker, from 404.0 ± 72.91 to 261.2 ± 65.96 ($P=0.0121$, $F(1.546, 10.83)=7.551$, $n=8$). Consistent with the effects of AVP alone, AVP in the presence of SR49059 did not change the first-spike Th (mV), at -34.09 ± 1.33 and -33.25 ± 2.33 ($P=0.2014$, $F(1.844, 12.91)=1.825$, $n=8$) before and after AVP, respectively.

Lastly, in the presence of the V1bR antagonist, Nelivaptan, AVP induced a significant depolarization of RMP (mV) from -74.24 ± 1.46 to -69.45 ± 1.74 ($P=0.0014$, $F(1.331, 10.65)=15.67$, $n=9$, RM one-way ANOVA) and a significant increase in R_{in} ($M\Omega$) (at -250 pA) from 124.9 ± 9.76 to 186.6 ± 24.80 ($P=0.0114$, $F(1.196, 9.565)=9.060$, $n=9$), as well as a significant decrease in R_h (pA) from 94.44 ± 5.86 to 84.26 ± 6.50 ($P=0.0272$, $F(1.507, 12.06)=5.441$, $n=9$). The first-spike Lat (ms) was significantly reduced when AVP was applied in the presence of the V1bR antagonist, Nelivaptan, from 377.2 ± 64.25 to 248.4 ± 37.86 ($P=0.0420$, $F(1.539, 12.31)=4.491$, $n=9$). Consistently with the effects of AVP alone, the first-spike Th (mV) was not changed, at -29.90 ± 1.76 and -24.24 ± 3.12 ($P=0.0610$, $F(1.077, 8.613)=4.558$, $n=9$) before and after AVP application, respectively.

These results suggest that AVP excites Type III BNST_{DL} neurons via a direct postsynaptic mechanism that involves OTR but not V1aR or V1bR activation.

4. The effect of OT on membrane properties of Type III BNST_{DL} neurons

OT did not induce a significant depolarization of the RMP (mV) in Type III BNST_{DL} neurons, at -68.54 ± 1.03 and -67.79 ± 0.87 ($P=0.2875$, $F(2, 13)=1.374$, $n=8$, mixed-effect analysis). R_{in} ($M\Omega$) (at -100 pA) significantly changed from 137.15 ± 23.61 to 142.41 ± 26.16 ($P=0.0251$, $F(0.8062, 3.628)=14.14$, $n=6$), as did R_h (pA), at 83.02 ± 4.81 and 69.33 ± 4.74 ($P=0.0007$, $F(2, 13)=13.22$, $n=8$). Similarly to the AVP effect, the first-spike Th (mV) was not changed by OT at -29.27 ± 1.86 and -29.49 ± 1.98 ($P=0.1480$, $F(0.04181, 0.2717)=2.479$, $n=8$) but the first-spike Lat (ms) significantly changed with OT application from 497.8 ± 63.95 to 281.05 ± 43.37 ($P=0.0027$, $F(1.827, 10.96)=11.13$, $n=8$).

5. The effect of OTR agonist, TGOT, on membrane properties of Type III BNST_{DL} neurons

The results above imply that AVP affects the membrane properties of Type III BNST_{DL} neurons via OTR. Thus, we next applied a potent OTR agonist, TGOT. TGOT induced a significant depolarization of the RMP (mV) from -71.86 ± 1.00 to -70.00 ± 1.22 ($P=0.0469$, $F(1.168, 8.177)=5.241$, $n=9$, mixed-effect analysis) and a significant increase in Rin (M Ω) (at -100 pA) from 85.79 ± 6.63 to 91.24 ± 7.02 ($P=0.0338$, $F(1.076, 4.841)=8.456$, $n=7$). TGOT significantly decreased Rh (pA) from 93.61 ± 9.88 to 82.69 ± 10.97 ($P=0.0174$, $F(1.776, 11.54)=6.129$, $n=9$) and decreased the first-spike Lat (ms) from 594.03 ± 76.46 to 355.243 ± 68.69 ($P=0.0373$, $F(0.9019, 5.412)=7.726$, $n=9$). Similarly to the effect of AVP and OT, TGOT did not significantly change the first-spike Th (mV), at -30.84 ± 0.98 and -30.79 ± 1.13 ($P=0.4439$, $F(1.120, 7.838)=0.6998$, $n=9$) before and after TGOT, respectively. These results confirm the primary contribution of OTR to the effects of AVP on membrane properties of Type III BNST_{DL} neurons.

6. The effect of V1aR agonist, FE 201874, on membrane properties of Type III BNST_{DL} neurons

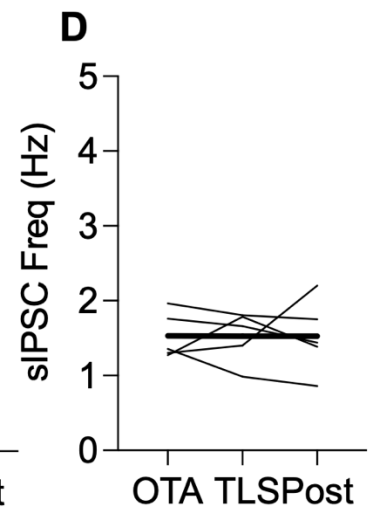
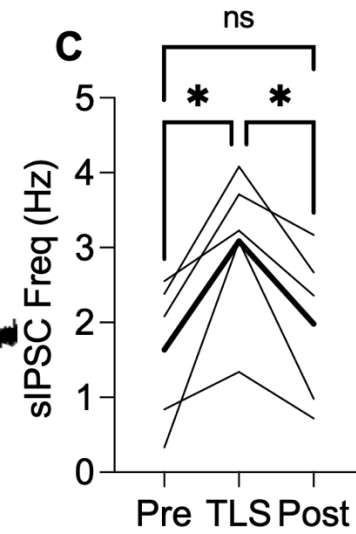
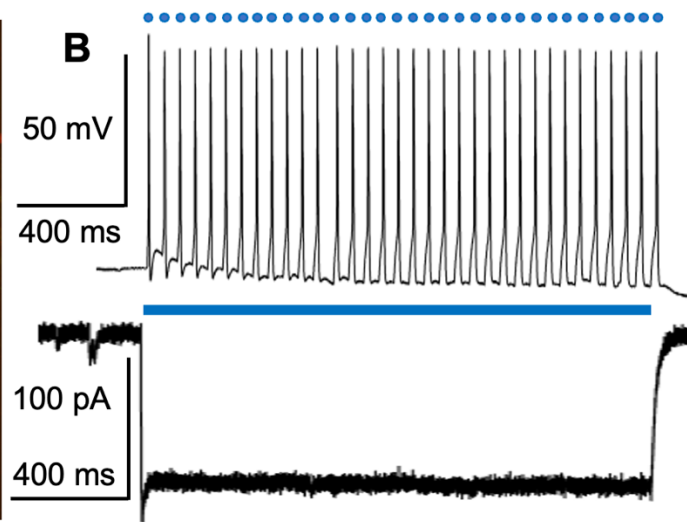
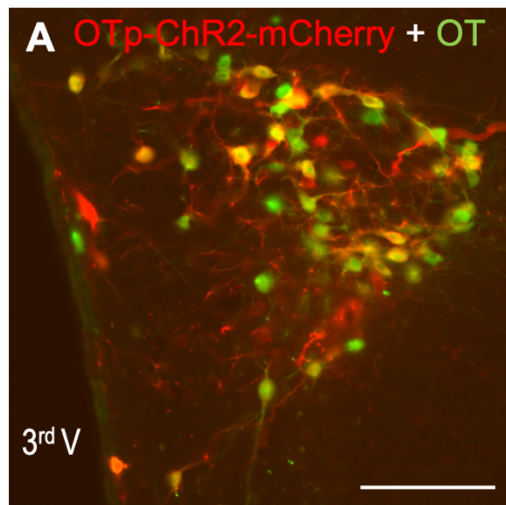
In contrast to TGOT, application of the selective rat V1aR agonist, FE 201874, did not change the RMP (mV) at -70.72 ± 0.9 and -69.44 ± 1.25 ($P=0.1068$, $F(1.242, 9.312)=3.093$, $n=10$, mixed-effect analysis), Rin (M Ω) (at -250 pA) at 118.21 ± 1.25 and 117.57 ± 9.69 ($P=0.70748$, $F(1.219, 6.094)=0.2128$, $n=7$, mixed-effect analysis), Rh (pA) at 77.83 ± 9.55 and 73.66 ± 10.5 ($P=0.2256$, $F(1.209, 9.066)=1.728$, $n=10$), first-spike Lat (ms) at 432.8 ± 65.72 and 345.3 ± 57.68 ($P=0.0610$, $F(1.710, 11.12)=3.780$, $n=9$), or first-spike Th (mV) at -30.45 ± 1.22 and -31.93 ± 1.1 ($P=0.1312$, $F(1.550, 11.63)=2.515$, $n=10$) before and after FE 201874 application, respectively.

7. The effect of V1bR agonist, d[Cha4]-AVP, on membrane properties of Type III BNST_{DL} neurons

V1bR agonist, d[Cha4]-AVP, did not change the RMP (mV) in Type III BNST_{DL} neurons, with a RMP of -70.42 ± 0.84 and -69.81 ± 1.15 pre and post V1bR agonist application, respectively ($P=0.2988$, $F(1.987, 12.91)=1.327$, $n=8$, mixed-effect analysis). Rin (M Ω) (at -250 pA) remained unchanged at 105.18 ± 7.85 and 110.98 ± 10.05 ($P=0.1532$, $F(0.9314, 6.054)=2.663$, $n=8$), as did Rh (pA), at 86.25 ± 5.96 and 81.46 ± 6.2 ($P=0.3195$, $F(1.160, 7.540)=1.193$, $n=8$). Similarly, the first-spike Th (mV) was not significantly changed at -33.38 ± 1.67 and -34.00 ± 1.79 by the V1bR agonist ($P=0.1666$, $F(0.9257, 6.017)=2.467$, $n=8$). However, the first-spike Lat (ms) was significantly changed from 475.1 ± 59.48 to 426.6 ± 60.20 before and after V1bR agonist ($P=0.0185$, $F(1.063, 5.848)=10.24$, $n=8$).

Supplementary figure 1 legend

TLS evokes OT release and increased inhibitory synaptic transmission in Type II BNST_{DL} neurons in an OTR-dependent manner. **A:** High somatodendritic expression of ChR2-mCherry (red) is observed in hypothalamic OT neurons (mouse anti-OT MAB5296 antibody, green) 3 weeks after AAV-OTp-ChR2-mCherry was injected to the PVN in male rats (20x, scale bar 100 μ m). **B:** Action potentials recorded from PVN neurons expressing ChR2-mCherry, evoked by 10 ms repeated (30 Hz, 1 sec) blue light stimulation (upper panel) and current induced by 1 sec continuous blue light (bottom panel). **C:** In the BNST_{DL} from rats injected as above, TLS (30 Hz train, single pulse duration 10 ms for 20 sec) increased frequency of spontaneous inhibitory postsynaptic currents (sIPSCs) in Type II BNST_{DL} neurons ($F(1.436, 7.182)=16.86$, $P=0.0028$, one-way ANOVA, $n=5$) but did not affect sIPSCs amplitude ($F(1.851, 7.404)=2.471$, $P=0.1520$, not shown). This effect mimics a well-established cellular effect of exogenous OT in the BNST_{DL}, which was shown to increase frequency of sIPSCs specifically in Type II BNST_{DL} neurons⁴⁰. **D:** Notably, TLS did not affect sIPSCs frequency in the presence of selective OTR antagonist, OTA ($F(1.565, 7.823)=0.0003$, $P=0.9985$, $n=5$). Fine lines represent individual Type II neurons responses, black thick lines - average responses, * $P<0.05$, 3rd V - Third ventricle.



Supplementary figure 2 legend

Fear-potentiated startle (FPS) components. Rats are tested for baseline acoustic startle response ASR, pre-shock, day 1) before fear conditioning on day 2 (context A). On day 3 fear recall is tested in context B: Cued fear is calculated as a percent change score of ASR amplitude from 'between conditioned stimulus (CS+)' to ASR 'during CS+'. Non-cued fear is calculated as a percent change score from post-shock to 'between CS+'. Note, during the fear recall test, post-shock ASR is measured before the first CS+ presentation. On day 4 rats are tested for contextual fear recall in context A with no CS presentations, calculated as percent change score from pre-shock on day 1 to ASR in context A on day 4.

